Experimental and Monte Carlo studies of Ca^{2+} channel function and fast transmitter release at presynaptic active zones of the frog neuromuscular junction

by

Fujun Luo

B.S., Nanjing University, 1999

M.S., Chinese Academy of Sciences, 2002

Submitted to the Graduate Faculty of

Arts and Sciences in partial fulfillment

of the requirements for the degree of

Doctor of Philosophy

University of Pittsburgh

2009

UNIVERSITY OF PITTSBURGH

School of Arts and Sciences

This dissertation was presented

by

Fujun Luo

It was defended on

June 23, 2009

and approved by

Committee Chairperson: Jon Johnson, Ph.D, Dept. of Neurosci.

Guo-Qiang Bi, Ph.D., Dept. of Neurobiol.

Jen-Wei Lin, Ph.D., Boston Univ.

Joel R. Stiles, M.D. Ph.D. Pitt Supercomputing Center.

Nathan Urban, Ph.D., Dept. of Biol., CMU

Dissertation Advisor: Stephen D. Meriney, Ph.D., Dep. of Neurosci.

Experimental and Monte Carlo studies of Ca^{2+} channel function and transmitter release at presynaptic active zones of the frog neuromuscular junction

Fujun Luo, PhD

University of Pittsburgh, 2009

During fast chemical synaptic transmission, neurotransmitter release is triggered by calcium (Ca^{2+}) influx through voltage-gated Ca^{2+} channels (VGCCs) opened by an action potential (AP) at the nerve terminal. The magnitude and time course of neurotransmitter release is critically determined by the coupling between Ca^{2+} channels and synaptic vesicles. Studies of the quantitative dependence of transmitter release on the number of VGCCs provide important information for our understanding of the mechanisms that underlie the control and modulation of presynaptic release probability and kinetics. Using high-resolution calcium imaging techniques and variance analysis, I have determined the number of functional VGCCs within individual active zones (AZs) of the adult frog neuromuscular junction (NMJ) and their opening probability in response to single AP stimulation. The results have shown that the average number of VGCCs within individual active zones was relatively small (~28) and the average opening probability of individual Ca^{2+} channels during a presynaptic AP was very low (~0.24). Therefore, it is predicted that an action potential induced opening of relatively few Ca^{2+} channels in a single active zone. Furthermore, by combining pharmacological channel block, calcium imaging, postsynaptic recording, and 3D Monte Carlo diffusion-reaction simulations, I have studied the coupling of single Ca^{2+} channel openings to the triggering of vesicle fusion. I have provided evidence that Ca^{2+} entry through single open Ca^{2+} channels at the nerve terminal can be imaged directly and that such Ca^{2+} flux is sufficient to trigger synaptic vesicle fusion. I have

further shown that following a single AP, the Ca^{2+} influx through a single open channel plays the predominant role in evoking neurotransmitter release, while Ca^{2+} ions derived from a collection of open Ca^{2+} channels are rarely required for vesicle exocytosis at this synapse.

TABLE OF CONTENTS

LIST OF TABLES

LIST OF FIGURES

1.0   INTRODUCTION

1.1   OVERVIEW

Neurons communicate with their target cells at synapses, the specialized intercellular junctions through which signals are transferred from the presynaptic neuron to the postsynaptic cell. Synapses are classified as electrical or chemical based on whether signal transmission occurs via direct propagation of electrical signals or via a chemical messenger. My thesis will focus exclusively on chemical synapses, referred to henceforth simply as synapses. During synaptic transmission, action potentials activate voltage-gated Ca^{2+} channels that control the flux of Ca^{2+} ions known to trigger transmitter release from specialized regions of the nerve terminal, called active zones. Both the number of Ca^{2+} channels in a single active zone and their probability of opening during an AP, which are critical determinants of AP-evoked Ca^{2+} signals, are poorly explored in part due to inaccessibility of most nerve terminals to direct patch-clamp recording. I imaged AP-evoked Ca^{2+} signals at adult frog motor nerve terminals, and used variance analysis of Ca^{2+}-dependent fluorescence fluctuations to calculate the number and opening probability of voltage-gated Ca^{2+} channels in sub-regions of presynaptic active zones. My analysis reveals that the number of voltage-gated Ca^{2+} channels within individual active zones is relatively small, roughly equivalent to the number of docked synaptic vesicles, and the average opening probability of individual Ca^{2+} channels during an AP is very low.

1

The roughly equivalent numbers of Ca^{2+} channels and docked synaptic vesicles at this synapse led me to hypothesize an interesting stoichiometric relationship: each docked synaptic vesicle might be tightly associated with a single Ca^{2+} channel, and the flux of Ca^{2+} through a single open Ca^{2+} channel may be the dominant Ca^{2+} signal that triggers vesicle fusion. By combining pharmacological channel block, calcium imaging, postsynaptic recording, and 3D Monte Carlo diffusion-reaction simulations, I have studied the coupling of single Ca^{2+} channel openings to the triggering of vesicle fusion within single active zones. The results provide strong evidence that Ca^{2+} entry through single Ca^{2+} channels is sufficient to trigger synaptic vesicle fusion. It is further shown that the Ca^{2+} influx through single open Ca^{2+} channels plays the predominant role in evoking neurotransmitter release whereas the sum of Ca^{2+} ions derived from a collection of several open Ca^{2+} channels are rarely required for vesicle exocytosis at this synapse.

1.2   ACTIVE ZONE

At the nerve terminal, AP-evoked Ca^{2+} influx and transmitter release take place in specialized active zone regions. There are two prominent features of Ca^{2+}-triggered transmitter release at synapses: it is fast and spatially restricted. These features are largely attributed to the unique structural and functional organization of active zones. The delay between the arrival of an AP and vesicle exocytosis is typically less than 1 millisecond (ms) at most synapses. To accomplish such rapid speed, it is thought that synaptic vesicles and voltage-gated Ca^{2+} channels must be in close proximity to one another (Rosenmund et al., 2003; Zhai and Bellen et al., 2004). In contrast to the regulated secretion of hormones, which can occur almost everywhere on the cell

membrane, the highly directed neurotransmitter release is localized to synaptic active zones. These active zones are generally very small with an area of ~0.1 μm^2 for central synapses (Schikorski and Stevens, 1997; Xu-Friedman et al., 2001; Satzler et al., 2002). Not surprisingly, complex protein interactions are necessary to coordinate synaptic vesicle docking, priming, Ca^{2+} entry and vesicle fusion at active zones (Garner et al., 2001; Rosenmund et al., 2003; Owald and Sigrist, 2009).

Ultrastructural studies of synapses in different organisms have revealed a relatively conserved architecture for active zones. These presynaptic specializations are characterized by the presence of electron-dense active zone material (AZM) near the plasma membrane, clustered synaptic vesicles, and close apposition with a postsynaptic density (Zhai and Bellen, 2005; **Figure 1.1**). The organization of the active zone is in apparent accordance with the temporal and spatial demands of neurotransmitter release. The electron-dense, proteinaceous active zone material suggests that a large number of proteins are clustered within this specialized region. Indeed, several proteins with multiple domains involved in protein-protein interaction, including bassoon, piccolo, RIM1, MUNC13/unc13, and CAST/ELKS, have been exclusively identified in the active zone cytomatrix (Garner et al., 2001; Rosenmund et al., 2003). These proteins may play important roles in assembly of the active zone and regulation of synaptic vesicle docking, priming and fusion with plasma membrane (Garner et al., 2001; Rosenmund et al., 2003 and the references therein). One of the best studied active zone macromolecular architecture is from the adult frog neuromuscular junction. In this model synapse, each AZM is about 1 μm long, 75 nm wide, and projects 50-75 nm into the cytoplasm (Harlow et al., 2001). Strikingly, using electron microscopy tomography, distinct structural components of AZM, such as beams, ribs and pegs, have been distinguished and demonstrated to be organized into a highly-ordered pattern (Harlow

et al., 2001). Along each edge of the AZM, there is a row of docked synaptic vesicles that seem to be connected with the AZM. The presynaptic membrane underneath the AZM contains a linear array of intramembraneous particles, which include voltage-gated Ca^{2+} channels (Heuser and Reese, 1974; Pawson et al., 1998). It has been proposed that the AZM may provide a structural linkage to the docked synaptic vesicles and VGCCs at the active zone of the frog NMJ (Harlow et al., 2001). Interestingly, a similar, unique structural and molecular organization of presynaptic active zones has also been resolved recently at the mouse NMJ synapse, despite a very different arrangement of docked synaptic vesicles with respect to the intramembraneous particles (Nagwaney et al., 2009; see **Error! Reference source not found.**). It should be noted, owever, that the mature AZ organization is not essential for synaptic vesicle exocytosis since transmitter release occurs before the developmental assembly of complex AZ structure (Sun and Poo, 1987; Kraszewski et al., 1995). Currently, the functional significance of AZ structural organization and architecture (as shown in **Error! Reference source not found.**) remains poorly nderstood, but the close proximity and functional interaction of individual proteins in the AZ is apparently important for AP-evoked fast neurotransmitter release. Indeed, many studies have shown that defects in proteins that appear to assemble AZ components into macromolecular complexes dramatically reduce the transmitter release efficiency of the synapse (Zhen et al., 1998; Kittel et al., 2006).

1.2.1   Synaptic vesicle and its trafficking cycle

In electron micrographs of synapses, there typically are abundant small (~35-50 nm) and round vesicles which are electron lucent and uniform in size. These synaptic vesicles appear to cluster around active zone regions of the nerve terminal. Synaptic vesicles are filled with a high
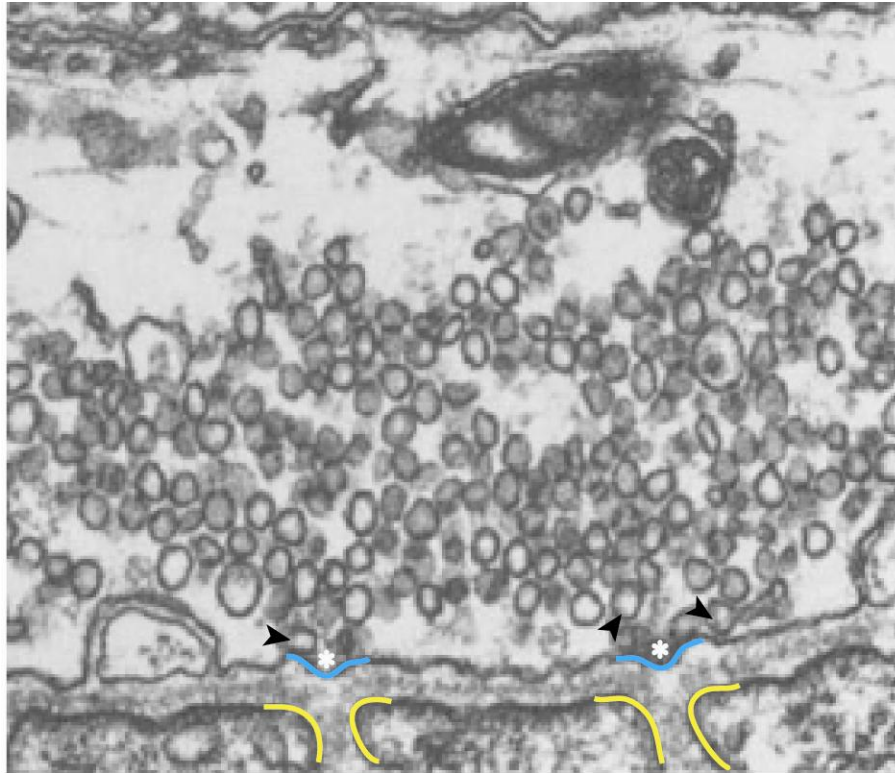
Figure 1.1 Active zone structure

An electron micrograph of the frog neuromuscular junction showing presynaptic active zones (blue), each of which directly opposes a postsynaptic junctional fold (yellow) that contains a high-density of acetylcholine receptors. A cluster of synaptic vesicles (arrowheads) within the presynaptic terminal docks at an electron-dense region of the active zone, and the electron-dense material (stars) consisting of many active zone-specific proteins are thought to facilitate synaptic vesicle docking, priming and fusion. The active zone regions also contain voltage-gated Ca^{2+} channels, but their presence is not apparent in this electron micrograph (but see **Figure 1.5**). After Heuser and Reese, 1974.

concentration of neurotransmitters, such as acetylcholine, glutamate, or GABA, which are released upon fusion of synaptic vesicle membrane with plasma membrane. Upon discharge, the neurotransmitters diffuse and bind to their receptors on the membrane of postsynaptic cells. The resultant activation of receptors may open or close ion channels and thus alter the membrane conductance and/or potential of the postsynaptic cell.

Synaptic vesicles undergo a continuous recycling in the nerve terminal for repeated use during sustained neuronal activity (see **Figure 1.2A**; for review see Sudhof, 2004). Briefly, synaptic vesicles are rapidly retrieved after exocytosis, either through a clathrin-dependent mechanism (Heuser and Reese, 1973; Murthy and De Camilli, 2003) or through a clathrin-independent, so called kiss-and run pathway (Ceccarelli et al., 1973; Valtorta et al., 1990; Fesce et al., 1994). The physiological importance of clathrin-mediated endocytosis in synaptic vesicle recycling has been well established, but seems to occur mostly during high-frequency stimulation (Brodin et al., 2000; Slepnev and De Camilli, 2000; Murthy and De Camilli, 2003; Sudhof, 2004). The kiss-and-run pathway provides an alternate but rapid route for vesicle recycling and may predominate under low frequency stimulation (Murthy and De Camilli, 2003; Royle and Lagnado, 2003). Newly endocytosed vesicles recycle directly (Murthy and Stevens, 1998), or fuse with an endosomal intermediate (Fesce et al., 1994). Neurotransmitters are actively transported into the synaptic vesicle by vesicular transmitter transporters in an ATP-dependent process. Neurotransmitter-filled synaptic vesicles are then mobilized and tethered to the active zone region for docking and priming in preparation for another round of exocytosis.

In response to high frequency stimulation, transmitter release drops quickly to a very low steady-state level, suggesting that there are different vesicle pools with distinct functional properties (Sudhof, 2004; Rizo and Betz, 2005). The precise number and identity of these pools,
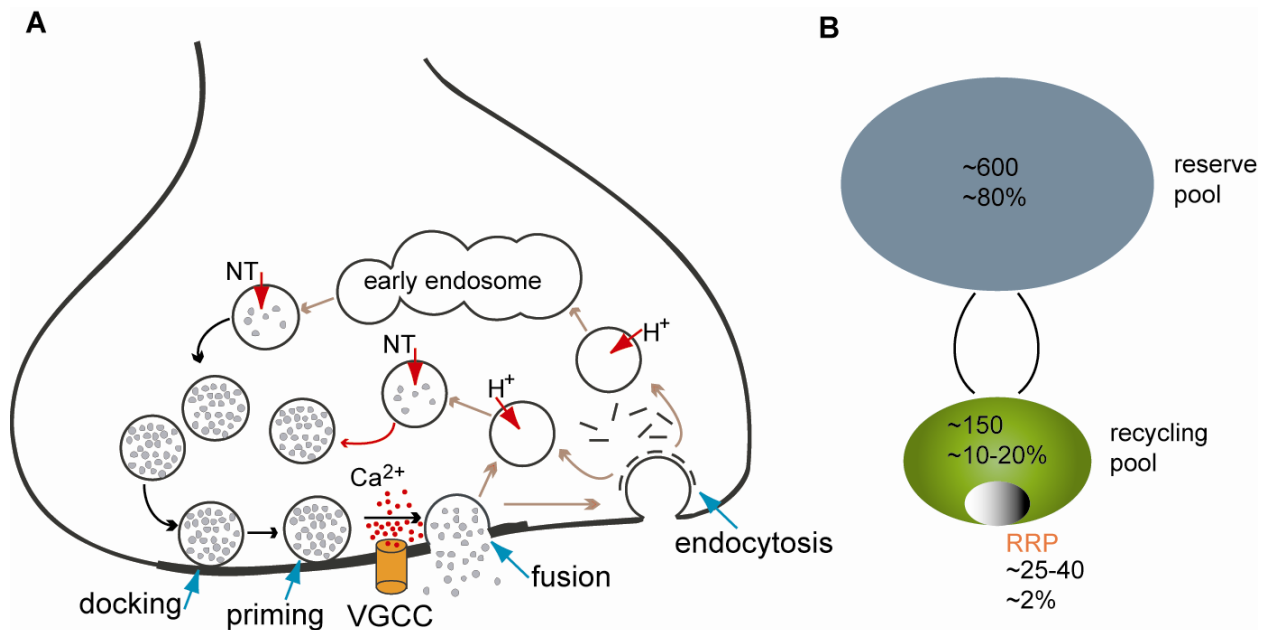
Figure 1.2 The synaptic vesicle cycle and vesicle pools.

(A) Synaptic vesicles are targeted to the active zone and dock at the plasma membrane. After priming, the docked vesicles become competent for fusion. Upon arrival of an action potential, the influx of Ca^{2+} through open voltage-gated Ca^{2+} channels triggers synaptic vesicle fusion with the plasma membrane. After exocytosis, the vesicle is retrieved by clathrin-mediated endocytosis and reacidified and reloaded for another round of exocytosis. (After Sudhof, 2004). (B) Different vesicle pools with distinct functional properties exist at a single active zone of the frog motor nerve terminal. Please see detail in the text. (After Rizo and Betz, 2005).

and their functional significance, are an active area of research and there is not complete

agreement in the literature. For the purposes of this discussion, I will present one scheme that I

feel is most consistent with studies from the frog NMJ (Rizo and Betz, 2005). In this scheme,

synaptic vesicles belong to one of three pools: reserve pool, recycling pool, and readily-

releasable pool (Rizo and Betz, 2005; see **Figure 1.2B**). The vesicles in reserve pool are

generally thought to be tethered to cytoskeleton (i.e. actin) through synapsin which renders them

immobile (Hilfiker et al., 1999). These vesicles make up about ~80-90% of all vesicles in most

nerve terminals, but do not participate in release during normal physiological activity. They may

only be mobilized for release after synapsin has been phosphorylated, which may only occur

after intensive stimulation (Greengard et al., 1993). The recycling pool is defined as those

vesicles that continuously recycle and are involved in vesicle fusion during physiological

stimulation. This pool contains about ~10-20% of all vesicles. The readily-releasable pool can

be thought of as a small part of the recycling pool and only contains those vesicles that are ready

to release immediately upon stimulation. The readily releasable vesicles make up only 1-2% of

total synaptic vesicles, and generally correspond to those docked synaptic vesicles at the active

zone observed with electron microscopy (Rosenmund and Stevens, 1996; S ätzler et al., 2002;

Schikorski and Stevens, 1997, 1999, 2001; Stevens and Tsujimoto, 1995; Rizo and Betz, 2005).

The number of docked synaptic vesicles per active zone is relatively small (ranging from 1 to 30

for central synapses; ranging from 25 to 40 for the frog active zones) and is often correlated with

the active zone area (S ätzler et al., 2002; Schikorski and Stevens, 1997; Stevens and Tsujimoto,

1995; Rizo and Betz, 2005). The release probability of a synapse, as well as its short-term

synaptic properties, is highly dependent upon the readily-releasable pool size (Rosenmund and

Stevens, 1996; Murthy et al., 2001; but see Xu-Friedman et al., 2001). The initial synaptic

depression caused by high-frequency stimulation typically reflects the depletion of vesicles in this pool. Although the concept of vesicle pools has been useful to delineate different synaptic vesicle populations with various release rates and/or probabilities, we know little about the mechanisms that underlie the regulation of these processes. It is possible that vesicles in different pools may have different calcium binding proteins with various affinities for Ca^{2+}, or that different vesicles are exposed to different Ca^{2+} dynamics due to their spatial coupling to various Ca^{2+} sources (Sun et al., 2007). In the present dissertation, it is assumed that all synaptic vesicles docked at presynaptic active zones of the frog NMJ are readily releasable upon AP-evoked Ca^{2+} entry and have the same calcium binding proteins.

1.2.2   Voltage-gated Ca^{2+} channels

Other essential components in the active zone for synaptic transmission are voltage-gated Ca^{2+} channels. These channels are transmembrane proteins and activate upon membrane depolarization to selectively mediate Ca^{2+} flux into the cell. Voltage-gated Ca^{2+} channels are composed of a primary α1 subunit and auxiliary subunits α2δ, β and γ. The α1 subunit is responsible for pore formation, voltage sensing and gating of the channel while the auxiliary subunits regulate the expression and gating properties of Ca^{2+} channels (Catterall, 2000; Ertel et al., 2000; Vacher et al., 2008). The α1 subunit consists of about 2000 amino acid residues and has four domains (I-IV), each formed by six transmembrane segments (S1-S6) and a loop connecting S5 and S6. Segment S4 is the primary voltage sensor. The ion conduction pore is formed by segments S5 and S6 and the loop between them (see **Figure 1.3**).

 There are multiple types of Ca^{2+} channels, and in different cells they perform a diversity of fundamental functions such as muscle contraction, hormone secretion, neurotransmitter

release and gene expression (Hofmann et al., 1999; Catterall, 2000; Ertel et al., 2000). The different types of Ca^{2+} channels are primarily defined by different α1 subunits (see **Figure 1.3**). Distinct genes encode 10 different Ca^{2+} channel α1 subunits that exhibit various pharmacological and physiological properties and functions (Catterall, 2000; Ertel et al., 2000; Catterall and Few, 2008; Vacher et al., 2008). Voltage-gated Ca^{2+} channels have been classified into three subfamilies. The Ca_V1 subfamily of Ca^{2+} channels includes $Ca_V1.1$, $Ca_V1.2$, $Ca_V1.3$ and $Ca_V1.4$, which mediate L-type calcium currents. The Ca_V2 subfamily of Ca^{2+} channels includes $Ca_V2.1$, $Ca_V2.2$, and $Ca_V2.3$, which conduct P/Q type, N-type and R-type calcium currents respectively. The Ca_V3 subfamily of Ca^{2+} channels includes $Ca_V3.1$, $Ca_V3.2$ and $Ca_V3.3$, which conduct T-type calcium currents. Both Ca_V1 and Ca_V3 subfamilies are rarely involved in initiating transmitter release and therefore are not discussed further in this thesis (see Dietrich et al., 2003). The diversity of Ca^{2+} channels is substantially increased by the expression of four types of β subunits, four types of $α_2δ$ subunits and their alternative splice variants (Catterall, 2000; Catterall and Few, 2008; Vacher et al., 2008).

At most chemical synapses, P/Q-type ($Ca_V2.1$) and N-type ($Ca_V2.2$) Ca^{2+} channels primarily control AP-evoked fast transmitter release (Dunlap et al., 1995; Stanley, 1997; Catterall, 2000; Augustine et al., 2003; Reid et al., 2003; Evan and Zamponi, 2006; Catterall and Few, 2008). In general, N-type Ca^{2+} channels play the primary role at peripheral synapses while P/Q type Ca^{2+} channels are predominant in triggering transmitter release at most central synapses (Reid et al., 2003; Evan and Zamponi, 2006; Catterall and Few, 2008). However, in some central synapses, N-type Ca^{2+} channels also play an important role in controlling transmitter release (Poncer et al., 1997; Wilson et al., 2001; Hefft and Jonas, 2005). At some synapses, especially during early development, Ca^{2+} influx through multiple Ca^{2+} channels triggers
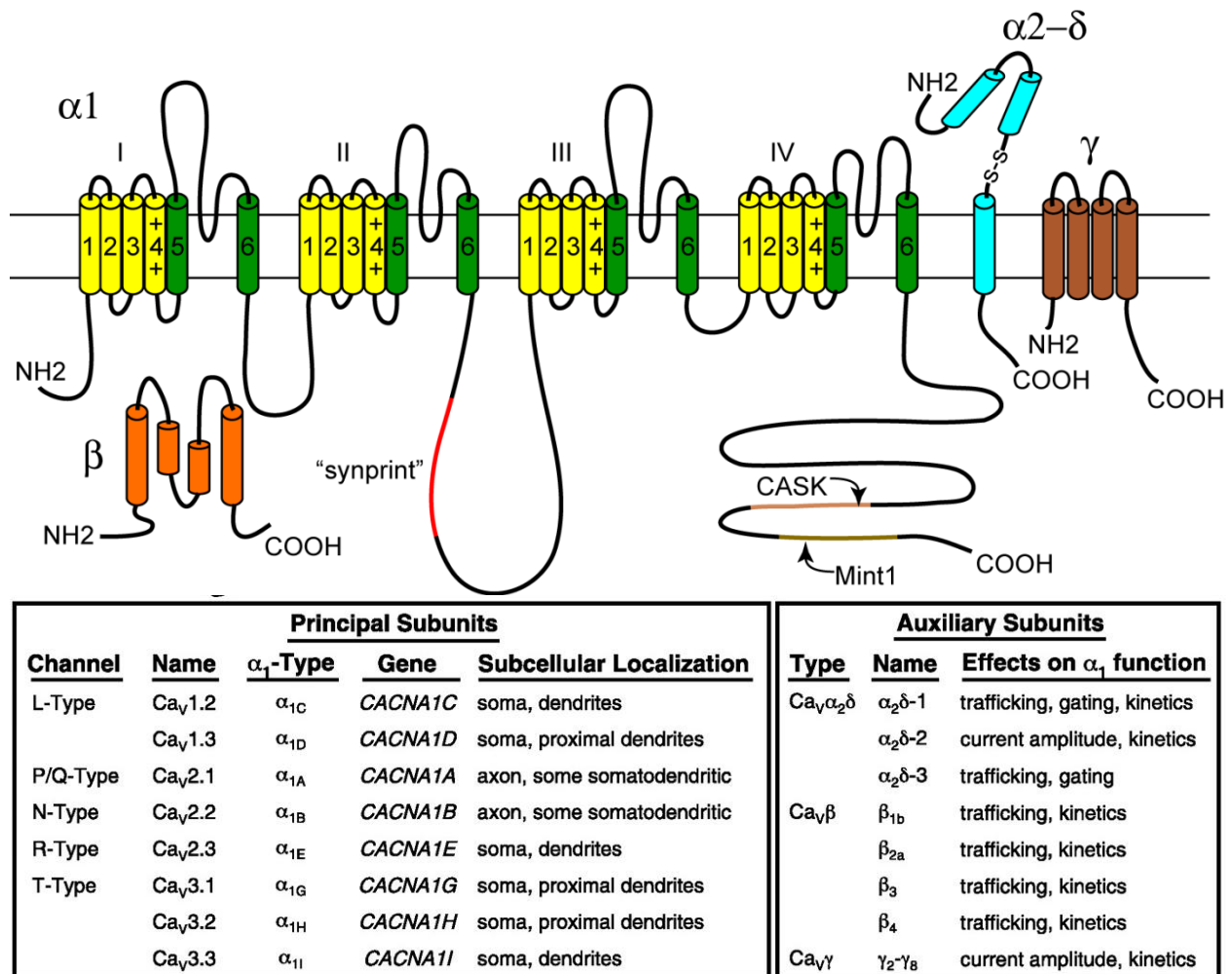
Figure 1.3 Voltage-gated Ca^{2+} channels in vertebrate neurons.

Diagram of the molecular structure of voltage-gated Ca^{2+} channels, composed of a primary α1 subunit and auxiliary β, α2δ and γ subunits. Bottom left box: classification, genetic nomenclature, and subcellular localization of α1 subunits. Bottom right box: classification of α2-δ, β and γ auxiliary subunits and their functional roles in regulating Ca^{2+} channels. (After Catterall and Few, 2008; Vacher et al., 2008)

11

neurotransmitter release in a coordinated manner (Wu et al., 1998; Iwasaki et al., 2000; Rozov et al., 201; Reid et al., 2003). It remains unknown what mechanisms selectively target specific subtypes of Ca^{2+} channels to a particular synapse. Also, it is unclear how the control of neurotransmitter release and synaptic plasticity is affected by the selective synaptic localization of various Ca^{2+} channels. At the adult frog neuromuscular junction, AP-evoked fast neurotransmitter release is predominately triggered by Ca^{2+} flux through N-type Ca^{2+} channels, which can be completely and irreversibly blocked by ω-conotoxin GVIA (Kerr and Yoshikami, 1984; Stocker et al., 1997). In contrast, at the mammalian neuromuscular junction, P/Q-type Ca^{2+} channels, which are specifically blocked by ω-agatoxin-IVA, are predominant in triggering AP-evoked transmitter release (Uchitel et al., 1992; Hong and Chang, 1995).

1.3   CA^{2+}-TRIGGERING OF FAST NEUROTRANSMITTER RELEASE

As an AP propagates down the axon to the nerve terminal, membrane depolarization activates voltage-gated Ca^{2+} channels, and the resulting Ca^{2+} entry triggers synaptic vesicle fusion with the plasma membrane and the subsequent release of transmitter (Katz, 1969). It should be noted that even at rest, synapses spontaneously release transmitter at a finite but low probability, generating miniature postsynaptic voltage responses that can be recorded with electrophysiological techniques (Katz 1969). AP-evoked Ca^{2+} transients dramatically increase the probability of transmitter release, triggering at least two components of with different release kinetics (Berrett and Stevens, 1972; Goda and Stevens, 1994; Sabatini and Regehr, 1996). The fast component is thought to be caused by synchronous release of a large number of quanta with a decay time constant of 5–10 ms. This phasic release predominates at most synapses during low frequency

AP stimulation (Sabatini and Regehr 1996). The second component is a slower asynchronous release which has a decay time constant in the range of 100-200 ms, and is typically overwhelmed by the fast component (Goda and Stevens, 1994). The existence and molecular mechanism of the asynchronous release and its physiological role in synaptic transmission and plasticity still remain elusive at most synapses (Barrett and Stevens 1972; Geppert et al. 1994; Goda and Stevens 1994; Atluri and Regehr 1998; Nishiki and Augustine, 2004a, b; Hefft and Jonas, 2005; Sun et al., 2007), and will not be discussed further in this dissertation.

1.3.1 How much Ca^{2+} is required to trigger fast neurotransmitter release?

One of the key questions related to AP-evoked fast neurotransmitter release is how much Ca^{2+} is necessary to trigger synaptic vesicle fusion with the plasma membrane. It has been estimated that the Ca^{2+} concentration at release sites ($[Ca^{2+}]_i$) can reach as high as hundreds of micromolar (Llinas et al., 1992; DiGregorio et al., 1999; Yazejian et al., 2000). Indeed, using flash photolysis of caged Ca^{2+} to uniformly elevate $[Ca^{2+}]_i$ in the synaptic terminal of retinal bipolar cells, Heidelberger et al (1994) showed that greater than 200 μM $[Ca^{2+}]_i$ was required to achieve rapid secretion. With the presence of large amounts of Ca^{2+} buffer inside the terminal, the peak Ca^{2+} signal is dramatically attenuated away from Ca^{2+} entry sites (Neher, 1998). Therefore, it is suggested that the Ca^{2+} sensor proteins on synaptic vesicles must be located within tens of nanometers of open Ca^{2+} channels (Augustine, 2001). This hypothesis is further supported by the experimental evidence that only BAPTA, a rapid Ca^{2+} buffer, but not EGTA, a slow Ca^{2+} chelator, effectively reduces transmitter release at some synapses, even though they have similar equilibrium affinity for Ca^{2+} (Adler et al., 1991; Bucurenciu et al., 2008).

In contrast, there is also strong evidence from recent studies at the Calyx of Held, a large auditory brainstem synapse, for a very different scenario. First, it was shown that injection of EGTA into the terminal reduced neurotransmitter release as effectively as injection of BAPTA, suggesting a relatively long diffusion distance of entering Ca^{2+} ions before binding to Ca^{2+} sensor proteins for transmitter release (Borst and Sakmann, 1996). Second, Ca^{2+} uncaging experiments at the calyx of Held demonstrated that only a few micromolar $[Ca^{2+}]_i$ can readily evoke transmitter release, and that 10~25 μM $[Ca^{2+}]_i$ was sufficient to induce a rapid release rate similar to that observed during AP stimulation (Bollmann et al., 2000; Schneggenburger and Neher, 2000).

Therefore, it has been proposed that Ca^{2+} sensor proteins with different Ca^{2+} affinity must control Ca^{2+}-triggered fast neurotransmitter release at different synapses, but their exact molecular identities remain unknown. In contrast to this dramatic difference in Ca^{2+} sensitivity of transmitter release between synaptic preparations, it has been widely observed that the quantitative dependence of transmitter release on extracellular Ca^{2+} concentration is highly consistent across different synapses and animals (Dodge and Rahamimoff, 1967; Augustine and Charlton, 1986; Bollmann et al., 2000; Schneggenburger and Neher, 2000; Beutner et al., 2001). A high power relationship (4~5 order) between neurotransmitter release and external Ca^{2+} concentration has been interpreted to reflect that synaptic vesicle fusion is triggered by the binding of at least four Ca^{2+} ions to the Ca^{2+} binding sites on synaptic vesicles (Dodge and Rahamimoff, 1967; Bollmann et al., 2000; Schneggenburger and Neher, 2000). Originally, it was proposed that there might be a vesicular membrane protein that contains four independent Ca^{2+} binding sites (stoichiometric model) or that a vesicle contains 4 or more Ca^{2+} receptors randomly distributed on the vesicle membrane (stochastic model). Both models could equally

14

well predict the observed fourth power dependence of transmitter release on extracellular Ca^{2+} (Dodge and Rahamimoff, 1967). More recently, the vesicular protein synaptotagmin 1, which can bind up to 5 Ca^{2+} ions through its C2A and C2B domains, has been demonstrated to be critical for Ca^{2+}-triggered fast neurotransmitter release (see section **1.3.3** below), and therefore is recognized as a primary candidate for the Ca^{2+} sensor. Based on this finding, molecular cooperativity hypotheses were developed and were dominated by the stoichiometric model. However, it remains unclear whether all Ca^{2+} binding sites on a single synaptotagmin 1 molecule can be bound by Ca^{2+} during the transient Ca^{2+} signals evoked by an AP. In addition, recent biochemical data has shown that each vesicle may have up to fifteen copies of synaptotagmin 1 (Takamori et al., 2006). Therefore, the details of how many Ca^{2+} ions need to be bound on each vesicular Ca^{2+} sensor and how many Ca^{2+}-bound vesicular Ca^{2+} sensors on each vesicle are sufficient and adequate to trigger vesicle fusion remains unresolved.

1.3.2 Spatial relationship between docked synaptic vesicles and voltage-gated Ca^{2+} channels

Another critical issue related to Ca^{2+}-triggered fast neurotransmitter release is the structural organization and physical relationship between presynaptic Ca^{2+} channels and docked synaptic vesicles in the active zone. The spatial distance between docked synaptic vesicles and Ca^{2+} entry sites can be inferred by examining the effectiveness of various exogenous Ca^{2+} chelators in blocking transmitter release (Alder et al., 1991; Bucurenciu et al., 2008). In the squid giant synapse and a synapse of parvalbumin-expressing GABAergic basket cells in the dentate gyrus of hippocampus, only BAPTA, but not EGTA effectively suppress transmitter release (Alder et al., 1991; Hefft and Jonas, 2005; Bucurenciu et al., 2008). These studies have been interpreted to

15

indicate that there is very tight coupling between Ca^{2+} channels and synaptic vesicles (Neher, 1998). At the calyx of Held synapse, however, the relatively slow Ca^{2+} buffer EGTA effectively inhibits release (Borst et al. 1995), suggesting a relatively loose coupling between most vesicles and Ca^{2+} channels. Consistently, it has been shown that different types of Ca^{2+} channels may control the same pool of readily releasable vesicles (Borst and Sakmann 1996; Wu et al., 1999).

Interestingly, the effectiveness of various Ca^{2+} channels in controlling transmitter release differ remarkably between synapses, which may reflect a different localization of Ca^{2+} channels relative to docked synaptic vesicles in different preparations (Wu et al., 1999). By applying specific Ca^{2+} channel toxins to titrate block of Ca^{2+} channels, and measuring the resultant effects on transmitter release, the possible spatial organization of Ca^{2+} channels relative to release sites can be estimated. For example, it has been proposed that the Ca^{2+} flux through a single Ca^{2+} channel may control each vesicle fusion event at the squid giant synapse and frog NMJ based on the observation that there is a nearly linear relationship between Ca^{2+} channel block and release inhibition (Yoshikami et al., 1989; Augustine et al., 1991). In contrast, a superlinear relationship has been observed at many central synapses and interpreted to mean that many Ca^{2+} channels need to open to create a summed Ca^{2+} flux to trigger transmitter release (Mintz et al., 1995; Borst and Sakmann, 1996, 1999; Wu et al., 1999).

1.3.3   Synaptic vesicle fusion and the Ca^{2+} sensor

The core protein machinery responsible for membrane fusion is assembled from a set of vesicle and target membrane proteins termed SNAREs (soluble N-ethyl maleimide sensitive factor attachment protein receptors; Sollner et al., 1993). The SNARE proteins are characterized by a special SNARE motif, a homologous sequences of 70 amino acid residues, which readily forms a

16

coiled-coil complex with other SNARE motifs (Poirier et al., 1998; Sutton et al., 1998; Rizo and Rosenmend, 2008; Sudhof and Rothman, 2009). In particular, the neuronal SNARE core complex is formed by syntaxin and SNAP-25, located at the plasma membrane, and synaptobrevin, located at the vesicle membrane (Weber et al., 1998; Tucker et al., 2004). The findings that these proteins are the targets of diverse *clostridia* neurotoxins, which completely block neurotransmitter release, demonstrate their key roles in synaptic exocytosis (Hayashi et al., 1994; Schiavo et al., 1992). *In vitro* reconstitution experiments have further shown that this minimal machinery is necessary and sufficient to mediate membrane fusion (Weber et al., 1998). In contrast to constitutive membrane fusion at other parts of the cell, however, synaptic vesicle exocytosis is highly restricted to the active zone region of the presynaptic terminals and tightly regulated by Ca^{2+} (Augustine, 2001; Schneggenburger and Neher, 2005). It has been commonly accepted that Ca^{2+}-triggered fast neurotransmitter release depends on the action of synaptotagmin 1.

Synaptotagmin 1, an integral vesicular membrane protein, has been proposed to function as the primary Ca^{2+} sensor for AP-evoked fast transmitter release (Perin et al., 1990; Augustine, 2001; Chapman, 2002; Sudhof, 2002; Koh and Bellen, 2003). Synaptotagmin 1 contains two consecutive cytoplasmic C2 domains, C2A and C2B (see **Figure 1.4**). Five highly conserved aspartate residues coordinate the binding of 3 and 2 Ca^{2+} ions at C2A and C2B domains respectively (Ubach et al., 1998; Fernandez et al., 2001). The intrinsic Ca^{2+} affinity of synaptotagmin 1 Ca^{2+} binding domains is far below the physiological intracellular Ca^{2+} concentration ($K_d > 0.1$ mM), but increase dramatically up to 5000 fold in the presence of phospholipids ($K_d = 1\sim20$ μM; Ubach et al., 1998; Zhang et al., 1998; Fernandez et al., 2001). The negative charges on phospholipids may provide additional coordination sites for Ca^{2+}

binding, since the apparent Ca^{2+} affinity of synaptotagmin 1 is sensitive to the phospholipid composition (Fernández-Chacón et al., 2001). Furthermore, it has been shown that both C2 domains of synaptotagmin 1 have the ability to penetrate the phospholipid membrane in a Ca^{2+}-dependent manner, which might function cooperatively in triggering synaptic vesicle fusion (Davis et al., 1999; Pang et al., 2006). In addition to phospholipid membranes, synaptotagmin 1 also binds to syntaxin as a function of Ca^{2+} (Chapmann et al., 1995; Kee and Scheller et al., 1996; Fernández-Chacón et al., 2001). Disruption of synaptotagmin 1 in various species, including worms, flies, and mice, has abolished AP-triggered fast transmitter release and thus demonstrated the critical role of synaptotagmin 1 in synaptic transmission (Littleton et al., 1993; Nonet et al., 1993; Geppert et al., 1994; Fernández-Chacón, et al., 2001; Koh and Bellen, 2003). Ca^{2+}-regulated membrane fusion has been reconstituted *in vitro* by co-expressing synaptotagmin 1 and SNARE complex proteins in phospholipids. Using this assay, it has been shown that the binding of Ca^{2+} to synaptotagmin 1 is necessary and sufficient to stimulate SNARE-mediated membrane fusion, suggesting that these proteins constitute the minimal protein machinery for Ca^{2+}-triggered exocytosis (Tucker et al., 2004). However, the specific roles of synaptotagmin 1 in calcium-dependent vesicle fusion are still under debate. One hypothesis proposes that synaptotagmin interacts with the SNARE complex in a Ca^{2+} -independent manner to prevent synaptic vesicle fusion with the plasma membrane (Chicka et al., 2008). This action may depend on interactions with another active zone protein, probably complexin, which aids in preventing spontaneous synaptic vesicle fusion mediated by the assembly of the SNARE complex (Tang et al., 2006; Maximov et al., 2009). Such inhibition is thought to be relieved by Ca^{2+} binding to synaptotagmin 1 upon the entry of Ca^{2+} ions into the nerve terminal (Tang et al., 2006; but see Xu et al., 2009).

A

NH2

TMD

C2A

C2B

B

synaptic vesicle

plasma membrane

| | synaptotagmin | | synaptobrevin | | Ca²⁺ |
| | syntaxin | | SNAP-25 | | |
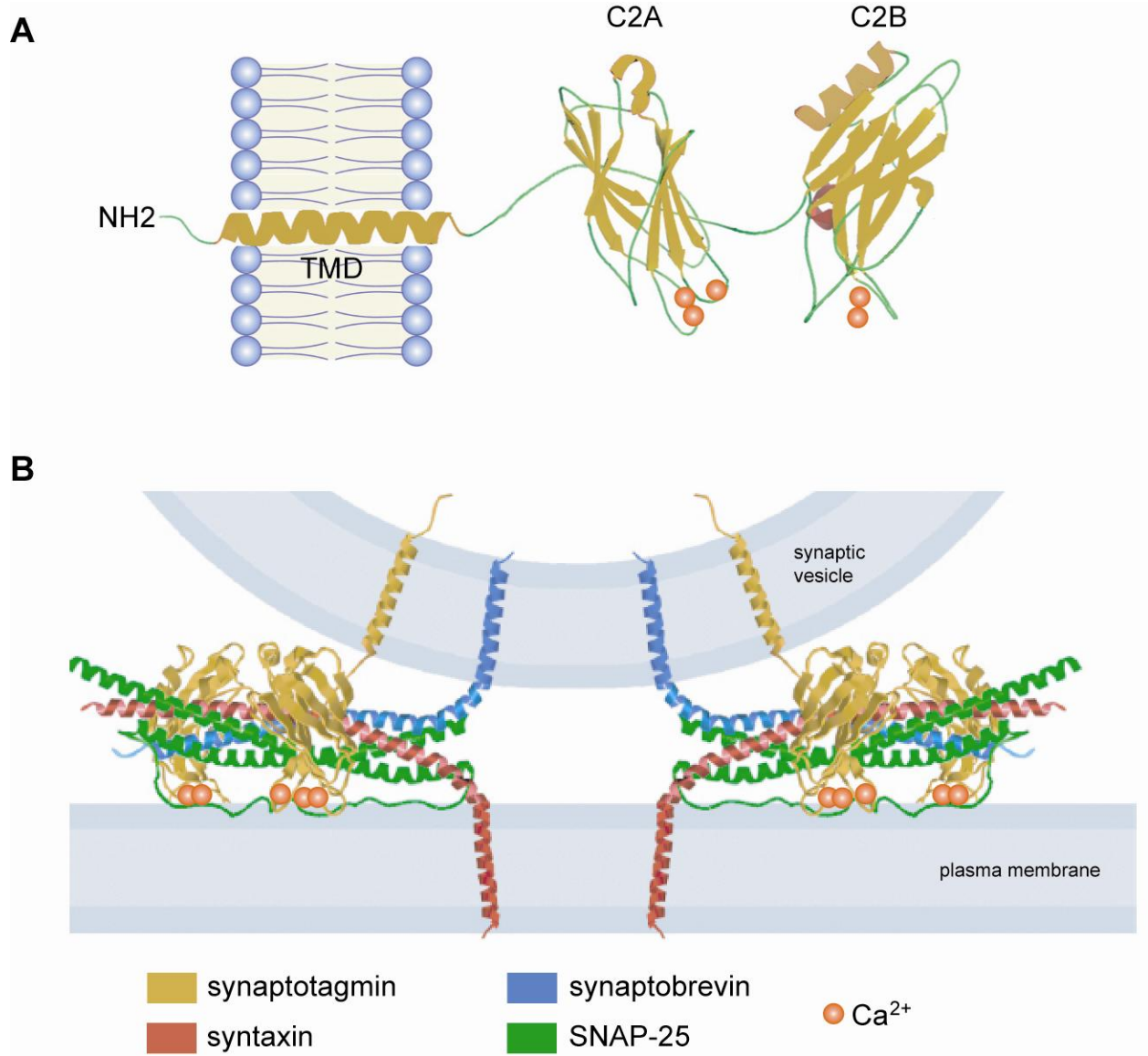
Figure 1.4 Synaptotagmin 1 and synaptic vesicle fusion

(A) Domain structure of synaptotagmin, showing the transmembrane domain (TMD) and the C2A and C2B domains, which can bind 3 and 2 Ca^{2+} (red spheres), respectively. (After Chapman, 2008)

(B) Model of SNARE-mediated vesicle fusion with plasma membrane, which is regulated by synaptotagmin 1 in a Ca^{2+} dependent manner. Upon the binding of Ca^{2+} to the C2A and C2B domains, synaptotagmin 1 is thought to penetrate the plasma membrane very rapidly and thus tightens the four-helix bundle formed by the SNARE proteins (syntaxin, synaptobrevin and SNAP-25). The zippering process may finally rip off the two opposing membranes and open a fusion pore for transmitter release. (After Koh and Bellen, 2003)

Numerous studies have suggested that C2A and C2B domains may play different roles in Ca^{2+}-triggered transmitter release. First, it has been shown that mutations in the Ca^{2+}-binding motif in the C2B domain abolished AP-evoked fast transmitter release (Mackler et al., 2002), whereas C2A mutants with a defect of Ca^{2+}-binding do not appear to block transmitter release *in vivo* (Robinson et al., 2002). Based on these results, it was proposed that that Ca^{2+} sensing by the C2B domain may play a dominant role in Ca^{2+}-evoked vesicle fusion (Koh and Bellen, 2003). However, in other studies, a point mutation in an amino acid residue that surrounds the calcium-binding sites in the C2A domain of synaptotagmin 1 caused a parallel reduction in the apparent calcium affinity of synaptotagmin and in the calcium sensitivity of neurotransmitter release in mutant mice, suggesting the C2A domain is also important for controlling fast synaptic transmission (Fernández-Chacón et al., 2001; Stevens and Sullivan, 2003).

Overall, it remains unclear how many Ca^{2+} ions are required to bind to each synaptotagmin 1 molecule, and how many synaptotagmin molecules on a given vesicle need to bind Ca^{2+}, for effective triggering of neurotransmitter release (Weber et al., 1998; Montecucco et al., 2005). Most release models assume all five Ca^{2+} binding sites on a single synaptotagmin molecule need to be bound by Ca^{2+} in order to for vesicle fusion to be triggered. This assumption seems primarily to be based on the well-known power relationship between release probability and $[Ca^{2+}]$ at the release sites (Dodge and Rahamimoff, 1967; Bollmann et al., 2000; Schneggenburger and Neher, 2000).

1.4   THE FROG NEUROMUSCULAR JUNCTION: A MODEL SYNAPSE

The neuromuscular junction (NMJ) is a synapse which connects a motor neuron and a skeletal

muscle fiber. In particular, the adult frog NMJ is a classic model synapse that has played a critical role in our understanding of the basic mechanisms of synaptic transmission (Katz, 1969). For example, the calcium hypothesis and the vesicle hypothesis of AP-evoked fast transmitter release were first proposed based on studies at the frog NMJ, and have since been demonstrated to be conserved across many synapses and species (Katz, 1969; Stevens, 2003).   The frog NMJ is known as a strong and reliable synapse in the sense that a single presynaptic action potential leads to the release of hundreds of quanta that are sufficient to bring the postsynaptic muscle cell to threshold, resulting in reliable muscle contraction (Wood and Slater, 2001). Ultrastructurally, the frog NMJ contains hundreds of large (1 μm long) active zones spaced regularly at ~1 μm intervals in a single nerve terminal (Heuser et al., 1974; **Figure 1.5**). These features make the frog NMJ an ideal preparation for physiological, ultrastructural and imaging studies. In addition, freeze fracture and electron microscope tomography have provided striking structural information related to the spatial organization of presynaptic active zone proteins (Heuser and Reese, 1977; Pawson et al., 1998; Harlow et al., 2001). Being one of the best studied model synapses, many parameters of Ca^{2+}-triggered neurotransmitter release from frog NMJ have been elucidated after more than 60 years of study. Furthermore, the putative regular arrangement of Ca^{2+} channels and docked synaptic vesicles at the frog NMJ active zone provides an ideal structure for spatially realistic simulations of the active zone function (Dittrich et al., 2009). Using the adult frog NMJ as a model system, I have combined a high resolution calcium imaging approach with powerful Monte Carlo simulations (see below) to address several important issues related to the Ca^{2+} channel regulation of transmitter release from presynaptic active zones.

A

axon

terminal

muscle fiber

presynaptic Ca²⁺ channels

postsynaptic ACh receptors

10 μm

B

Intramembraneous particle

C

synaptic vesicle

100 nm
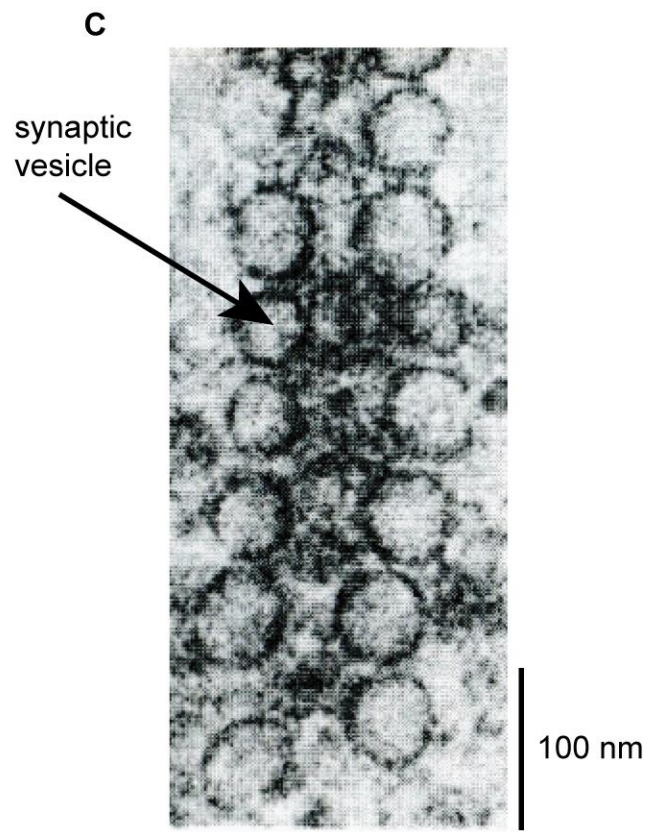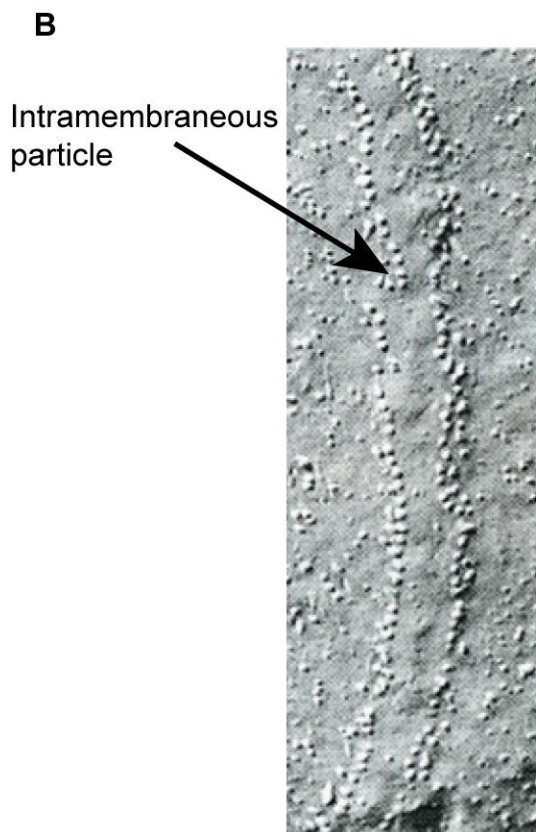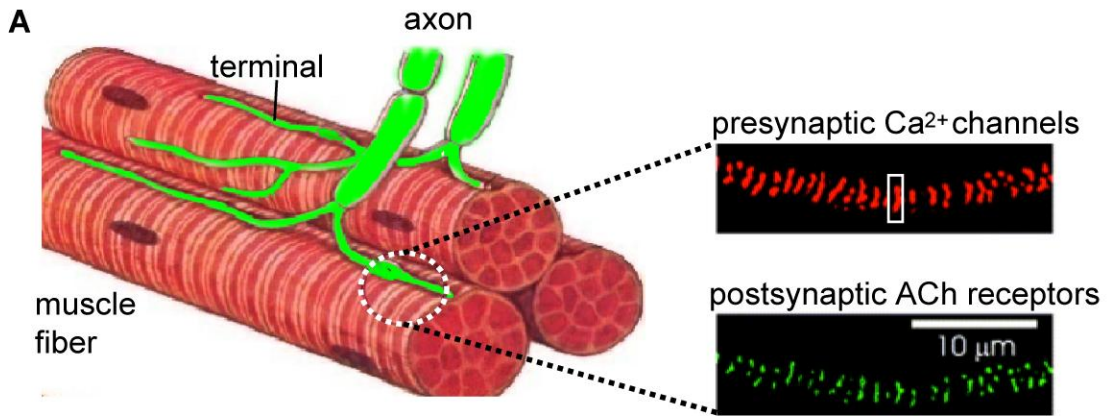
Figure 1.5 Frog neuromuscular junction as a model synapse

(A) The presynaptic nerve terminal of the frog motor neuron innervates single muscle fibers with hundreds of active zones arranged in a linear array, as shown by labeling presynaptic N-type Ca^{2+} channels with ω-conotoxin GVIA (red) or postsynaptic acetylcholine receptors with fluorescence-conjugated α-bungratoxoin (green). The postsynaptic staining, which is precisely aligned with the presynaptic staining of Ca^{2+} channels, provides a useful landmark for identifying well-focused active zones during our calcium imaging experiments.

(B) Within a single active zone, freeze-fracture electron micrographs have shown that there is a linear array of 200-250 intramembraneous particles (about 10 nm in diameter), including Ca^{2+} channels, which are arranged in parallel double rows.

(C) Transmission electron micrograph of a fraction of a single active zone, showing two lines of synaptic vesicles. It has been estimated that there are 25-40 docked synaptic vesicles on the outside edge of each particle array within single active zones. (A after Robitaille et al., 1990; B after Heuser and Reese, 1979; C after Couteaux and Pecot-Dechavasine, 1970).

1.5   MONTE CARLO SIMULATION OF CA^{2+}-EVOKED TRANSMITTER RELEASE

Monte Carlo simulation is an alternative approach to modeling based on deterministic differential equations. This approach has been widely used in simulations of synaptic transmission in a number of studies (Bartol et al., 1991; Stiles and Bartol, 2001; Stiles et al., 2001, Stiles et al., 2004). MCell (Monte Carlo Cell) is a program implementing Monte Carlo algorithms and has been designed for realistic simulation of molecular diffusion and reaction in a complex 3-D subcellular microenvironment (www.mcell.psc.edu). Using 3D random walk theory, individual diffusing molecules, e.g. Ca^{2+} ions, can be traced discretely in space and time as they freely move and react with other molecules, e.g. Ca^{2+} sensors for transmitter release. The membranes and membrane-bound molecules are defined as surface objects and effector sites and their positions can be constrained in realistic space. When diffusing molecules encounter other molecules or surfaces, the outcome is decided by comparing the value of a random number to a Monte Carlo probability value. Surfaces can be reflective, transparent, absorptive, or occupied by an effector site with an associated chemical reaction mechanism, and these properties determine the possible outcomes of each encounter. Random numbers are also used to decide between all other possible reaction mechanism transitions that might occur during each time-step. For example, bound molecules may unbind, and effector sites may change from one defined state to another, simulating a protein conformational change.

A spatially realistic 3-D MCell model of the presynaptic active zone has been developed and used to explore the molecular mechanism of synaptic vesicle release at the frog NMJ (Dittrich et al., 2009). The topology, spatial dimensions, and number of synaptic vesicles in the active zone modal are constrained by published data (Heuser et al., 1974; Pawson et al., 1998; Harlow et al., 2001). The total number of Ca^{2+} channels and their opening probability during an AP are

25

constrained by the calcium imaging experiments described below (see Chapter 2). For simplicity in this dissertation, there were 26 voltage-gated Ca^{2+} channels in each active zone and that each was positioned in a one-to-one topographic relationship with a single docked synaptic vesicle with an average distance from the vesicle of 40 nm. A similar model was adapted for simulating the titration effects of Ca^{2+} channel blockade on AP-evoked Ca^{2+} entry and neurotransmitter release. The quantitative relationship between single Ca^{2+} channel openings and synaptic vesicle fusion was also examined using this realistic active zone model.

2.0 SINGLE PIXEL OPTICAL FLUCTUATION ANALYSIS OF CA^{2+} CHANNELS AT ACTIVE ZONES OF THE FROG MOTOR NERVE TERMINAL

2.1 ABSTRACT

Action potentials activate voltage-gated Ca^{2+} channels, and the flux of Ca^{2+} into the presynaptic space triggers synaptic vesicle fusion and transmitter release from specialized active zone regions of the nerve terminal. I performed high-resolution optical imaging of Ca^{2+}-evoked fluorescence signals at adult frog motor nerve terminals. Optical fluctuation analysis of AP-evoked Ca^{2+} signals allowed us to determine the number of Ca^{2+} channels within individual active zones and their opening probability during an AP. I conclude that single active zones contain a relatively small number of Ca^{2+} channels and each opens with very low probability during an AP. The low probabilistic release of transmitter from each active zone at this synapse appears to be governed by the small number of Ca^{2+} channels opened by an AP.

2.2 INTRODUCTION

Neurotransmitter release is typically restricted within specialized regions of the nerve terminal, called active zones, which are highly organized for synaptic vesicle docking and fusion (Zhai and Bellen, 2004). As a model system in studies of synaptic transmission, the adult frog

27

neuromuscular junction (NMJ) has played an important role in our understanding of the basic mechanisms of Ca^{2+}-triggered transmitter release (Katz, 1969). The NMJ is known as a strong and reliable synapse in the sense that a single presynaptic AP leads to the release of hundreds of quanta that are sufficient to bring the postsynaptic muscle cell to threshold, resulting in reliable muscle contraction (Wood and Slater, 2001). Electron microscope tomography studies have revealed that each NMJ is constructed using hundreds of linear active zones, each with 25-40 "docked" synaptic vesicles tightly associated with vesicle release machinery and "ready" for Ca^{2+}-triggered fusion (Heuser et al., 1979; Harlow et al., 2001; Rizzoli and Betz, 2005). Each active zone, however, appears to be a low probability release site, with an average of only one vesicle released following every other AP stimulus (Katz and Miledi, 1979; see Poage and Meriney, 2002). Despite more than 60 years of study, many details of the relationship between presynaptic Ca^{2+} entry and vesicle fusion remain unresolved. For example, freeze fracture studies have documented that there are normally ~200-250 intramembraneous particles that line each active zone (Heuser et al., 1979; Pawson et al., 1998), but it is not known what fraction of these proteins are voltage-gated Ca^{2+} channels. Also unknown is the probability that individual voltage-gated Ca^{2+} channels in the active zone open in response to an AP stimulus. A determination of both the number and opening probability of presynaptic Ca^{2+} channels during an AP will provide insights into the stoichiometric relationship between Ca^{2+} channels and docked synaptic vesicles, and constrain our interpretation of the mechanisms that underlie Ca^{2+}-triggered vesicle fusion in the active zone.

Combining high resolution calcium imaging techniques with variance analysis of imaged Ca^{2+} signals has enabled the study of voltage-gated Ca^{2+} channel properties in small neuronal compartments inaccessible to standard electrophysiological approaches (see Sabatini and

Svoboda, 2000). This approach has previously been applied to reveal the stochastic opening of a

small number of Ca^{2+} channels in both presynaptic boutons and postsynaptic spines (Frenguelli

and Malinow 1996; Sabatini and Svoboda, 2000; but see Brenowitz and Regehr, 2007).

Following the previous work demonstrating the feasibility of imaging presynaptic Ca^{2+} entry at

the frog NMJ active zones (Wachman et al., 2004), I have used variance analysis of imaged AP-

evoked Ca^{2+} fluctuations to estimate the number of Ca^{2+} channels at single active zones and the

opening probability of individual Ca^{2+} channels during an AP. The results predict that there are

relatively few Ca^{2+} channels that line a single frog NMJ active zone, and that an AP normally

opens only a small fraction of these presynaptic Ca^{2+} channels. These data contribute to our

understanding of the mechanisms that govern the low probability of transmitter release from

single active zones at the frog NMJ.

2.3   METHODS

2.3.1   Dye-loading of cutaneous pectoris nerve-muscle preparations

Adult frogs (*Rana pipiens*) were decapitated and pithed following anesthesia in 0.1% tricaine

methane sulfonate. Cutaneous pectoris muscles were dissected bilaterally and bathed in normal

frog Ringer (NFR; in mM: 116 NaCl, 2 KCl, 1.8 $CaCl_2$, 1 $MgCl_2$, 5 HEPES, pH 7.4). The nerve

was cut near its entrance into the muscle, and the cut end was drawn into a Vaseline well

containing 30 mM Calcium Green-1 (3000 MW dextran conjugate; Molecular Probes) dissolved

in distilled water. After 7-8 hours of dye loading at room temperature, the preparation was

rinsed in NFR and stored at 4°C for 2-3 hours. For stimulation and imaging, preparations were

pinned over an elevated Sylgard (Dow Corning) platform in a 35 mm dish mounted on the microscope stage. The nerve was drawn into a suction electrode and stimulation threshold was determined by observation of muscle twitch. Postsynaptic acetylcholine receptors then were blocked and labeled using 2 μg/ml Alexa 594-conjugated α-bungarotoxin (α-BTX) for 10 minutes. α-BTX staining was used to locate and focus the postsynaptic receptor bands, which are directly opposed to the presynaptic active zones, and to evaluate possible z-axis drift over the course of data collection. Superficial nerve terminals were chosen for study, and most lay in a single focal plane as judged by α-BTX staining. Except as noted, all Ca^{2+} imaging was performed in NFR containing 10 μM curare to prevent nerve-evoked muscle contractions not completely blocked by α-BTX.

2.3.2 Calcium imaging and nerve stimulation protocol

Images were collected at 0.5 Hz using a 1 ms laser illumination time. An acousto-optic tunable filter (AOTF; ChromoDynamics, Inc.) was used to select wavelengths and gate the laser with sub-millisecond time resolution (Krypton-Argon laser; Innova 70 Spectrum, Coherent). The laser was fiber-coupled to the epi-illumination port of an upright fluorescence microscope (Olympus BX61WI) equipped with a long working-distance water-immersion objective (100x, 1.0 NA; Lumplan/FL IR, Olympus). Calcium Green-1 was excited at 488 nm and emitted light was collected through a 530 ±20 nm filter. Alexa 594-α-BTX was excited at 567 nm and emitted light collected using a 620 ±30 nm filter. Images were recorded on one of two cooled, back-thinned CCD cameras (LN1300B, Roper Scientific, or Ixon DV887, Andor), which provided the high sensitivity and low noise necessary for 1 ms illumination times. Pixel size was 200 nm (LN1300B) or 160 nm (Ixon DV887). The spatial resolution of the microscope was

estimated using a point spread function measured using 20 nm fluorescent beads (width at half-maximum amplitude = 450 nm; see **Figure 2.1C**). Furthermore, a plot of the cross-correlation analysis of fluorescent signals detected by adjacent pixels revealed a width at half-maximum amplitude of 410 nm (**Figure 2.1D**). Analysis of data from either camera gave similar results.

During acquisition, images were collected in sets of 20. Within each set, the first 10 were obtained without nerve stimulation to obtain resting (background) fluorescence, while each of the second 10 followed nerve stimulation at $5 \times$ threshold to obtain AP-dependent fluorescence. Based on previous studies, we know that a delay of 1.5 ms between stimulation and illumination accounted accurately for nerve conduction delay in this preparation and therefore was used in all imaging experiments (Wachman et al., 2004). In most experiments, 10 sets of trials were performed sequentially to obtain a total of 100 background images interleaved with 100 images following stimulation. Between sets, I confirmed/adjusted focus based on α-BTX staining, and discarded image sets from analysis if they showed noticeable z-axis drift or significant changes in average background fluorescence. In some experiments, the preparation subsequently was exposed to the potassium channel blocker 3,4-diaminopyridine (DAP; 5 μM for 30 minutes), and another 10 sets of images were obtained in the continued presence of DAP. In these acute experiments, DAP treatment prolongs the AP and thus indirectly increases the probability that Ca^{2+} channels open after nerve stimulation while leaving the number of channels unchanged. This differential effect allows subsequent analysis of fluorescence fluctuations across repeated trials to determine the number of Ca^{2+} channels and opening probability on a per pixel basis (see below).

2.3.3 Image registration and analysis

Prior to analysis, each set of images was registered to the first image of the first dataset to correct for slight fluctuations in the x-y (or lateral) position of the preparation during data collection. Registration software was written at the National Resource for Biomedical Supercomputing (www.nrbsc.org) at the Pittsburgh Supercomputing Center. Although the software was capable of generalized rotational and non-linear corrections, virtually all of the adjustments necessary for these experiments were simple interpolated translational movements of one pixel or less. Stimulus-dependent changes in fluorescence intensity were small (typically 3-4% above background, see Results), and so the registration step brought the shape of the nerve terminal into alignment without being confounded by large and variable changes in signal strength within regions of terminals.

Analysis of registered images was performed using MATLab. To create difference images showing stimulus-dependent fluorescence changes (Δf_s) for each pixel, I calculated each pixel's average background fluorescence ($\overline{f_b}$), subtracted it from the fluorescence (f_s) obtained after a stimulation trial, and then normalized the resulting differences to $\overline{f_b}$, i. e., per pixel $\Delta f_s = \frac{f_s - \overline{f_b}}{\overline{f_b}}$. Resulting difference images were displayed in pseudocolor.

For each pixel, I also calculated the background variance (σ_b^2), the mean fluorescence ($\overline{f_s}$) and variance (σ_s^2) after nerve stimulation, and the mean fluorescence ($\overline{f_{Ds}}$) and variance (σ_{Ds}^2) after stimulation combined with DAP treatment. Within image sets from individual terminals, the variance of background fluorescence arises from dark noise and photon shot noise, and under our experimental conditions was dominated by Gaussian shot noise. On the other hand, background photoelectron counts from different visualized terminals varied according to

differences in geometry and dye loading, and ranged from 1500 to 6000 per pixel.

2.3.4 Determination of *n* and *p*

Over the course of repeated stimulation trials, the mean fluorescence intensity $\bar{f}_s$ is expected to

exceed the mean background level $\bar{f}_b$ for pixels that overlie a sub-region of an active zone and

periodically detect Ca^{2+} influx through one or more open Ca^{2+} channels. The mean of the

stimulus-dependent fluorescence signals before and after DAP treatment are:

$$\Delta F_s = \frac{\bar{f}_s - \bar{f}_b}{\bar{f}_b} \times 100\% \qquad (1a)$$

$$\Delta F_{Ds} = \frac{\bar{f}_{Ds} - \bar{f}_b}{\bar{f}_b} \times 100\% \qquad (1b)$$

Note that I used Δf_s and ΔF_s to represent the single trial and the mean of the stimulus-

dependent fluorescence signals, *i.e.*, for a particular pixel ΔF_s equals to the average of 100-trial

Δf_s. I limited the subsequent analysis to those pixels within AZ regions that reported significant

AP-evoked fluorescence signals under control conditions by using the criterion that the mean

fluorescence after stimulus should be at least $1 \times \sigma_b$ above the mean background fluorescence

intensity. I demonstrated that the choice of selection criterion had little or no effect on the

estimates of the number of Ca^{2+} channels and their opening probability by comparing results

using this criterion with a Student's t-test employing different levels of significance (see Table 1

and **Figure 2.6**).

For individual pixels that sample active zone regions of the nerve terminal, I defined that

the number of Ca^{2+} channels that can be detected by a particular pixel is n and each Ca^{2+} channel

open independently with the same probability p during an AP. I calculated n and p for selected

pixels using the ratio method (see below and Sabatini and Svoboda, 2000). I defined R_F as the

ratio of stimulus-dependent fluorescence signals before and after DAP treatment:

$$R_F = \frac{\Delta F_s}{\Delta F_{Ds}} \tag{1c}$$

Similarly, the coefficient of variation in the stimulus-dependent fluorescence signals before and after DAP treatment are:

$$CV_s = \frac{\sqrt{\sigma_s^2 - \sigma_b^2}}{\bar{f}_s - \bar{f}_b} \tag{2a}$$

$$CV_{Ds} = \frac{\sqrt{\sigma_{Ds}^2 - \sigma_b^2}}{\bar{f}_{Ds} - \bar{f}_b} \tag{2b}$$

R_{CV} is defined as:

$$R_{CV} = CV_s^2 \Big/ CV_{Ds}^2 = \frac{\sigma_s^2 - \sigma_b^2}{(\bar{f}_s - \bar{f}_b)^2} \Big/ \frac{\sigma_{Ds}^2 - \sigma_b^2}{(\bar{f}_{Ds} - \bar{f}_b)^2} \tag{2c}$$

To calculate n and p from the experimental R_F (Eq. 1c) and R_{CV} (Eq. 2c) values, I assume that each Ca^{2+} channel acts independently and opens during an AP with probability (p) before DAP treatment and (p_D) after DAP treatment. The corresponding probabilities of remaining closed are $(1 - p)$ and $(1 - p_D)$, respectively. Under each condition, the number of channels that open from trial to trial is expected to follow a binomial distribution. From standard binomial theory, individual pixels that sample active zone regions containing n Ca^{2+} channels, the average number of channels that will open (μ) before DAP treatment is given by:

$$\mu = n \times p \tag{3}$$

Assuming a linear detection system (see results), the mean fluorescence arising from Ca^{2+} entering through open channels (ΔF_s, Eq. 1a) will be proportional to μ, thus

$$\Delta F_s \propto \mu = n \times p \tag{4}$$

Similarly, after DAP treatment, the mean fluorescence arising from entering Ca^{2+} (ΔF_{Ds}, Eq. 1b) will be proportional to the average number that will open (μ_D) after DAP treatment:

$$\Delta F_{Ds} \propto \mu_D = n \times p_D \qquad (5)$$

Since it is assumed that Ca^{2+} channels are distributed regularly in a linear array, the distances between a given pixel and different Ca^{2+} channels may differ significantly. Therefore, Ca^{2+} channels locating at various distances from a given pixel may contribute different amounts of Ca^{2+} ions, which produce an additional variability beyond the fluctuation of single Ca^{2+} channel current (see below). We know Ca^{2+} ions can move very rapidly in the solution (diffusion coefficient 220 μm^2/sec; Albritton et al., 1992). However, the presence of Ca^{2+} buffers restricted the free diffusion of Ca^{2+} ions inside the terminal. The apparent diffusion distance of free Ca^{2+} ions depends on the diffusion coefficient of Ca^{2+}, the concentration and forward binding rate constants of diffusible, unbound buffer(s) (Neher, 1998b). It has been predicted that the peak Ca^{2+} concentration attenuates steeply within tens of nm with increasing distance from the open channel (Neher, 1998a). Because of the lack of knowledge of the real distribution of Ca^{2+} channels and detail information on the concentration and properties of Ca^{2+} buffers within the frog motor nerve terminal, in the present thesis, I was unable to estimate the magnitude of this variability caused by Ca^{2+} channels distribution. However, based on the experimental data that increasing extracellular Ca^{2+} concentration only increased the magnitude of Ca^{2+}-dependent fluorescence signals without changing the coefficient of variation of the fluorescence signal, I argued that various distances between a given pixel and different Ca^{2+} channels may have little, if any, significant effect on the single pixel optical fluctuation analysis (see discussion in Chapter 2). Therefore, the mean stimulus-dependent fluorescence signals

before and after DAP treatment appears to be governed primarily by the number of Ca^{2+} channels opened by an AP.

From Eqs. (1c), (5), and (6), I now have:

$$R_F = \frac{\Delta F_s}{\Delta F_{Ds}} = \frac{n \times p}{n \times p_D} = \frac{p}{p_D} \tag{6}$$

where I assume that DAP treatment does not affect the number of functional Ca^{2+} channels n as well as the amount of Ca^{2+} flux through single open channels (see results).

Again from standard binomial theory, the predicted variance for the number of open channels before DAP treatment (σ^2) is:

$$\sigma^2 = n \times p \times (1 - p) \tag{7}$$

The standard deviation (σ) is thus:

$$\sigma = \sqrt{n \times p \times (1 - p)} \tag{8}$$

Using Eqs. (3) and (8), the coefficient of variation in the number of open channels is:

$$CV_{open} = \frac{\sigma}{\mu} = \sqrt{\frac{1-p}{n \times p}} \tag{9a}$$

$$CV_{open}^2 = \frac{1-p}{n \times p} \tag{9b}$$

If all of the variance in measured stimulus-dependent fluorescence arises from the random openings of channels from trial to trial, then from Eqs. (2a) and (7):

$$(\sigma_s^2 - \sigma_b^2) \propto \sigma^2 = n \times p \times (1 - p) \tag{10}$$

and from Eqs. (2a) and (9b):

$$CV_s^2 \propto CV_{open}^2 = \frac{1-p}{n \times p} \tag{11}$$

Similarly, after DAP treatment:

$$CV_{Ds}^2 \propto \frac{1-p_D}{n \times p_D} \tag{12}$$

Therefore, from Eqs. (2c), (11), and (12), we have:

$$R_{CV} \equiv CV_s^2 \Big/ CV_{Ds}^2 = \frac{1-p}{n \times p} \Big/ \frac{1-p_D}{n \times p_D} = \frac{\frac{1-p}{p}}{\frac{1-p_D}{p_D}} \tag{13}$$

where again I assume that DAP treatment does not affect the number of functional Ca^{2+} channels n as well as the amount of Ca^{2+} flux through single open channels.

In Eqs. (6) and (13) we have the two measured ratios R_F and R_{CV}, as well as the two unknown probabilities p and p_D. Rearranging Eq. (6) for (p_D) yields:

$$p_D = \frac{p}{R_F} \tag{14}$$

After using Eq. (14) to substitute for p_D in Eq. (13), algebraic rearrangement now provides an expression for p that includes only the measured ratios R_F and R_{CV}:

$$p = \frac{R_{CV} \times R_F - 1}{R_{CV} - 1} \tag{15}$$

Eq. (15) was therefore used to calculate p and Eq. (14) was used to calculate p_D. Finally, a rearranged form of Eq. (11) was used to estimate n:

$$n = \frac{1-p}{p \times CV_s^2} \tag{16}$$

2.4   RESULTS

2.4.1   Trial-to-trial variability of AP-evoked calcium influx at presynaptic active zones

The adult frog motor nerve terminal consists of hundreds of linear active zones at a regularly spaced interval of ~1 µm. A single active zone is about 1 µm long and contains a linear array of

~200-250 intramembraneous particles arranged in parallel double rows which include voltage-gated Ca^{2+} channels. These morphological features allow imaging of presynaptic Ca^{2+} entry within a single active zone (**Figure 2.1A** and **2.1B**). For Ca^{2+} imaging, I loaded the frog motor nerve terminals with Calcium Green-1dexdran (3000 MW, K_D of ~540 nM). I identified well-focused active zones by labeling postsynaptic acetylcholine receptors with Alexa 594-conjugated α-bungarotoxin (**Figure 2.1E**). I imaged AP-evoked Ca^{2+} signals within active zone regions during low frequency nerve stimulation (0.5 Hz), which were quantified using a measure of relative fluorescent change (see experimental procedures). To estimate the resolution of our imaging system, I measured the point spread function (PSF) of the optical system using 20 nm fluorescent beads (full width at half-maximum amplitude = 450 nm; **Figure 2.1C**). As expected, the cross-correlation of Ca^{2+}-evoked fluorescent signals detected by adjacent pixels (half width = 410 nm; **Figure 2.1D**) was mainly determined by the PSF. As a result of these measurements, in comparison with the average length of a single active zone (~1 μm), I estimated that each pixel in our imaging system samples about one half of an active zone.

Following repeated stimulation, I observed a large trial-to-trial variability in stimulus-evoked Ca^{2+} signals (**Figure 2.1F**). It has been previously shown that AP-evoked Ca^{2+} signals imaged in this manner arise exclusively from Ca^{2+} entry through N-type Ca^{2+} channels, with no contribution from Ca^{2+}-induced Ca^{2+} release, and are restricted to active zone regions of the nerve terminals (Wachman et al., 2004). To quantitatively characterize this variability, I chose imaging pixels for variance analysis using an SD criterion that the mean fluorescence after stimulus should be at least 1 σ_b above the average background fluorescence (i.e. $\bar{f}_s > \bar{f}_b + \sigma_b$; see **Figure 2.2E** and methods for details). The pixels selected by this criterion reported significant AP-evoked fluorescence signals and were restricted to active zone regions of nerve

A Axon, Nerve terminal, Postsynaptic ACh receptor clusters, Muscle cell

B pixels, Docked vesicles, Estimated optical resolution, Active zone proteins, ΔF_s (%)

C normalized fluorescence vs distance (μm)

D correlation coefficient vs distance (μm)

E

F Δf_s (%)
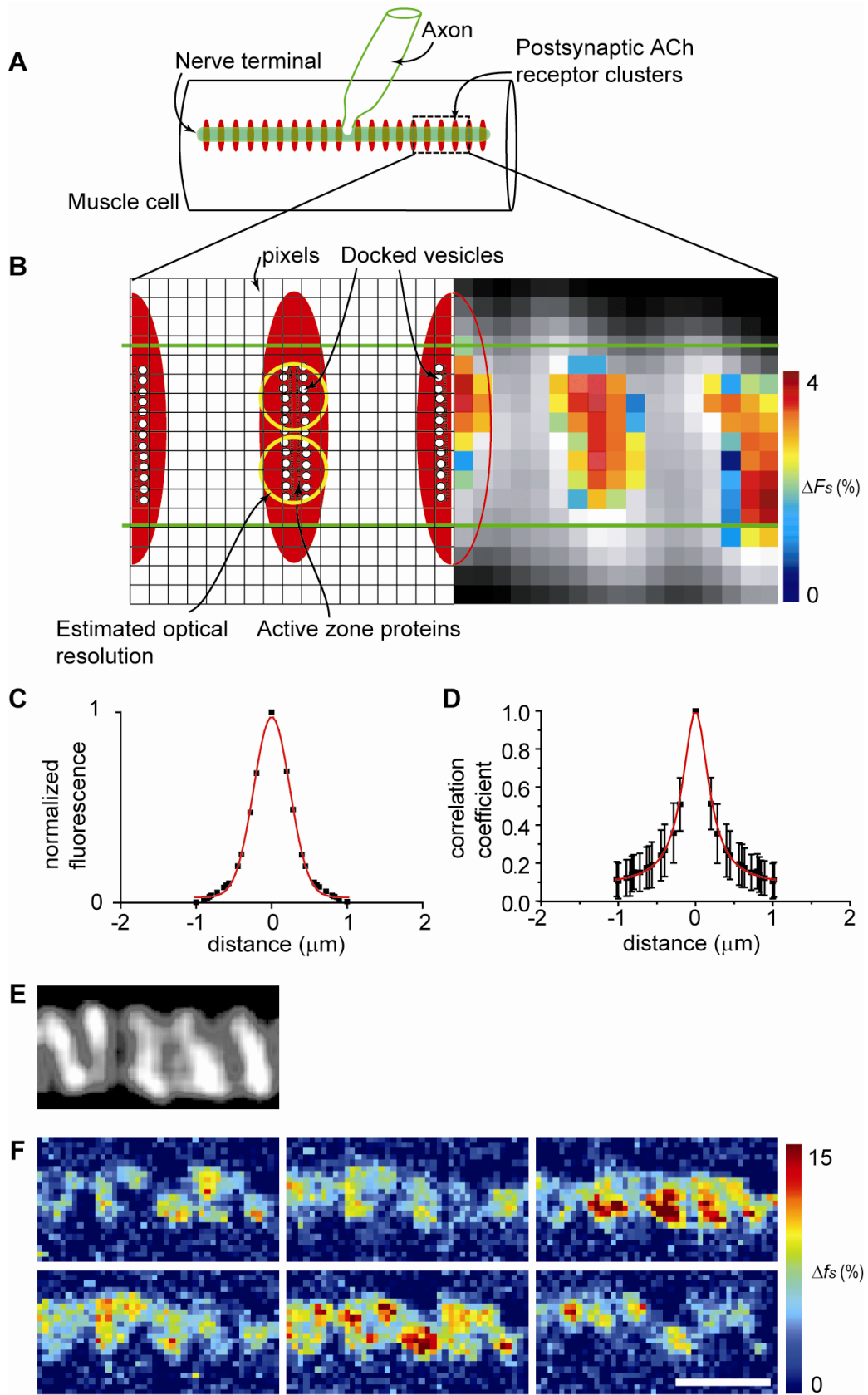
Figure 2.1 Calcium imaging in the adult frog neuromuscular junction

(A) Diagram of a single nerve terminal at an adult frog neuromuscular junction. Active zones within the nerve terminal (green) overlie regularly spaced clusters of postsynaptic acetylcholine receptors (red).

(B) Magnified active zones (boxed region in A) with highly-organized active zone proteins, which include voltage-gated Ca^{2+} channels, and docked synaptic vesicles. The estimated relationship between active zone dimensions, pixel size, and optical resolution are also shown (Left). For comparison, a composite image that includes fluorescent staining of postsynaptic acetylcholine receptors (background, grayscale) overlaid with Ca^{2+}-evoked fluorescent signals after nerve stimulation (foreground, false color) is shown on the right half of this panel. For clarity, only the edge of nerve terminal is illustrated (green line).

(C) Experimentally measured point spread function of the optical system from a fluorescent bead with diameter of 0.02 μm. The Gaussian fit (red) has a width at half-amplitude of 0.45 μm. I thus estimated that about half the length of a single active zone can be resolved optically.

(D) Correlation coefficient of neighboring pixels that detected AP-evoked fluorescence signals following repeated low-frequency nerve stimulus tightly depends on the distance between pixels. The Lorentzian fit (red) has a width at half amplitude of 0.41 μm. The residual correlation coefficient between pixels with long distance may be caused by the presence of several Ca^{2+} entry sources when multiple Ca^{2+} channels open by an AP.

(E) Predicted active zone regions of a representative frog motor nerve terminal identified by labeling the postsynaptic acetylcholine receptor clusters with Alexa 594-α-bungarotoxin.

(F) Representative difference images showed a large trial-to-trial variability in the spatial distribution of calcium entry evoked by single APs. Scale bar = 2 μm.

A BTX

B resting $(\overline{f_b})$

C stimulated $(\overline{f_s})$

D Diff ΔF_s (%)

E SD criterion $(\overline{f_s} > \overline{f_b} + \sigma_b)$

Mask

F # CV$_s$
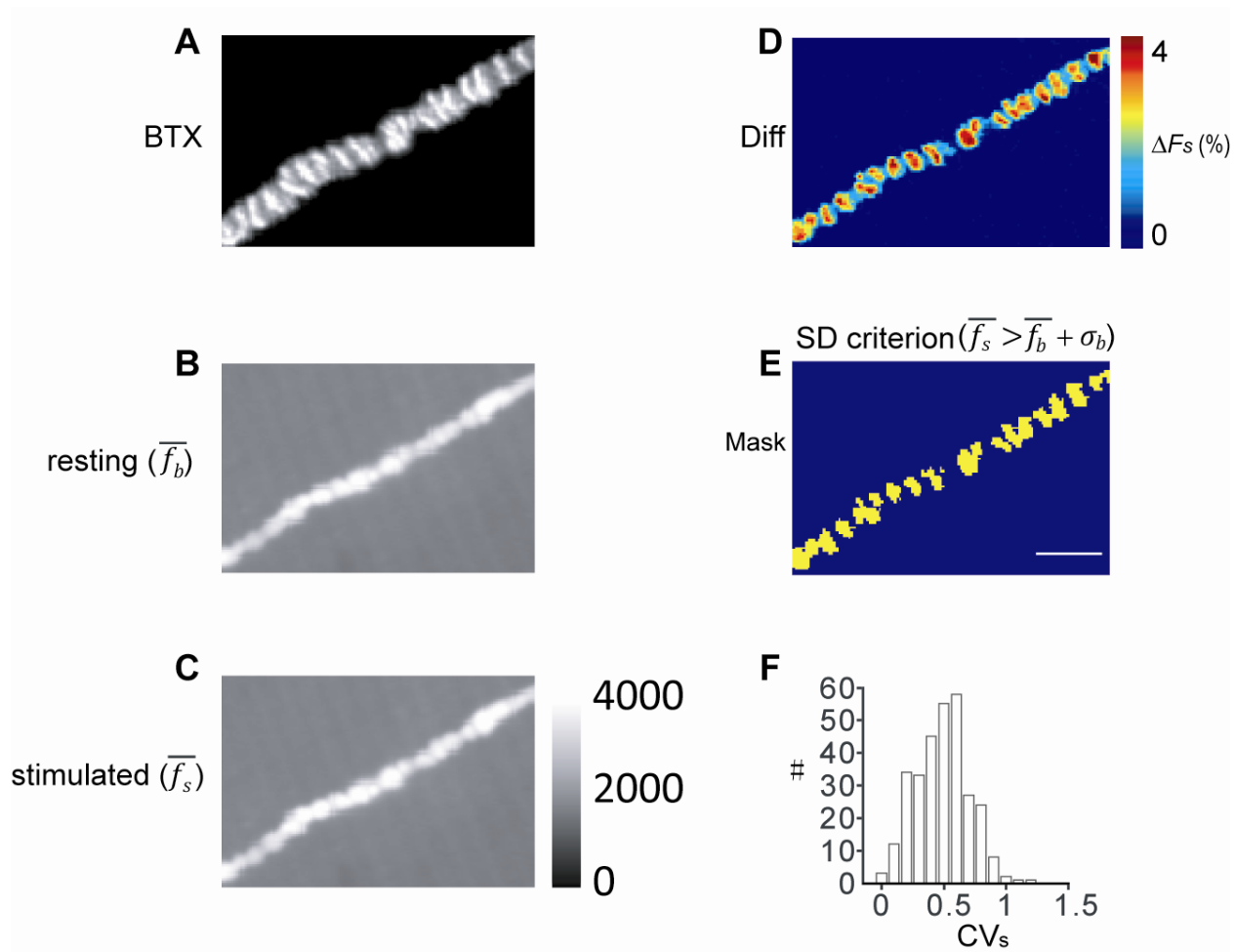
Figure 2.2 Method used to define active zone regions of the nerve terminal within which action potential-evoked Ca^{2+} influx is restricted

(A) Postsynaptic acetylcholine receptor distribution determined using Alexa 594-conjugated α-bungarotoxin (BTX).

(B) Resting fluorescence image of a frog motor nerve terminal averaged over 100 trials.

(C) Fluorescence image of the nerve terminal following a single AP stimulation averaged over 100 trials. Note the similarity between (B) and (C), which is primarily caused by the small increase in fluorescence intensity after nerve stimulation (ΔF_s is typically 5-10%, see D).

(D) Average (100 trials) Ca^{2+} influx within active zone regions of the nerve terminal evoked by a single AP. The pattern of Ca^{2+} influx averaged over 100 stimulus trials decorates nerve terminals with fluorescence signals that can visually identify active zone regions.

(E) Masking the active zone regions with the criterion that pixels have a mean stimulated fluorescence intensity exceeding $1 \times SD$ above resting fluorescence. Scale bar: 5 μm.

(F) Histogram distribution of CV_s over 100 stimulus trials for selected pixels using the criterion shown in (E).

terminals (see **Figure 2.2**). The coefficient of variation (CV_s) of stimulus dependent fluorescent signals for the pixels examined at a representative nerve terminal had a median value of 0.54 (**Figure 2.2F**). Similar CV_s were obtained from a total of 7 nerve terminals with a mean 0.51 ± 0.07 (range 0.41 to 0.62). I hypothesized that the large variability in AP-evoked Ca^{2+} signals was caused by a low probability of opening of a small number of Ca^{2+} channels within single active zones.

2.4.2 Ca^{2+} channels open with low probability during an AP at presynaptic active zones

In our system, I estimated that individual pixels sample about one half of an active zone region (see **Figure 2.1**). Assuming this sub-active zone region contains n Ca^{2+} channels that open independently with an average probability p during an AP, the number of open channels per trial follows a simple binomial distribution with mean ($\mu = n \times p$), variance $\sigma^2 = (1 - p) \times n \times p$, and coefficient of variation ($CV = \sqrt{(1 - p)/(n \times p)}$). The magnitude of the AP-evoked Ca^{2+} signal (measured by ΔF_s) is governed by the average number of open channels while the coefficient of variation in the measured Ca^{2+} signal (CV_s) is typically dominated by the fluctuations in the number of channels that open (but see below in results and discussion). The distribution of stimulus-dependent fluorescence signals detected by a single pixel across multiple trials therefore should follow a binomial distribution which is governed by both n and p. Figure 2.3 shows representative histogram distributions of resting fluorescence intensities and fluorescence intensities after stimulus, normalized to the mean resting fluorescence. Although it is clear that stimulus-dependent fluorescence signals were significantly above the fluctuation of resting fluorescence, the overlapping distributions of resting fluorescence and stimulated

fluorescence signals led to difficulty of identifying which trials failed to open any calcium channels. The relatively short (1 ms) exposure time and relatively small increase in Ca^{2+}-dependent fluorescence of calcium green 1-dextran may primarily limit our ability to estimate the failure rate. As can be seen in Figure 2.3 (D-F), at terminals treated with high concentration ω-conotoxin GVIA (600 nM), which blocked over 90% of available calcium channels, the stimulus-dependent fluorescence intensities were relatively low, as compared to the fluctuation of resting fluorescence. In all cases, it is impossible to use the direct method which relies on the CV and failure rate to estimate the n and p (see Sabatini and Svoboda, 2000).

I therefore turned to the ratio method (see method section **2.3.4**). Theoretically, increasing the probability of channel opening is expected to increase ΔF_s while decreasing CV_s in the measured Ca^{2+} signal. Using the ratios of ΔF_s and CV_s during such a manipulation, the probability that Ca^{2+} channels open during an AP (p) can be extracted (see methods). To experimentally manipulate Ca^{2+} channel opening probability, I treated the frog NMJ with 5 μM 3,4-diaminopyridine (DAP) for 30 minutes. DAP is known to block selectively potassium channels, and as a result, broaden the presynaptic AP (Bostock et al., 1981; Thomsen and Wilson, 1983; Augustine, 1990). This is predicted to increase the probability of opening of Ca^{2+} channels following an AP (Augustine, 1990; **Figure 2.7**). For these acute experiments, I assumed DAP treatment caused no change in the total number of functional Ca^{2+} channels within the active zone. Figure 2.4 shows an example of calcium imaging data from the same terminal before (**Figure 2.4A**) and after DAP exposure (**Figure 2.4B**). As compared to control, DAP exposure strongly increased the magnitude of single AP-evoked fluorescence signals, and decreased the coefficient of variation of these signals (**Figure 2.4C** and **D**, respectively), consistent with the expected increase in opening probability of Ca^{2+} channels. For individual
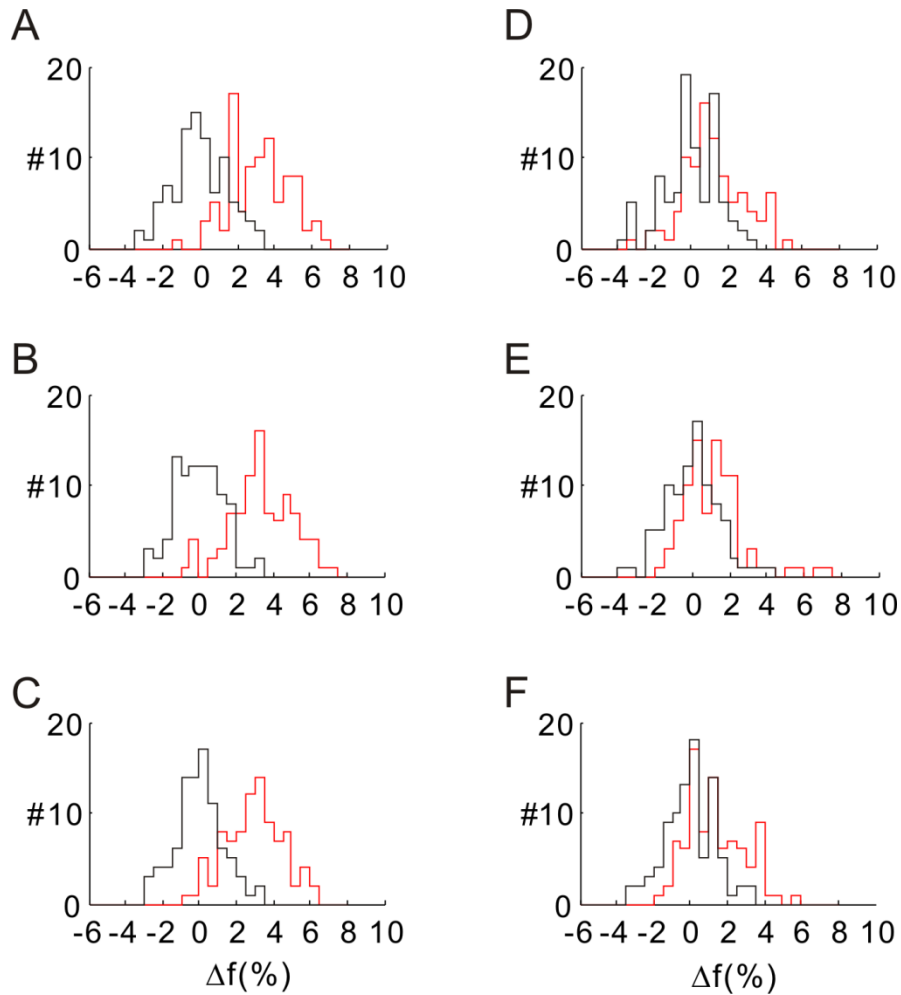
Figure 2.3 The histogram distribution of normalized fluorescence intensities detected by individual pixels before and after stimulation.

(A-C) The distribution of resting fluorescence intensities (black) and stimulus-dependent fluorescence intensities (red) of three representative pixels that sample active zone regions in a control nerve terminal.

(D-F) The distribution of resting fluorescence intensities (black) and stimulus-dependent fluorescence intensities (red) of three representative pixels that sample active zone regions in a 600 nM CgTX-treated nerve terminal.

45

pixels selected using the criterion described above, the stimulus dependent CV_s and F_s were measured and used to calculate the p value in both control and DAP-treated conditions (see method). Since a small fraction of selected pixels reported a p value that is smaller than 0 or larger than 1, which is physiologically meaningless, those pixels were also excluded in our determination of n and p (see **Figure 2.6** below). **Figure 2.4E** shows the distribution of Ca^{2+} channel opening probability for the representative terminal under control conditions. Because these values were not normally distributed, I used the median value ($p = 0.22$) to represent my estimate of the average opening probability of Ca^{2+} channels at this terminal. This value was increased to 0.72 after exposure to DAP. Similar results were obtained from four nerve terminals from which I pooled all the data from individual pixels and generated a histogram distribution of opening probability of Ca^{2+} channels under control conditions (**Figure 2.4F**). As described for the representative nerve terminal above, I used the median value of this distribution ($p = 0.24$) as my estimate of the probability of opening for Ca^{2+} channels at frog NMJ active zones, which was applied for my subsequent data analysis described below.

My variance analysis approach depends on a linear relationship between ΔF_s and $\Delta[Ca^{2+}]$. To confirm this, I varied extracellular calcium and measured changes in signal detected. After doubling the extracellular Ca^{2+} concentration from 1.8 mM to 3.6 mM (which enhances Ca^{2+} influx per open channel) the Ca^{2+} signal detected within active zone regions of the nerve terminal increased by $102 \pm 2\%$ (n = 4 terminals). However, the CV_s of stimulus-dependent fluorescence signals in high extracellular Ca^{2+} was not significantly different from that measured in normal extracellular calcium (P > 0.05, one-way ANOVA with Tukey's post hoc test; see **Figure 2.5**). This doubling in Ca^{2+} signal, coupled with an unchanged CV_s supports the conclusion that the reduced CV_s measured following exposure to DAP was indeed caused by an increase in opening

probability of Ca^{2+} channels, and not by a potential saturation of measured fluorescence signals. In this analysis, it is clear that the concentration of extracellular Ca^{2+} (and thus the magnitude of Ca^{2+} influx through open channels) does not alter my quantitative analysis of variability in presynaptic fluorescence signals. Therefore, this experiment also serves as a control for the validity of my method of variance analysis since CV_s (and thus estimated p and n values) does not change as extracellular Ca^{2+} is varied.

A lack of significant dye saturation during low frequency stimulation might be expected given the ordered geometry of adult frog NMJ active zones (long, linear arrays of presynaptic Ca^{2+} channels distributed spatially at some distance from one another; see **Figure 2.1**), combined with the prediction that there are few Ca^{2+} channel openings within each active zone during a single AP (Wachman et al., 2004). Therefore, a single pixel that is positioned to detect Ca^{2+} signals from some number of well distributed sources will be able to detect linear change in signals that are dependent on the number of open Ca^{2+} channels. The absence of significant dye saturation under similar imaging conditions at this synapse was also reported by Shahrezaei et al. (2006).

2.4.3   The number/density of Ca^{2+} channels within presynaptic active zones

Individual active zones of the adult frog motor nerve terminal are tightly organized into a linear array of ~200-250 intramembraneous particles arranged in parallel double rows which are associated with ~25-40 docked synaptic vesicles (Heuser et al., 1979; Pawson et al., 1998; Rizzoli and Betz, 2005; see **Figure 2.1A**). Previous studies have led to the hypothesis that these intramembraneous particles include the presynaptic Ca^{2+} channels that trigger vesicle fusion (Pumplin et al., 1981; Robitaille et al., 1990; Cohen et al., 1991). Considering the existence of

47
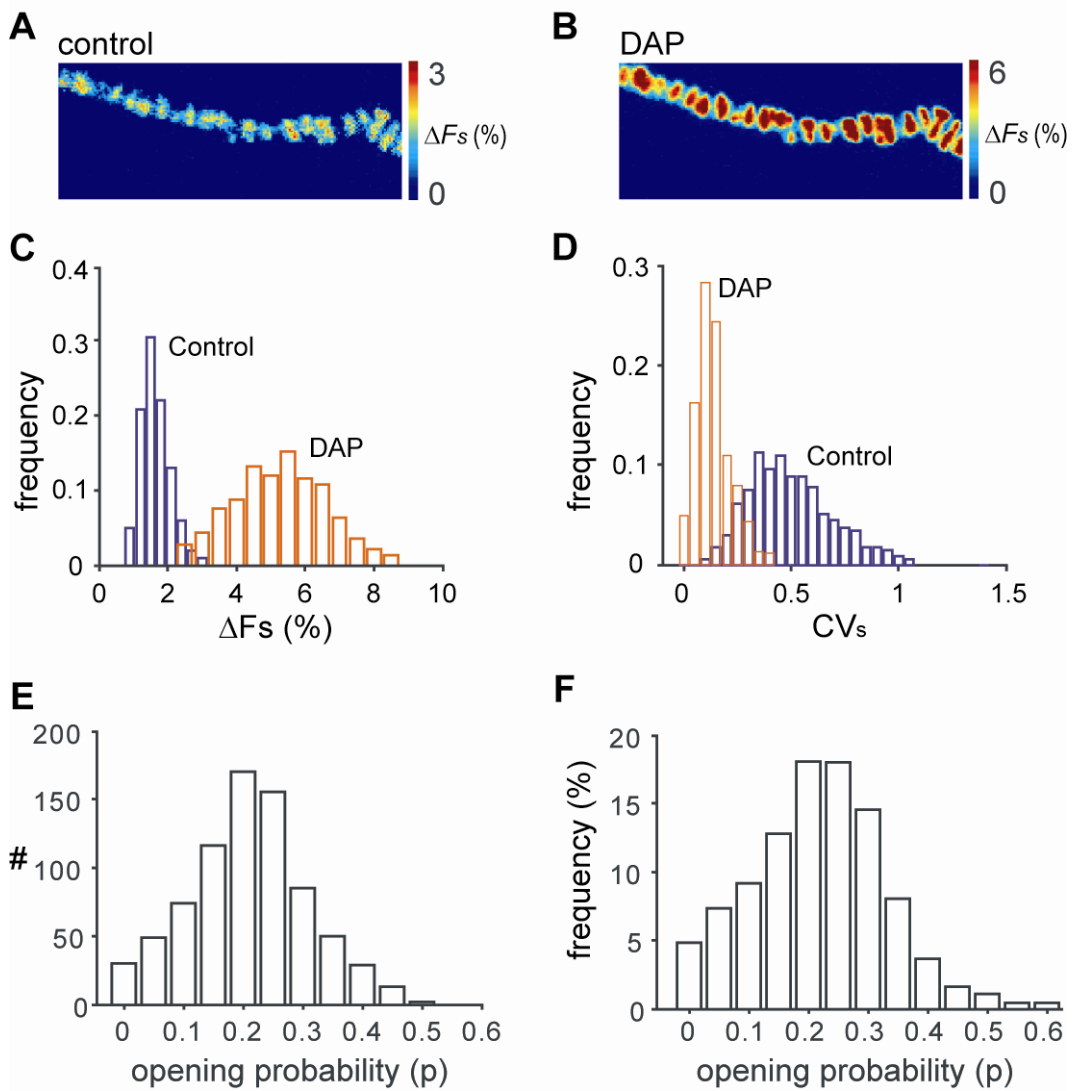
Figure 2.4 Opening probability of Ca^{2+} channels during an action potential

(A) Averaged 100-trial single AP-evoked Ca^{2+} influx under control condition.

(B) Averaged 100-trial single AP-evoked Ca^{2+} influx after 5 μM 3,4-diaminopyridine treatment.

Scale bar: 5 μm.

(C) Histogram distribution of the fluorescence intensity reported by individual pixels before

(blue) and after drug treatment (red).

(D) Histogram distribution of the coefficient of variation of individual pixels before (blue) and

after drug treatment (red).

(E) Histogram distribution of opening probability of Ca^{2+} channels during an action potential for

the example terminal shown in (A and B) .

(F) Histogram distribution of the average opening probability of Ca^{2+} channels during an action

potential reported by individual pixels pooled from a total of 4 nerve terminals.

Ca^{2+}-activated potassium channels (Robitaille et al., 1993) and core release machinery proteins that are also known to be selectively expressed in the active zone, it is reasonable to expect that only some of the large intramembraneous particles observed in freeze fracture replicas are voltage-gated Ca^{2+} channels.

Using the p value for presynaptic Ca^{2+} channels derived above, and the measured CV_s, I can calculate the number of Ca^{2+} channels within sub-active zone regions sampled by individual pixels (see equation 16 in method). I first estimated n at the nerve terminals treated with DAP. For each terminal, the median p and CV_s of all selected pixels was used to calculate the average n. I found that the average n ranged from 13 to 21 with mean (17.1 $\pm$ 3.6) for all four nerve terminals examined.

Next I analyzed untreated control nerve terminals. As previously shown in Figure 2.2F, the pixels selected from these untreated terminals reported a relatively large CV_s (mean: 0.51 $\pm$ 0.07; range: 0.41-0.62). Because I did not have an independent determination of p for each of these untreated nerve terminals, I used the p value determined above (0.24), in combination with the median CV_s value from each terminal to calculate the average n. For all 7 untreated terminals examined in this manner, I found that n averaged 12.8 $\pm$ 3.8 (range 8 to 19), which was not significantly different than the number reported using the DAP experimental data (17.1 $\pm$ 3.6; unpaired student t-test, P = 0.1). Therefore, when I pooled all the data from eleven nerve terminals examined in this manner, the average number of Ca^{2+} channels within sub-active zone regions sampled by individual pixels was 14.3 $\pm$ 4.2. Considering the resolution of our imaging system (see **Figure 2.1**), I predict that an entire active zone has only about 28 voltage-gated Ca^{2+} channels distributed among the ~200-250 intramembraneous particles described in freeze

fracture replicas of the active zone. So, I conclude that the adult frog NMJ active zones have a relatively small number of presynaptic Ca^{2+} channels.

Finally, as a test for the validity of my analysis approach, I also examined the effects of exposure to a sub-maximal concentration of ω-conotoxin GVIA (CgTX; 100 nM). This treatment is known to completely and irreversibly block (over the course of our experiments) a subset of N-type Ca^{2+} channels without affecting the probability of opening for channels that remain unblocked (Kerr and Yoshikami, 1984; Stocker et al., 1997). An exposure to 100 nM CgTX blocked total Ca^{2+} entry evoked by an AP by 70 ± 5.9 % (mean $\pm$ SD, 5 nerve terminals). As a result, the stimulus-dependent fluorescence signals were very weak, and only the Student's t-test method could be applied to select pixels for variance analysis (see **Figure 2.6** and Table 1). Using a Student's t-test to select active zone pixels ($P < 0.01$; see **Figure 2.5** and Table 1), the average CV_s after CgTX treatment increased significantly above control to a value of 0.77 ± 0.12 (one-way ANOVA with Tukey's post hoc test, $P < 0.05$; mean $\pm$ SD, 5 nerve terminals). Using the estimated p (0.24) determined above and the CV_s from CgTX treated nerve terminals, the average ($n = 5.7 \pm 2.0$) was significantly decreased as compared with control (one-way ANOVA with Tukey's post hoc test, $P < 0.01$). This decrease in n is consistent with the expected effects of CgTX. Therefore, my method of variance analysis is sensitive to treatments known to alter either p (DAP) or n (CgTX), as the measured CV_s values vary as expected (see **Figure 2.5**).
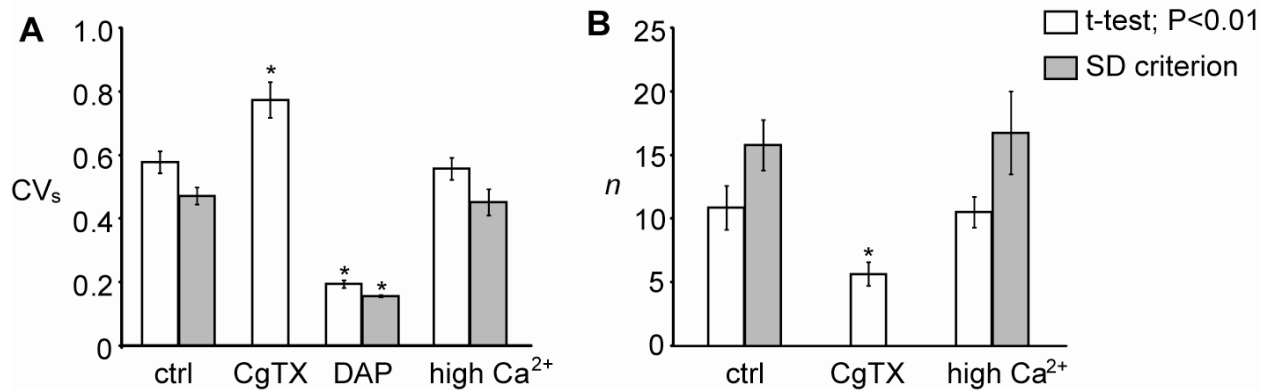
Figure 2.5 Summary data for measured CV values and calculated n values under different treatment conditions

(A) Calculated CV values (mean + SEM) for pixels sampling active zone regions of control nerve terminals (ctrl), those exposed to 100 nM ω-conotoxin GVIA (CgTX), 5 μM 3,4-diaminopyrindine (DAP), or elevated extracellular calcium (3.6 mM; high Ca^{2+}).

(B) Calculated number of Ca^{2+} channels (n) sampled by active zone pixels (mean + SEM) under control conditions (ctrl), after exposure to 100 nM ω-conotoxin GVIA (CgTX), and after increasing extracellular calcium to 3.6 mM (high Ca^{2+}).

In both (A) and (B), open bars represent values calculated after using a student's t-test (P < 0.01) to select active zone pixels that detect a significant stimulus-dependent signal, and shaded bars represent values calculated using the criterion that the stimulus-dependent signal be at least one standard deviation above resting levels (see experimental procedures). For the CgTX treatment condition, signal intensity was so weak that only the student's t-test method for selecting pixels resulted in identifying a significant number of pixels for analysis.

* Significantly different from control, one-way ANOVA with Tukey's post hoc test, P < 0.05.

2.4.4 Impact of pixel selection criteria on the estimates for *n* and *p*

To control for the impact of my pixel selection method on the variance analysis, I compared the results described above with those obtained after using a Student's t-test to choose pixels that detected significant AP-evoked fluorescence signals above rest ($\Delta F_s > 0$, at various significance levels; $P < 0.01$, 10^{-3}, 10^{-6} or 10^{-9}). As shown in **Figure 2.6** and Table 1, the t-test method selects different numbers of pixels for analysis depending on the significance level chosen (P value). I found that unless the t-test P values used for significance testing were very stringent (10^{-6} or 10^{-9}), this approach selected pixels for analysis that were outside of active zone regions of the nerve terminal. Even under these conditions however, my estimates for *p* did not change (see Table 1). Because the ratio method used to estimate the opening probability of Ca^{2+} channels during an AP was very robust and little influenced by the pixel selection criterion, I am

pixel selection criteria	Selected pixels	*p*	CV_s	*n*
Student's t-test, $P < 10^{-2}$	3079	0.26 ± 0.11	0.51 ± 0.12	9.7 ± 1.6
Student's t-test, $P < 10^{-3}$	2674	0.26 ± 0.11	0.48 ± 0.12	11.2 ± 1.5
Student's t-test, $P < 10^{-6}$	2260	0.25 ± 0.10	0.43 ± 0.07	12.8 ± 2.2
SD criterion	2005	0.24 ± 0.11	0.41 ± 0.07	17.1 ± 3.6

Table 1: Pixel selection criteria and their impact on my estimates for *n* and *p* based on DAP-treated nerve terminals (values represent mean $\pm$ standard deviation, total 4 terminals). Note the number of selected pixels is for the representative nerve terminal as shown in **Figure 2.6**.

confident that my estimate of the probability of opening of Ca^{2+} channels during an AP represents an unbiased evaluation. However, when non-active zone pixels were selected using less-stringent criteria, my calculation of n was moderately underestimated (Table1). It appears that pixels satisfying more stringent criteria tend to overlie the center region of an active zone (**Figure 2.6**) and have lower CV values, which is consistent with the idea that these pixels may detect more Ca^{2+} channels than pixels overlying the edge of an active zone.

2.4.5 Evaluating the effect of fluctuation in single Ca^{2+} channel current on the estimate for n

For simplicity, I have used the measured coefficient of variation in stimulus-dependent fluorescence signals to estimate the number of Ca^{2+} channels within sub-active zone regions of frog motor nerve terminals. But in reality, the variability in stimulus-dependent fluorescence signals is contributed by two sources: 1) variability in the number of channels that open during an action potential, which is governed by the binomial distribution, and 2) variability in the amount of Ca^{2+} flux through an open channel. The Ca^{2+} flux through an open channel varies according to differences in open time and the latency of opening during a complex AP waveform (due to dynamic changes in the driving force at different time points during an action potential waveform).

In order to evaluate the contribution of variability in single channel current to the total variability of action potential-evoked Ca^{2+} signals, I have used Monte Carlo stochastic simulations of modeled single Ca^{2+} channel gating and influx (Stiles et al., 1996; Stiles et al., 2001). Our kinetic model of the N-type voltage-gated Ca^{2+} channel contained 3 closed and a single open state connected by time dependent rates. AP-driven Ca^{2+} flux rates were modeled

54

A

SD criterion

P < 10^{-2}

P < 10^{-3}

P < 10^{-6}

P < 10^{-9}

B

C

D BTX

E

pixels

10^{-2} 10^{-3} 10^{-6} 10^{-9} SD criterion

t-test P values

55
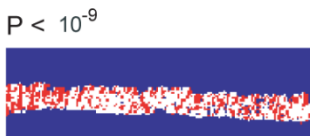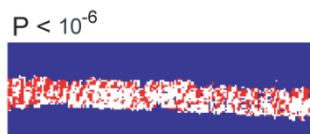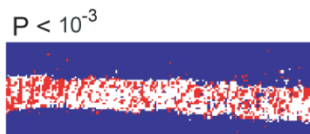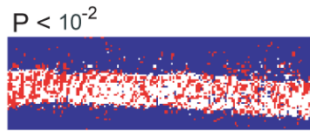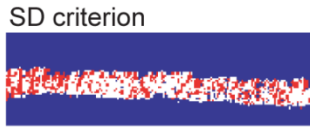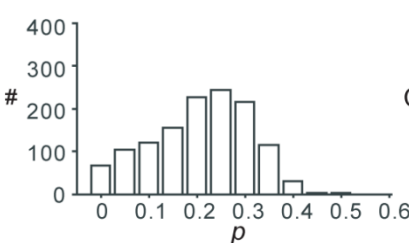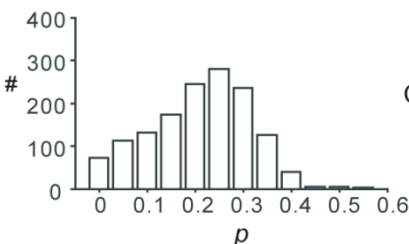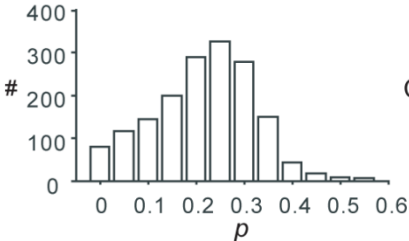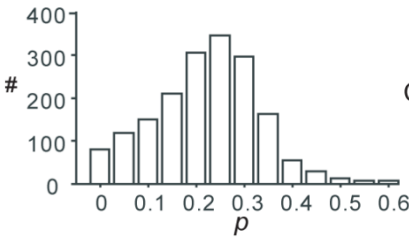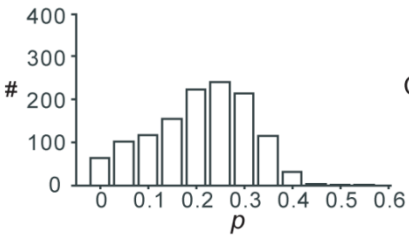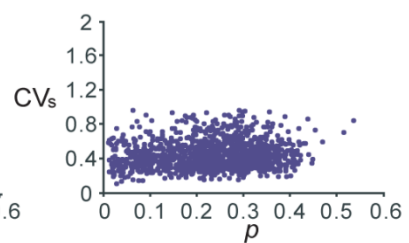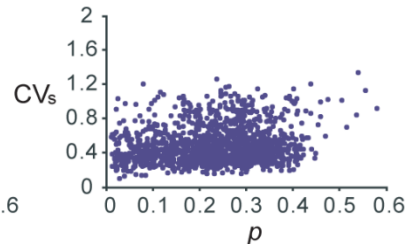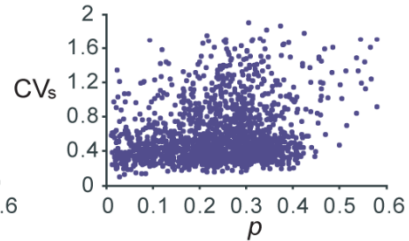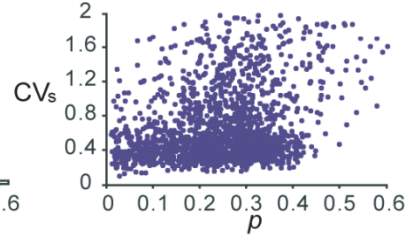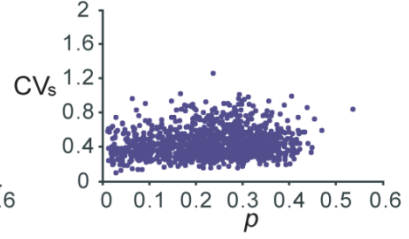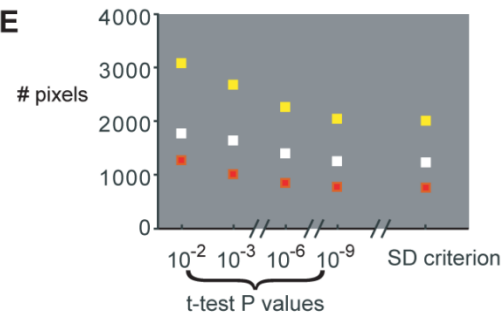
Figure 2.6 Varying the criterion for pixel selection does not bias the estimate for the probability that Ca^{2+} channels open during an action potential

(A) Mask for the pixels selected after using different criteria, i.e., SD criterion, or a Student's t-test using different significance levels ($P < 10^{-2}$, 10^{-3}, 10^{-6}, or 10^{-9}). All pixels selected are shown in either red or white; only the pixels shown in white could be used to derive a meaningful p (i.e. $0 < p < 1$).

(B) Histogram distribution of opening probability calculated from the selected pixels under each criterion.

(C) In each graph, CV_s is plotted against opening probability to reveal subsets of the data that are selected under each criterion. Comparing panels (B) and (C) demonstrates that the distribution of opening probability of Ca^{2+} channels during an AP is not changed as more restrictive criteria eliminate a subset of the data.

(D) Predicted active zone regions of the example nerve terminal identified by labeling the postsynaptic acetylcholine receptor clusters with Alexa 594-α-bungarotoxin. Scale bar: 5 µm; also applies to the image in (A).

(E) Plot of the total number of pixels selected by each criterion (yellow), and the corresponding subset of these pixels that either do (white), or do not (red) resolve a meaningful p (i.e. $0 < p < 1$).

based on the single channel conductance (2.4 pS) estimated under physiological extracellular

calcium (Church and Stanley, 1996). The computed action potentials based on the equations of

Hodgkin and Huxley (1952) were generated by the software Neuron 7.0 (Hines and Carnevale,

1997). To model the effect of 3,4-diaminopyridine on single Ca^{2+} channel currents I reduced the

maximum conductance of the delayed rectifier potassium channels g_{max} by ~50% and 75%,

which broadened the APs (see Augustine, 1990). The resulting AP waveforms are shown in

Figure 2.7A and are in good agreement with the observed effects of DAP on APs recorded from

cultured Xenopus motoneurons (Meriney, unpublished observations).

    For each of the three AP waveforms shown in **Figure 2.7A**, we ran 10,000 single Ca^{2+}

channel simulations. As individual channels opened, the total number of inflowing Ca^{2+} was

counted as the integral of single channel current. The distribution of single Ca^{2+} channel current

integral was plotted in **Figure 2.7B** and was characterized by a log-normal histogram distribution.

This is in sharp contrast to the expected exponential distribution of mean open times for Ca^{2+}

channels recorded with a step voltage command. Such shift in distribution is driven by the

dynamic change in driving force as channels open at different points during the AP waveform

(see above). The prolonged action potential resulted in little change in the magnitude of single

channel Ca^{2+} current integrals (**Figure 2.7B**), but a dramatic increase in the opening probability

of individual Ca^{2+} channels during an AP (Table 2), consistent with previous studies (Augustine,

1990). For fast AP waveforms, the probability of calcium channel openings does not reach a

maximum until the AP has begun to repolarize (Pattillo et al., 1999). Broadening the AP

significantly increases the number of calcium channels that open during an AP. On the other

hand, since the driving force for calcium influx through a single open channel near the peak of

the AP is very small, this may offset the increase in time that calcium channels open

A

B

C

$$CV^2_{open} = 0.92 * CV^2_s - 0.053$$
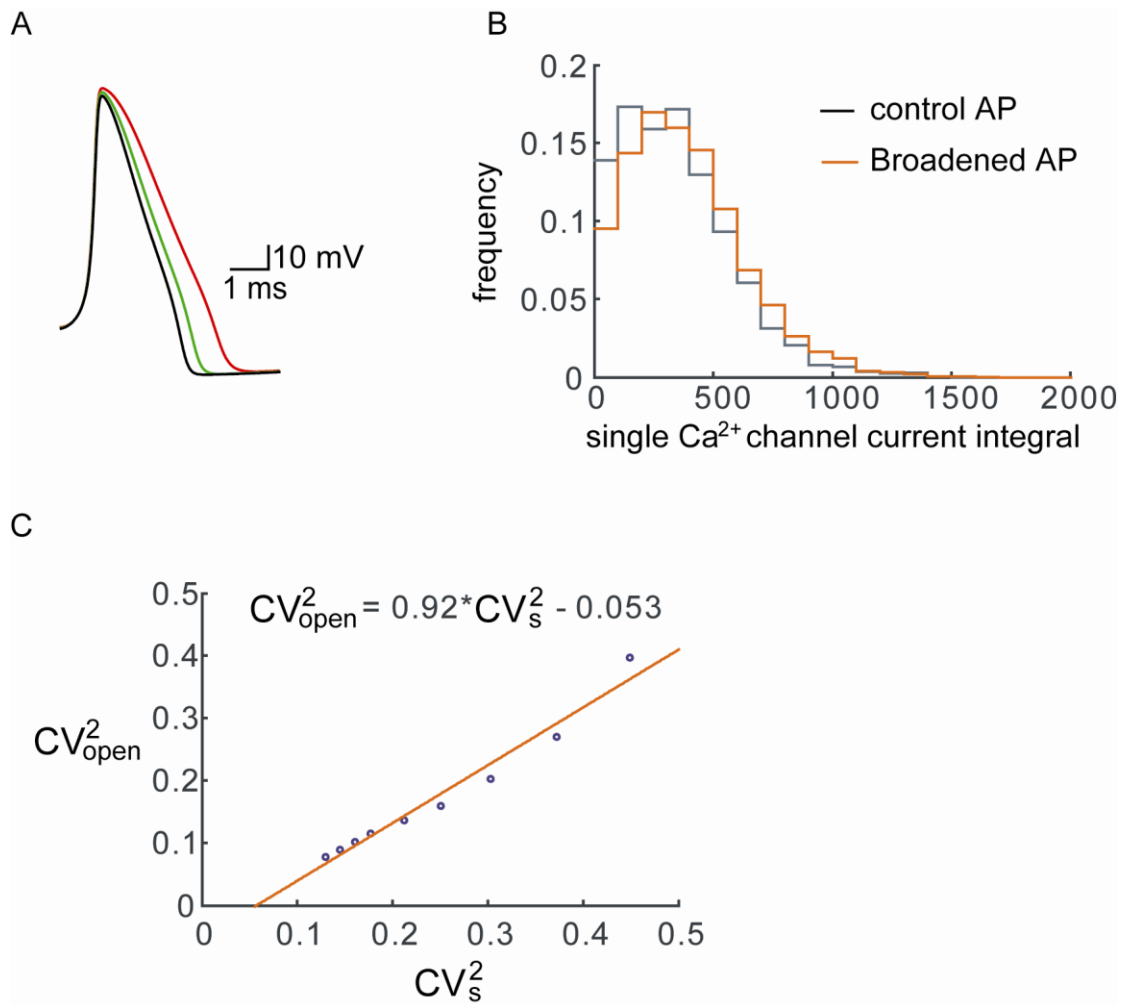
Figure 2.7 Computer simulations of presynaptic APs and AP-evoked Ca^{2+} influx through single open channels were used to estimate the relationship between CV_{open} and CV_s

(A) The computed action potential waveforms based on the equations of Hodgkin and Huxley (1952) and the effects of prolonging the duration of repolarization by reducing maximum conductance of the delayed rectifier potassium channels by 50% (green) and 75% (red) of the control (black).

(B) The distribution of single Ca^{2+} channel current integral evoked by the control AP and broadened AP (reduction of potassium conductance by 75%) exhibited a similar lognormal shape.

(C) For each simulation, the known number of Ca^{2+} channels and probability of opening allowed us to calculate the CV_{open} , which is governed by the fluctuating number of open channels based on the binomial distribution. The CV_s, which is affected by the fluctuation in the single channel calcium current, was computed directly from trial-to-trial variability in the total amount of Ca^{2+} flux through all the channels that open during an AP (circles). As the number of Ca^{2+} channels increased (from 10 to 50 with increment of 5), both CV_{open} and CV_s decreased. The relationship between CV_{open} and CV_s can be best fit by a linear regression with a slope of 0.92 (red line).

during the prolonged AP. Therefore, the amount of calcium ions flowing through open channels, which is determined by both driving force and open duration of calcium channels, remained relatively unchanged for the control and the prolonged AP. Furthermore, I showed that no significant change occurred in the distribution of single Ca^{2+} channel current integrals evoked by the broadened APs, as compared to control. Therefore, similar magnitudes of coefficient of variation in AP-evoked single Ca^{2+} channel current integrals (CV_{ch}) were found for all AP waveforms (see Table 2). Interestingly, simulation results showed that most channels flickered open once, with only 1-3% of channels flickering open twice during either a control AP or one of the broadened APs. The computed opening probability of our simulated channels during an AP under control conditions, and after 75% block of potassium channels, are in agreement with our experimentally derived values for the probability of opening of Ca^{2+} channels during an AP (0.24 vs 0.72 before and after DAP treatment).

experiment	CV_{ch}	p	CV_{open}^2 / CV_s^2
Control	0.68	0.19	0.68
DAP 50%	0.63	0.46	0.71
DAP 75%	0.61	0.66	0.73

Table 2: Variability in simulated Ca^{2+} influx through single open channels and its contribution to the total variance of Ca^{2+} signals.

Next, I explored the quantitative relationship between CV_{open} (the coefficient of variation of the number of Ca^{2+} channels that open during an AP, which is governed by the binomial distribution) and CV_s (the coefficient of variation of total amount of Ca^{2+} ions fluxing through all the open Ca^{2+} channels, which is strongly affected by single channel fluctuation) in a systematic

way by varying the number of Ca^{2+} channels in our simulation. As n increased, both CV_{open} and CV_s decreased by similar magnitudes, resulting in a linear relationship between CV_{open}^2 and CV_s^2 which was best fit with a slope 0.92 (**Figure 2.7C**). The ratio of $\frac{CV_{open}^2}{CV_s^2}$ becomes larger as CV_s increases, for example, when n is smaller. The mean is equal to 0.68 ± 0.08 (n = 9, see Table 2). Since I used CV_s as a substitute for CV_{open} in our experimental data to estimate n (see equation 14 in experimental procedures), our simulations presented here led to the conclusion that I underestimated the true number of Ca^{2+} channels in an active zone by approximately 10-30%.

2.5   DISCUSSION

In this study I have combined variance analysis with high-resolution calcium imaging techniques to estimate the number and probability of opening of Ca^{2+} channels within presynaptic active zones. Our results predict that a single active zone at the frog NMJ contains a relatively small number of Ca^{2+} channels, each with low probability of opening during an AP.

2.5.1   Single pixel optical fluctuation analysis of presynaptic Ca^{2+} signals within active zones

I have validated the optical fluctuation analysis method with several experiments. The measured CV_s of AP-evoked fluorescent signals was shown to be sensitive to changes in either n (by reducing the number of Ca^{2+} channels using CgTX) or p (by broadening the AP with DAP),

but not to the changes in extracellular Ca^{2+} concentration (**Figure 2.5**). These results are consistent with our expectation that the variance in AP-evoked Ca^{2+} signals are predominately affected by the fluctuating number of open Ca^{2+} channels which follows the binomial distribution governed by n and p.

I performed variance analysis on individual imaging pixels which sample about one-half of a single active zone of the frog NMJ, instead of averaging the signal across an entire single active zone for two main reasons. First, it was difficult to identify which pixels should be included in the representation of a single active zone for most nerve terminals. Second, due to various sizes of active zones, it was also difficult to determine how many pixels should be averaged. Therefore, I could perform single pixel analysis without bias of associating any particular pixel to a particular active zone. However, single pixel analysis introduced the question of how to extend the n value reported by individual pixels to our estimate for the total number of Ca^{2+} channels within single active zones. One simplistic solution was to compare the resolution of single pixels (~0.45 μm) with the length of single active zones (~1 μm) and double the n value reported by individual pixels. However, since the Ca^{2+} channels at the center region of active zones may be detected by several pixels, the total number of Ca^{2+} channels in an active zone obtained by this simplistic approach would be overestimated. Indeed, as I compared the n values using different pixel selection criteria, it is evident that pixels satisfying more stringent criteria tend to overlie the center region of active zone (**Figure 2.6**) and have lower CV values, which is consistent with the idea that these pixels may detect more Ca^{2+} channels than pixels overlying the edge of an active zone (Table 1).

Another issue concerning single pixel analysis is that differences in the distance of individual channels from the center of a pixel may impose significant variability on the total

62

variance of fluorescent signals detected by the pixel, which would result in an underestimate in either n or p value. As described above, the measured CV_s across trial-to-trial variability of AP-evoked fluorescent signals was not sensitive to changes in extracellular Ca^{2+} concentration. If different Ca^{2+} channels with various distances to a particular pixel contributed significantly different amount Ca^{2+}, I should expect a decrease in the measured CV_s with the increase in apparent Ca^{2+} diffusion length, which is sensitive to the concentration of free calcium buffer. However, I did not see a significant decrease in the measured CV_s in high Ca^{2+} as compared to the control condition. Further, the distribution of single channel current integrals during an AP is relatively broad (see below; **Figure 2.7**), and this may dominate the variability in detection of single channel fluxes and therefore minimize the contribution of variability due to channels at different distances from any given pixel.

2.5.2 The opening probability of active zone Ca^{2+} channels during AP stimulation

The probability that presynaptic Ca^{2+} channels open in response to a single AP is primarily determined by the activation kinetics of Ca^{2+} channels and the shape of the AP. Indeed, by broadening the AP with DAP, I have shown that the opening probability of presynaptic Ca^{2+} channels increases significantly. In a limited number of cases it has been possible to determine the opening probability of Ca^{2+} channels from patch clamp recordings of presynaptic Ca^{2+} current. At the squid giant synapse (Pumplin et al., 1981; Augustine, 1990), the chick ciliary ganglion calyx (Bertram et al., 1996), and the cultured *Xenopus* neuromuscular varicosity (Poage and Meriney, 2002), it has been estimated that opening probability is relatively small (0.1-0.3). In contrast, evidence from the rat calyx of Held (Borst and Sakmann, 1998), hippocampal mossy fiber boutons (Bischofberger et al., 2002), and the synapse between cerebellar granule cells and

Purkinje neurons (Sabatini and Regehr, 1997), indicate that single APs activate a large fraction

of available Ca^{2+} current (0.7-0.9). Thus, it is likely that the proportion of presynaptic Ca^{2+}

channels that open with AP stimulation may be variable between synaptic preparations.

Furthermore, Ca^{2+} channels have characteristic gating kinetics that depend on Ca^{2+} channel type,

splice variant, and auxiliary subunits (Jones and Marks, 1989; Lin et al., 1997; 1999). In fact,

striking differences in the rate of activation (~15 fold) have been observed when comparing two

isoforms of the α_{1B} N-type Ca^{2+} channel derived from rat brain (Stea et al., 1999). Therefore,

Ca^{2+} entry during an AP depolarization can vary widely when examined across synapses and

model preparations, and even within the same family of Ca^{2+} channel types.

Our analysis approach assumes that all Ca^{2+} channels sampled in our experiment have the

same probability of opening during an AP. Thus, our calculation of the probability of opening

during an AP represents an average of the actual values for individual Ca^{2+} channels. It would be

interesting to know how much variability in probability of opening exists among individual

active zone Ca^{2+} channels. Further, it is likely that the probability of Ca^{2+} channel opening

during an AP can be modulated under various conditions (i.e. disease, altered synaptic activity,

or pharmacologic treatment). In particular, this characteristic may underlie the homeostatic

modulation of presynaptic transmitter release (Wang et al., 2004; Frank et al., 2009).

2.5.3   The number of Ca^{2+} channels within single active zones of the motor nerve terminal

In spite of previous work presenting evidence that the 200~250 active zone intramembraneous

particles include the voltage-gated Ca^{2+} channels (Pumplin et al., 1981; Robitaille et al., 1990;

Cohen et al., 1991) as well as Ca^{2+}-activated potassium channels (Robitaille et al., 1993), it

remains unknown how many of these active zone intramembraneous particles actually represent

presynaptic Ca^{2+} channels. Further, the stoichiometric relationship between presynaptic Ca^{2+}

channels and the docked synaptic vesicles that line both sides of the active zone is unknown. In

our experiments, an average of ~14 Ca^{2+} channels was reported by individual active zone pixels.

When I extended this single pixel estimate to the number that would be expected to be present in

an entire active zone (based on the optical resolution of the system, see **Figure 2.1**), I estimate

that each active zone has only about 28 voltage-gated Ca^{2+} channels along its entire length.

Because I used the measured variance of fluorescence signal to calculate the number of Ca^{2+}

channels in the active zone, other sources of variance (i.e. fluctuating Ca^{2+} flux through single

channels) can influence this estimate. The impact of such additional variability can be evaluated

by determining the variability in flux through single Ca^{2+} channel currents. With the aid of

Monte Carlo simulation of single Ca^{2+} channel currents (**Figure 2.7**), I have shown that a large

percentage of the trial-to-trial variability of Ca^{2+} signal evoked by single APs derived from the

fluctuating number of Ca^{2+} channels whereas only ~10-30% of the variance may come from

fluctuations in single channel currents. Based on our calculations of the extent to which

variations in single channel flux influence our estimates, I calculated that I have underestimated

n by about 10-30%. As such, the actual number of Ca^{2+} channels within an active zone may be

about 30~36. Therefore, our results suggest that the number of Ca^{2+} channels in an entire active

zone (~30~36) still constitutes only a small proportion (~15-20%) of total intramembraneous

particles (200-250) observed in freeze-fracture active zone replicas. Given the average

probability of opening that I calculated during an AP (~0.24), on average only about 7-8 Ca^{2+}

channels are expected to open in each active zone during each AP. Interestingly, our data also

predict that the total number of presynaptic Ca^{2+} channels within an individual active zone

coincides roughly with the number of docked synaptic vesicles. This quantitative relationship

suggests the interesting possibility that each docked synaptic vesicle is tightly associated with only a single voltage-gated Ca^{2+} channel (see **Figure 2.8**). While this idea is consistent with the highly ordered Ca^{2+}-regulated release machinery at the active zone (Harlow et al., 2001), I am unable to exclude the possibility of a heterogeneous distribution of Ca^{2+} channels along the active zone.

Of course, our analysis only estimates the number of functional presynaptic Ca^{2+} channels present in the active zone. There may be additional Ca^{2+} channels present that are 'silent' due to some form of regulation such that they do not open during our experiments. A 'silencing' of ion channels has been observed for leak potassium channels as a result of sumoylation (Rajan et al., 2005; Wilson and Rosas-Acosta, 2005), and something similar could occur with synaptic Ca^{2+} channels using any of a variety of potential mechanisms (Pun et al., 1986; Lipscombe et al., 1989; Faber et al., 1991; Voronin and Cherubini, 2004; Toselli et al., 2005). Changes and/or variability in the number of Ca^{2+} channel in an active zone then could be explained by some mechanism that underlies a 'silent' to 'functional' interconversion. Under this scenario, it is possible that some of the particles identified in freeze-fracture replicas of the frog neuromuscular junction may be 'silent' Ca^{2+} channels.

2.5.4 The Ca^{2+} channel-vesicle release relationship

The question of how many Ca^{2+} channels must open to trigger a single release event is particularly intriguing and contributes to our understanding of how Ca^{2+} regulates synaptic vesicle fusion in the nerve terminal. At a single active zone of the frog NMJ, my data predict that an average of about 7-8 Ca^{2+} channels open following an AP, but the release probability of a whole active zone is only ~0.5. Therefore, it appears that these open Ca^{2+} channels trigger

vesicle fusion with a relatively low probability. One possible explanation is that each vesicle release event requires the summed Ca^{2+} flux through many open Ca^{2+} channels. However, previous studies at this synapse have suggested that Ca^{2+} flux through only 1~2 Ca^{2+} channels can trigger transmitter release (Yoshikami et al., 1989; Shahrezaei et al.2006). If only a few Ca^{2+} channel openings are required to trigger vesicle fusion, it is possible that these openings need to occur in close proximity to one another in the active zone to be effective at evoking transmitter release. The probability that two channel openings would occur in close proximity is low, which could therefore limit the occurrence of vesicle fusion from each active zone. Alternatively, each vesicle fusion event might be controlled predominately by the tightly-associated single Ca^{2+} channel positioned nearby, but the Ca^{2+} flux through these single open channels might only trigger vesicle fusion with a low probability (5~10%). Under these conditions, the release probability within individual active zones would be determined by both the number of open Ca^{2+} channels and the probability that a single open Ca^{2+} channel triggers vesicle fusion.
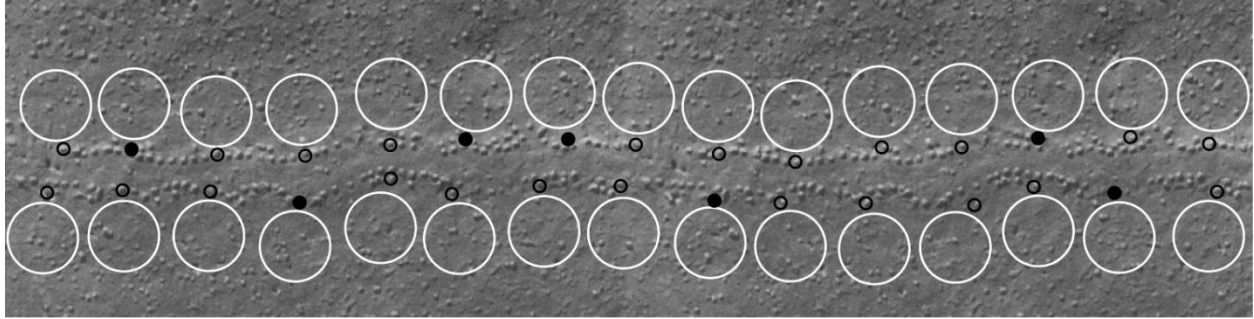
Figure 2.8 Conceptual model of a single active zone showing graphically the stoichiometric and functional relationship between Ca^{2+} channels and docked synaptic vesicles

Replica from a freeze-fractured frog neuromuscular junction (adapted from Heuser and Reese, 1981) showing a linear array of intramembraneous active zone particles. Superimposed on this image is a graphic representation of the hypothesized number and position of associated synaptic vesicles (white circles), voltage-gated Ca^{2+} channels (black circles), and the number of these voltage-gated Ca^{2+} channels that are predicted to open after stimulation by a single action potential (filled black circles).

3.0 QUANTITATIVE ANALYSIS OF SINGLE CA^{2+} CHANNEL OPENINGS AND EVOKED TRANSMITTER RELEASE FROM PRESYNAPTIC ACTIVE ZONES

3.1 ABSTRACT

The quantitative relationship between presynaptic calcium influx and transmitter release critically depends on the spatial coupling of presynaptic Ca^{2+} channels with synaptic vesicles. When there is a close association between Ca^{2+} channels and synaptic vesicles, the flux through a single open Ca^{2+} channel may be sufficient to trigger transmitter release. With increasing spatial distance, however, a larger number of Ca^{2+} channels might be required to open and contribute the calcium ions necessary to trigger vesicle fusion. Here I used a combination of pharmacological Ca^{2+} channel block, high-resolution calcium imaging, postsynaptic recording, and 3D Monte Carlo diffusion-reaction simulations to investigate this problem at adult frog neuromuscular junctions. Our findings demonstrate that calcium ions entering the nerve terminal through a single open Ca^{2+} channel can trigger vesicle fusion. Further, I show that the calcium flux through a single open channel plays the predominant role in evoking neurotransmitter release even when multiple channels open in the active zone.

3.2   INTRODUCTION

Fast neurotransmitter release is triggered by calcium influx through voltage-gated Ca^{2+} channels opened by an action potential. It has previously been shown that the magnitude and time course of neurotransmitter release is highly stochastic and tightly dependent on the coupling between Ca^{2+} channels and synaptic vesicles (Augustine and Neher, 1992; Meinrenken et al., 2002). Understanding the mechanisms that underlie the control and modulation of presynaptic release probability and kinetics is crucial for understanding synaptic transmission and plasticity.

The stoichiometric relationship between presynaptic Ca^{2+} channels and synaptic vesicles has been studied at many model synapses by either directly reducing the number of available Ca^{2+} channels using specific toxins, or changing the action potential waveform shape and thus varying the number of open channels indirectly. Using these approaches to estimate the quantitative contribution of Ca^{2+} channels to vesicle release has led to variable results. At some synapses, it has been argued that there is a tight coupling between presynaptic Ca^{2+} channels and synaptic vesicles (Yoshikami et al., 1989; Stanley, 1993; Bucurenciu et al., 2008). In these cases, several lines of evidence predict that calcium flux through a single open Ca^{2+} channel can trigger vesicle fusion.   At other synapses, the summed calcium ions derived from many open channels appear to be required to trigger synaptic vesicle fusion, suggesting a loose coupling between individual presynaptic Ca^{2+} channels and the transmitter release machinery (Borst and Sakmann, 1996; Wu et al., 1999; Meinrenken et al., 2002).

Combining pharmacological channel block, high-resolution calcium imaging, postsynaptic recording, and 3D Monte Carlo diffusion-reaction simulations, I have fully investigated the contribution of single open Ca^{2+} channels to the triggering of vesicle fusion at a model fast synapse: the adult frog neuromuscular junction. This synapse features hundreds of linearly

70

organized active zones that are each characterized by double rows of presynaptic ion channels and synaptic vesicles (Heuser et al., 1974). Further, our previous imaging studies (Wachman et al., 2004; Luo et al., submitted) predict that the number of presynaptic voltage-gated Ca^{2+} channels in each active zone is roughly equivalent to the number of docked synaptic vesicles, suggesting an active zone structure compatible with a tight association between a single presynaptic Ca^{2+} channel and each docked synaptic vesicle. By reducing the number of available Ca^{2+} channels using a relatively high concentration of ω-conotoxin GVIA (CgTX; a selective N-type Ca^{2+} channel blocker), I show that calcium entry through the remaining spatially distinct individual Ca^{2+} channels can be imaged directly. Furthermore, transmitter release can still be triggered under these conditions. These findings suggest that a single open Ca^{2+} channel is able to trigger quantal release at this synapse and permit a characterization of this calcium-release coupling.

The interpretation of our experimental data was aided by a 3D Monte Carlo diffusion-reaction simulation of a realistic active zone model which included docked synaptic vesicles, action potential-driven stochastic Ca^{2+} channel gating and ion permeation, and vesicle-associated Ca^{2+}-binding sites based on predicted synaptotagmin copy number and C2 domain properties (see Dittrich et al., 2009). During simulations, individual calcium ions were followed as they entered the nerve terminal and bound to sensor sites, and the modeling quantitatively reproduced the effect of titrated Ca^{2+} channel block on quantal release and release latency. Under normal conditions, our model predicted that a significant fraction (~1/3) of release events would be triggered by calcium ions entering through a single open channel. In the remaining ~2/3 of release events, however, vesicle fusion was predicted to be triggered by calcium ions derived from at least two Ca^{2+} channels. Strikingly, even in these cases, the Ca^{2+} ions that triggered

71

transmitter release were predominately derived from a single Ca^{2+} channel that was positioned nearest to the vesicle (providing >80% of the ions bound).

3.3   METHODS

3.3.1   Calcium imaging

Imaging AP-evoked Ca^{2+} entry into active zone regions of the adult frog NMJ synapse was performed as described above (2.2.1 and 2.2.2). When quantifying the effect of various CgTX doses on average Ca^{2+} entry, only 10 resting fluorescence images and 10 stimulus-evoked fluorescence images were collected from individual nerve terminals before and after CgTX treatment. When quantifying the probability of detecting Ca^{2+} entry within active zone regions after high concentrations of CgTX treatment, up to 100 stimulus trials were collected (see 3.3.2. below).

3.3.2   Image analysis

For each dose of CgTX, the sum of pixel fluorescent intensities over an entire in-focus active zone region of interest was calculated before and after the CgTX treatment. Their ratio was used to estimate the average blocking effects of various doses of CgTX on AP-evoked Ca^{2+} entry into the nerve terminal.

I was also interested in quantifying the Ca^{2+} flux through isolated single Ca^{2+} channel openings after blockade of a majority of Ca^{2+} channels within active zones using relatively high-

concentrations CgTX. Because total Ca^{2+} entry was remarkably low after exposure to a

relatively high concentration of CgTX (600 nM, ~93% decrease), for quantitative analysis of the

imaged calcium flux through isolated single Ca^{2+} channel openings under this condition, I used a

nerve terminal mask (based on resting fluorescence in dye loaded nerve terminals) to restrict the

analysis only to nerve terminal regions. Within these nerve terminal regions, I quantified the

number of distinct Ca^{2+} entry sites within individual active zones for each AP stimulus trial. The

goal of this approach is to represent the number of single Ca^{2+} channel openings. This is distinct

from the approach described above in Chapter 2 where I wanted to perform optical fluctuation

analysis using all of the pixels that sampled active zone areas of the nerve terminal. In Chapter 2,

the SD criterion was performed on the mean stimulated fluorescent signal (including failures)

with the goal of defining pixels that sampled active zone regions of the nerve terminal. Here, I

needed a criterion that could distinguish, in each stimulus trial, the fluorescent signal caused by

the Ca^{2+} influx through an open Ca^{2+} channel from the background fluctuation caused by shot

noise. For this purpose, I collected as many as 100 trials of stimulus-evoked fluorescence

images for the nerve terminals exposed to high concentrations of CgTX. Furthermore, I used the

criterion that the stimulated fluorescence change above rest (Δf_s) should exceed 3 times the

standard deviation ($3 \times \sigma_b$) of the resting fluorescence of each pixel. There are several reasons for

our choice of a $3 \times \sigma_b$ criterion for this purpose. First, an examination of pixels selected using a

variety of criteria demonstrates that the $3 \times \sigma_b$ criterion appears to be most reasonable at

identifying calcium entry sites within active zone regions of the nerve terminal. Since resting

fluorescence follows a Gaussian distribution, a $2 \times \sigma_b$ cutoff may lead to 3% false positive error

and therefore have a significant impact on our estimate of the number of detected Ca^{2+} channel

openings, the probability of which is expected to be relatively low based on the results described

in Chapter 2. Indeed, the use of $2 \times \sigma_b$ criterion leads to false positive identification of Ca^{2+} channel openings as reported by a large number of pixels between active zones, and even under unstimulated conditions. The use of $4 \times SD$ criterion eliminates most Ca^{2+} channel openings such that there are almost none detected within active zone regions. Second, in testing a variety of criteria (2, 3, or $4 \times SD$), I evaluated the number of Ca^{2+} channel openings that were reported in comparison with expectations based on the use of such a high concentration of CgTX (600 nM). This CgTX treatment decreases total average calcium entry into the nerve terminal by 93% (see table 3 below). Based on my previous analysis of variance for calcium signals at untreated control synapses, I calculated that there are ~28 Ca^{2+} channels in each active zone, and that each opened during an action potential with a probability of ~0.2 (see Chapter 2). Therefore, a 93% reduction in total calcium entry would predict that only ~2 Ca^{2+} channels would remain in each active zone, and that the probability that only one channel would open during an action potential would be ~32%. Using the $3 \times SD$ criterion leads to a detection of a number of calcium entry sites that is consistent with these expectations (see **Figure 3.5**).

For statistical analysis, the number of detected Ca^{2+} entry sites was normalized (as Ca^{2+} channel openings per AZ per AP) for each terminal by dividing the total number of Ca^{2+} entry sites by the number of AZs and the number of stimulation trials.

3.3.3 Electrophysiology

Intracellular recordings from the adult frog cutaneous pectoris nerve-muscle preparation were performed as described previously (Meriney and Grinnell, 1991). In brief, the nerve of the cutaneous pectoris muscle was stimulated via a suction electrode at $5 \times$ the threshold intensity required to elicit muscle twitch. Intracellular micropipettes were made from glass pipettes

(Warner Instruments, filament glass G100F-4, O.D. 1mm, I.D. 0.58mm) and had a resistance of ~25MΩ after filling with 3M potassium acetate. Surface muscle fibers were penetrated close to nerve endings under visual control with a long working distance water-immersion objective (40x, 3mm working distance). Only muscles with a resting potential more negative than -70mV were recorded for analysis. Data were amplified using a Dagan BBC 700 amplifier and acquired using Clampex 9 software (Axon Instruments, Foster City, CA). Clampfit 9.2 was used for data analysis.

3.3.4   Drug treatment

CgTX is known to block N-type Ca^{2+} channels in a manner that is essentially irreversible over the time-course of these studies (Stocker et al., 1997). For titrating channel block, the frog nerve-muscle preparation was incubated with various doses of CgTX for 45-60 minutes and then washed in NFR. Superficially positioned nerve terminals and muscle fibers were chosen for study to avoid variability in toxin access to nerve terminals positioned at different depths of the preparation. Effects on transmitter release and calcium influx were determined in separate experiments to optimize the health of the terminal for imaging experiments and to avoid potential complications due to the buffering effects of calcium-sensitive dye during recordings of transmitter release.

3.3.5   Monte Carlo simulation

A spatially realistic 3-D model of the presynaptic active zone, which employs a Monte Carlo algorithm, has been developed and used to explore the molecular mechanism of synaptic vesicle

release (Dittrich et al., 2009). A similar model was adapted for simulating the titration effects of CgTX on calcium entry and neurotransmitter release. In brief, the topology, dimensions, and number of synaptic vesicles of the 3-D model active zone were based on published ultrastructural data from the adult frog NMJ (Heuser et al., 1974; Pawson et al., 1998; Harlow et al., 2001). The AZ encompassed a volume approximately 1.6 μm^3 (length $\times$ width $\times$ height: $1.52 \times 1.13 \times 0.95$ μm). This simulated AZ included two rows of docked synaptic vesicles (50 nm diameter) positioned on either side of a centre groove which contained simulated voltage-gated Ca^{2+} channels. Within each row there were 13 vesicles positioned 70 nm from the centre of the AZ and 4 nm above the presynaptic membrane. The total number of Ca^{2+} channels and their opening probability following single APs were constrained by our recent calcium imaging experiments. For simplicity, there were 26 voltage-gated Ca^{2+} channels and that each was positioned in a one-to-one topographic relationship with a single docked synaptic vesicle with an average distance from the vesicle of 40 nm.

For quantifying transmitter release, our Ca^{2+} sensor model was constructed based on the known biochemical properties of synaptotagmin 1 and the predicted number of copies of this molecule per synaptic vesicle (see **Section 1.3.3 Synaptic vesicle fusion and the Ca2+ sensor**). As such, an individual synaptic vesicle contained a total of 40 Ca^{2+} binding sites that represented a total of eight synaptotagmin molecules, each with five binding sites (see Dittrich et al., 2009). Our simulation of vesicle fusion used a cooperative fusion model in which at least 3 of these modelled synaptotagmin molecules must bind at least 2 calcium ions (one each in the C2A and C2B domains). Therefore, a minimum of 6 calcium ions must bind in pairs (to both C2 domains) to trigger vesicle fusion (see Dittrich et al., 2009). This Ca^{2+} sensor model is consistent with the predicted number of copies of synaptotagmin per synaptic vesicle and the essential role of both

C2A and C2B domains in AP-evoked neurotransmitter release (Takamori et al., 2006; Fernández-Chacón et al., 2001; Mackler et al., 2002; Stevens and Sullivan, 2003). Furthermore, it has been shown the presence of excess calcium binding sites on each vesicle is necessary and sufficient to reproduce accurately the experimentally observed relationship between transmitter release and external Ca^{2+} concentration (see Dittrich et al., 2009). Our release model is in contrast with a popular previous model that assumed all calcium binding sites on a single synaptotagmin 1 molecule must be occupied to trigger vesicle fusion. This relatively simple older model seems to have been supported by the purely coincidence evidence that the cooperative dependence of transmitter release on calcium concentration (slope of 4-5) is equal to the total number of calcium binding sites on each synaptotagmin molecule (5). In this older model, the properties of synaptotagmin, the number of synaptotagmin molecules on each vesicle, as well as the SNARE complex formed by each vesicle, are not taken into account in triggering vesicle release. Therefore, this older model cannot explain the reduction in calcium cooperativity caused by an experimentally decreased level of some components of the SNARE complex (Stewart et al., 2000). Further, the older model is apparently incompatible with the vesicle fusion model mediated by SNARE complex (Yoshihara and Littleton, 2002). For the model I have used in this thesis, for each binding site, the on and off rates were $1 \times 10^8 \, M^{-1} \, s^{-1}$ and $6 \times 10^3 \, s^{-1}$, respectively (Davis et al., 1999). The other parameters used in the simulation included immobile Ca^{2+} buffers (at 2 mM with on ($1 \times 10^8 \, M^{-1} \, s^{-1}$) and off ($1 \times 10^4 \, s^{-1}$) rates based on published experimental data), and freely diffusing Ca^{2+} ions (diffusion coefficient of $6 \times 10^{-6} \, cm^2 \, s^{-1}$).

MCell 3.1 (www.mcell.psc.edu) software was used for the simulations. Each simulation was run using at least 1000 seeds on a single processor of a High Performance Computing platform at

the Pittsburgh Supercomputing Center (codon.psc.edu, a cluster of 23 dual processor machines, each with two 1.6 GHz AMD Opteron processors and 8 gigabytes of memory). Data analyses were performed with custom written scripts.

3.4   RESULTS

To study the characteristics of presynaptic calcium flux I imaged presynaptic active zone regions of adult frog motor nerve terminals filled with a Ca^{2+}-sensitive dye. To evoke calcium entry, the nerve was stimulated at low frequency (0.5 Hz) and action potential-induced fluorescence transients were demonstrated to arise exclusively from Ca^{2+} entry through N-type Ca^{2+} channels as evidenced by complete block following exposure to 2 μM CgTX, and the lack of significant change following block of Ca^{2+}-induced Ca^{2+} release from internal stores (see Wachman et al., 2004). In order to reduce complications associated with Ca^{2+} diffusion within the nerve terminal after entry, and to facilitate analysis at single pixel resolution, I limited the laser illumination of the calcium-sensitive dye to 1 ms with a 1.2~1.5 ms delay after nerve stimulation. Under these conditions, the spatial profile of detected calcium entry was constrained by the resolution of our imaging system (~450 nm, see Chapter 2 methods).

3.4.1   The relationship between presynaptic calcium entry domains and triggering of transmitter release

In order to address the question of how many Ca^{2+} channel openings trigger transmitter release at the frog neuromuscular junction, I titrated the concentration of CgTX to block different fractions

78

of presynaptic calcium entry. I measured changes in calcium influx and transmitter release in separate experiments to avoid the buffering effects of calcium-sensitive dye on our measures of transmitter release. **Figure 3.1A** shows an average fluorescence change over 10 single AP stimulus trials at the control nerve terminal. Following exposure to 100 nM CgTX, AP-evoked fluorescence signals decreased dramatically. The ratio of total calcium influx evoked by single APs before and after drug treatment was calculated and used as an index of the blocking percentage of presynaptic Ca^{2+} channels by various concentrations CgTX (see Table 3).

I next examined the effects of the same concentrations of CgTX on the magnitude of neurotransmitter release using intracellular recording of endplate potentials (EPPs). EPPs were recorded from the same muscle fiber before and after incubation with CgTX. For these recordings, 3-7 μM curare and 2 μM μ-conotoxin PIIIA (a muscle-specific sodium channel blocker) were added to the Ringer bathing the preparation to block muscle contraction. The concentration of curare was titrated to reduce EPP amplitude to less than 10 mV to avoid significant effects of nonlinear summation of quantal events underlying the EPP, while still permitting the EPP to be measured both before and after exposure to various concentrations of CgTX. **Figure 3.1B** shows an example of averaged EPP traces before and after exposure to 100 nM CgTX and the summary data are reported in Table 3.

[CgTX] (nM)	25	50	75	100	400	600
%Ca^{2+} entry blocked (mean $\pm$ SD)	22 $\pm$1.0	41 $\pm$2.6	59 $\pm$4.6	70 $\pm$5.9	85 $\pm$8.0	93 $\pm$1.0
%transmitter release blocked (mean $\pm$ SD)	34 $\pm$2.4	64 $\pm$2.9	79 $\pm$5.0	84 $\pm$1.8	96 $\pm$2.5	98 $\pm$1.4

Table 3: The effect of CgTX titration on single AP-evoked calcium entry and

neurotransmitter release.

To determine the quantitative relationship between presynaptic calcium entry and transmitter release, the effects of titrating CgTX on both calcium entry and transmitter release were compared. As shown in **Figure 3.1C**, the fraction of transmitter release was plotted on a log-log scale against the fraction of presynaptic calcium entry that remained following exposure to various concentrations of CgTX. The resulting relationship is not completely linear over the range of CgTX doses examined. At low doses of CgTX (25-50 nM) the relationship appeared to fall on a line with a slope of ~2, but as the concentration of CgTX was increased, this relationship appeared to approach a slope of 1. These results suggest that under control conditions, very few Ca^{2+} channels open to contribute the calcium ions required to trigger each release event, consistent with previous observations at this synapse (Yoshikami et al., 1989; Shahrezaei et al., 2006). However, as presynaptic Ca^{2+} channels are blocked, release events depend increasingly on single open channels.

I then tested whether a spatially realistic AZ model constrained by experimental data (Dittrich et al., 2009) was able to reproduce the effect of titrating blockade of presynaptic calcium entry on transmitter release. This model has been shown to reproduce many properties of neuromuscular transmission including the normal release rate, the 4th power relationship between release rate and extracellular calcium concentrations, and synaptic delay. To model CgTX titration in the current study, an increasing number of Ca^{2+} channels were randomly removed from the active zone and the resulting release probability following a single AP stimulation was simulated. As shown in **Figure 3.2A** and Table 4, the model reproduced accurately the experimental observations (compare with **Figure 3.1C** and Table 3).
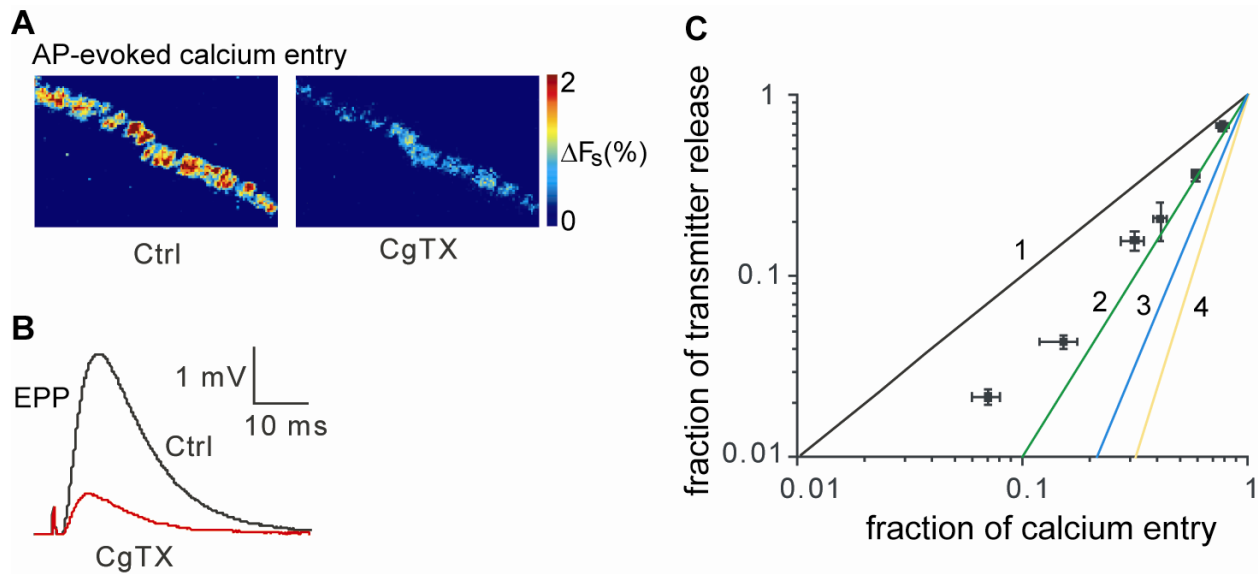
Figure 3.1 Titrating ω-CgTX GVIA blockade reveals a low Ca^{2+} channel cooperativity in transmitter release

(A)　CgTX (100 nM) remarkably reduced single AP-evoked calcium entry into the nerve terminals.

(B)　EPP amplitude decreased significantly after exposure to 100 nM CgTX.

(C)　A log-log plot of calcium entry and neurotransmitter release after treatment with various concentration of CgTX (25, 50, 75, 100, 400, and 600 nM) reveals a relationship with a slope between 1 and 2.

AZ channel number	26	20	15	11	8	4	2
% channel blocked	control	23	42	58	69	85	92
% transmitter release blocked	control	32	57	70	79	91	96

Table 4: The effect of titrating blockade of Ca^{2+} channels on AP-evoked neurotransmitter release using Monte Carlo simulation.

Since our experimental data indicated that very few, but likely more than one Ca^{2+} channel contributed calcium ions to triggering single vesicle release from the terminals under control conditions, I used the MCell simulation to estimate the percentage of released vesicles that bound calcium ions derived from one, two, or more Ca^{2+} channels (**Figure 3.2B**). On average, the model predicted that 5.2 ± 0.3 Ca^{2+} channels would open in each active zone following a single AP stimulation. Interestingly, however, it was found that about 34% of vesicles were triggered to fuse by calcium ions derived from a single open Ca^{2+} channel, and 41% of vesicle fusion events were triggered by calcium ions derived from only two open Ca^{2+} channels. Vesicle fusion triggered by more than two Ca^{2+} channel openings was less likely. On average, synaptic vesicle fusion was triggered by calcium ions derived from 1.9 Ca^{2+} channels, consistent with expectations based on our experimental data. As expected, this relationship changed when I decreased the number of available Ca^{2+} channels in the model (see Figure 3.2B inset). In particular, when 80% of Ca^{2+} channels were blocked, the average number of Ca^{2+} channels that open per simulation seed was reduced to 1.0 ± 0.2 and the release probability of single active zone was reduced to 0.06 ± 0.007. Under these conditions, using large simulation runs to increase the reliability of our estimates (10000 seeds), I determined that 460 out of 550 (84%) released vesicles were bound by calcium ions from a single Ca^{2+} channel. Therefore, the model predicts that vesicle fusion will still occur when most Ca^{2+} channels in the active zone are
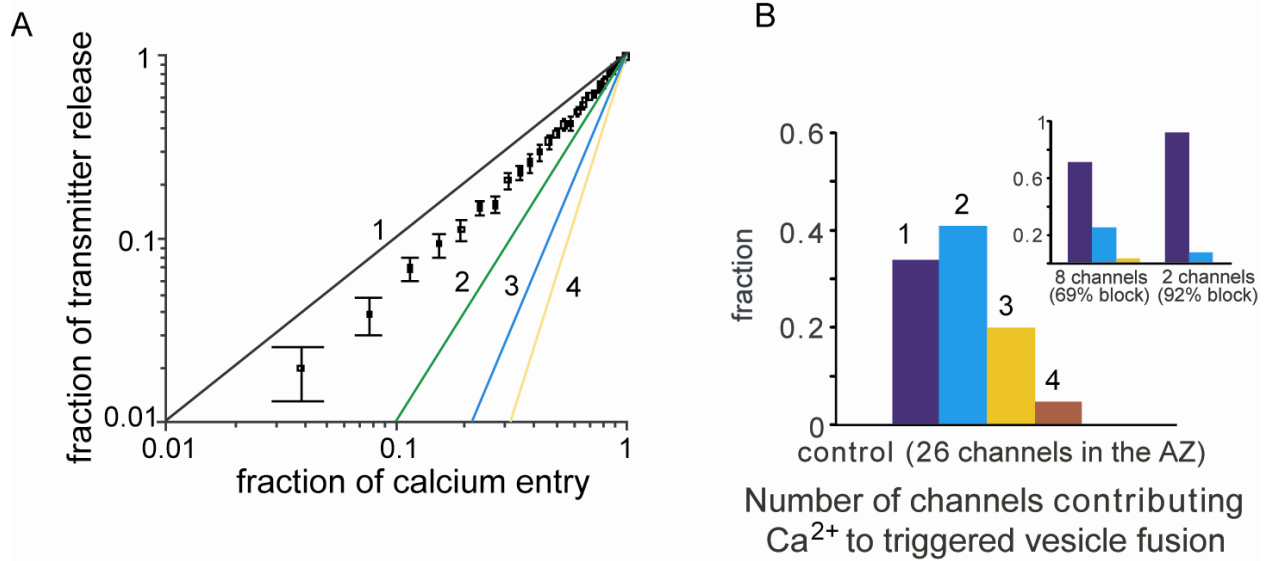
Figure 3.2 MCell computer simulations reproduce experimental data (compare with figure 3.1) and predict that each vesicle fusion event is normally triggered by the calcium flux through very few Ca^{2+} channels.

(A)   A log-log plot comparing changes in calcium entry and predicted neurotransmitter release after randomly removing different numbers of Ca^{2+} channels from the modeled active zone. The data fall on a slope between 1 and 2.

(B)   Histogram distribution of the fraction of released synaptic vesicles that bound calcium ions contributed by various numbers of Ca^{2+} channels under control conditions (26 Ca^{2+} channels in the active zone). Inset shows the fraction of released synaptic vesicles that bound calcium ions contributed by a single open Ca^{2+} channel increases as the number of available Ca^{2+} channels is reduced by 69% (8 channels remaining in the active zone) or 92% (2 channels remaining in the active zone).

not available, and as expected, the great majority of these events will be triggered exclusively by calcium ions derived from a single Ca^{2+} channel opening.

3.4.2 Single Ca^{2+} channel openings predominate in contributing calcium ions that trigger vesicle fusion even when more than one channel opens in the active zone

To more completely explore the Ca^{2+} channel contribution of calcium ions that trigger vesicle release, I used our model to track the pattern of open Ca^{2+} channels for a given fused vesicle. Interestingly, I found that when a particular vesicle was released, 94% of the time the nearest, closely-associated Ca^{2+} channel opened (**Figure 3.3A**). For these cases, I determined the specific Ca^{2+} channel source of each calcium ion that bound to the released vesicle and found that 81% of the calcium ions bound originated from the nearest, closely-associated Ca^{2+} channel (**Figure 3.3B**, left panel). In our model, a released vesicle (with 40 calcium binding sites, see methods) bound an average of 7~8 calcium ions. Therefore, our model predicts that among the calcium ions that bind to trigger vesicle fusion, 6~7 of these are derived from the closest Ca^{2+} channel and only 1~2 Ca^{2+} ions are derived from another open Ca^{2+} channel (**Figure 3.3B**, right panel). In contrast, in a few cases predicted by our model (6% of total vesicle fusion events), when a particular vesicle was released, the nearest, closely-associated Ca^{2+} channel did not open (see **Figure 3.3A**). Under these rare conditions, the Ca^{2+} ions that bound to the fused synaptic vesicle derived predominately from a nearby cluster of 3-5 Ca^{2+} channels, with each of these channels contributing 1-2 Ca^{2+} ions to the synaptic vesicle binding sites (**Figure 3.3C**). In conclusion, our model predicts that AP-evoked transmitter release at the frog NMJ is most often controlled by the Ca^{2+} ions that derive predominantly from the opening of one closely-associated Ca^{2+} channel, even when several Ca^{2+} channels open in the active zone (**Figure 3.3A** and **B**).

3.4.3 Experimental evidence confirmed that single channel openings can trigger synaptic vesicle release

In order to provide experimental evidence that single Ca^{2+} channel openings can trigger vesicle release, I sought to image directly the calcium influx through single Ca^{2+} channels at the frog motor nerve terminal (following exposure to high concentrations of CgTX) and determine effects on transmitter release. Based on our previous calcium imaging data (Wachman et al., 2004; Luo et al., submitted), I have argued that each active zone in the adult frog neuromuscular junction has relatively few presynaptic Ca^{2+} channels (30~36), and that each Ca^{2+} channel must have a relatively low opening probability (0.24). Therefore, very few Ca^{2+} channels within each active zone would be predicted to open (~6-8) during a single AP. Given this scenario, I expected that it might be possible to reduce the number of available Ca^{2+} channels so that a single AP may open at most one Ca^{2+} channel within individual active zones. An exposure to 600 nM CgTX greatly reduced AP-evoked calcium entry by 93 $\pm$ 1% (n = 3). Following a reduction of this magnitude, the number of available presynaptic Ca^{2+} channels within single AZs is expected to be very small (~1-2), and given the probability of opening (0.2), the likelihood that more than one would open in the same AZ during a single AP stimulus would be very small (~0.05). In agreement with this expectation, the pixels that detected significant calcium signal after exposure to 600 nM CgTX had a very large coefficient of variation (CV = 1.6 $\pm$ 0.5), as compared to control terminals (CV = 0.5 $\pm$ 0.3), suggesting a large reduction in the number of channels that can be detected by individual pixels. To increase the number of calcium signals detected for these experiments, I collected 70-100 stimulus-evoked images after treatment with high concentrations of CgTX. As shown in **Figure 3.4C**, after exposure to 600 nM CgTX, I detected discrete, sparse and spatially distributed signals evoked by single APs within well-focused
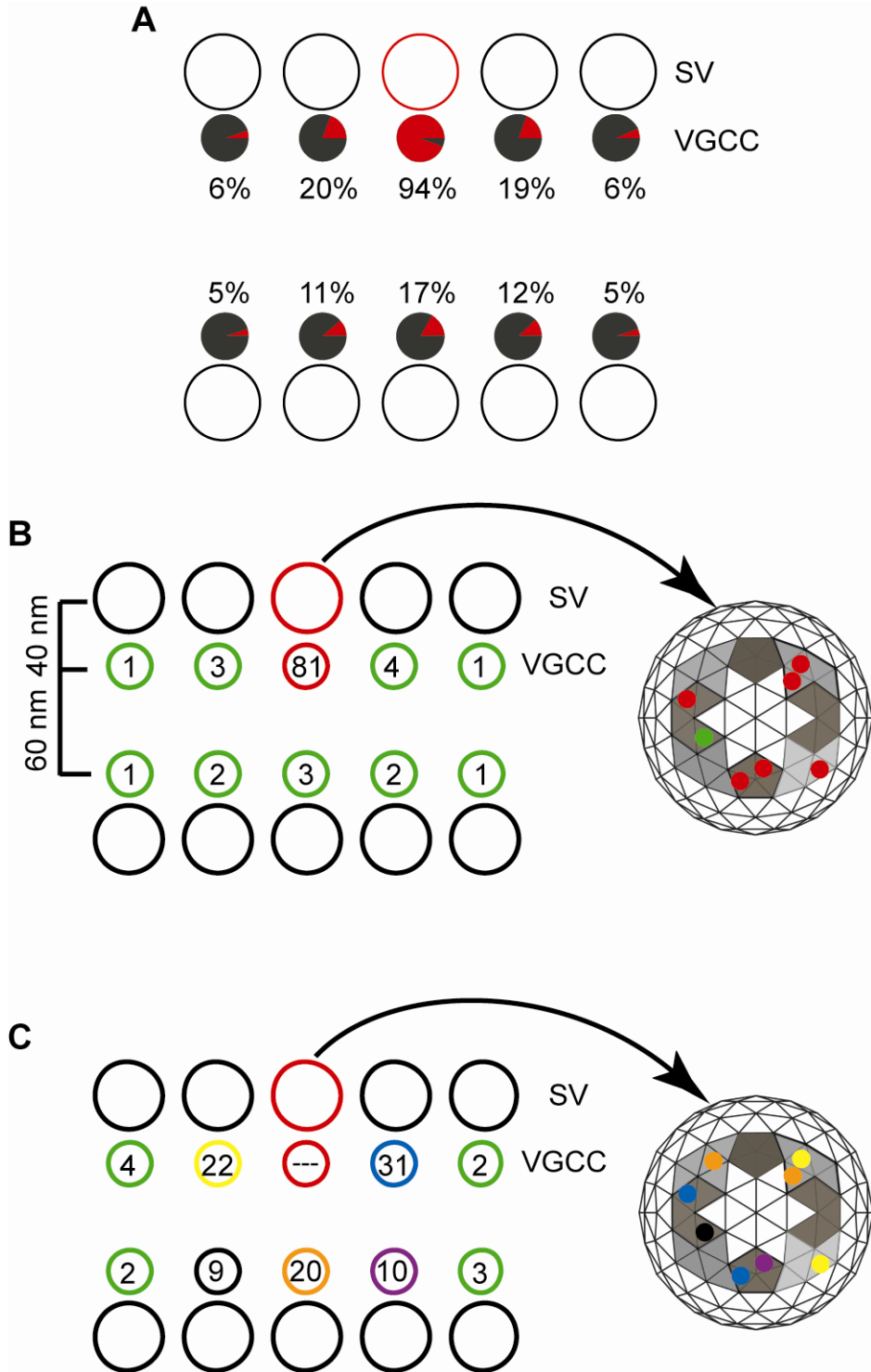
Figure 3.3 Single Ca^{2+} channel openings primarily provide the calcium ions that trigger neurotransmitter release at the modeled frog NMJ active zone.

(A)   Given a particular vesicle fusion event (red circle), the probability that different Ca^{2+} channels have opened is represented by the red area in the pie chart and the corresponding number below each channel icon.

(B)   *left panel:* For the majority of vesicle fusion cases in which the closely-associated Ca^{2+} channel has opened (94% as represented in A above), the number in each Ca^{2+} channel circle indicates the percentage of calcium ions from each Ca^{2+} channel position in the active zone that bound to the released vesicle (red circle). *right panel:*   Model schematic of the under surface of the synaptic vesicle triggered to fuse when the closely-associated Ca^{2+} channel has opened. Gray areas represent different synaptotagmin molecules and colored dots represent individual calcium ions that are color coded for their Ca^{2+} channel source in the active zone. The model was predicted based on the average behavior of the released vesicles, which has bound on average total 7~8 Ca^{2+} ions.

(C)   *left panel:* For the minority of vesicle fusion cases in which the closely-associated Ca^{2+} channel has not opened (6% as represented in A above), the number in each Ca^{2+} channel circle icon indicates the percentage of calcium ions from each Ca^{2+} channel position in the active zone that bound to the released vesicle (red circle). *right panel:*   Model schematic of the under surface of the synaptic vesicle triggered to fuse when the closely-associated Ca^{2+} channel has not opened. Gray areas represent different synaptotagmin molecules and colored dots represent individual calcium ions that are color coded for their Ca^{2+} channel source in the active zone.

regions of the nerve terminal.

When the signal intensity of individual pixels detecting channel openings was plotted as a histogram, the distribution took a lognormal form (**Figure 3.4E**) that was similar to the single channel current integral distribution measured using cell-attached patch-clamp measurements of single N-type Ca^{2+} channels gated by a frog motoneuron action potential waveform (**Figure 2.7** and Dittrich et al., 2009). This distribution is generated as single channels open with variable mean open time under conditions of rapidly changing driving force at different times during the AP waveform. Furthermore, this lognormal form of the distribution could also be reproduced using a computational model of single channel calcium ion flux gated by an AP waveform (Dittrich et al., 2009). The similarity in these histogram distributions is consistent with our prediction that at most only one Ca^{2+} channel opens in each AZ following a single AP stimulation. This same lognormal distribution was also observed after exposure to 400 nM CgTX; a treatment condition that reduced total calcium influx evoked by a single AP to 15.3 $\pm$ 3.3% of control. In contrast, for control terminals, the distribution of signal intensities from individual pixels was remarkably shifted to higher magnitude and took a more Gaussian shape (**Figure 3.4E**). I hypothesized that exposure to either 400 or 600 nM CgTX blocked sufficient numbers of Ca^{2+} channels in each active zone that imaged calcium signals were derived a great majority of the time from a single open channel. Under these conditions, I predict that transmitter release would be rare, but when it occurred, it would be triggered by sparse single channel openings.

Next, I carried out postsynaptic recording of end-plate potentials (EPPs) from the muscle fibers after exposure to either 600 nM or 400 nM CgTX to test whether a single AP could trigger transmitter release. In support of our hypothesis, I detected significant transmitter release from

nerve terminals after exposure to either 400 or 600 nM CgTX (**Figure 3.4F**). After exposure to

400 nM CgTX quantal content measured 15.1 ±8.8, while after exposure to 600 nM CgTX

quantal content was only 7.6 ±4.9. These values are much lower than what has been reported in

untreated control nerve terminals (~350; Katz and Melidi, 1979; Cho and Meriney, unpublished

observations), but suggest that isolated single Ca^{2+} channel openings can trigger transmitter

release from these presynaptic terminals.

3.4.4 Measuring the probability of transmitter release triggered by the calcium flux through a single Ca^{2+} channel opening

In order to evaluate transmitter release probability triggered by the opening of single Ca^{2+}

channels, I estimated the frequency of observing Ca^{2+} channel openings and normalized this

value to the number of AZs. Then I compared this value with the corresponding release

probability calculated from a single AZ under each treatment condition. For calculating Ca^{2+}

channel openings per AZ per AP, I limited our analysis to those nerve terminal regions where I

could clearly identify each active zone by postsynaptic labeling of acetylcholine receptors using

Alexa 594-conjugated α-bungarotoxin. As shown above in **Figure 3.4A**, 31 active zones can be

distinguished with the region of interest identified in this representative nerve terminal. After

exposure to 600 nM CgTX, I collected imaging data from 100 stimulus trials and calculated that

a single AP evoked an average of 0.23 Ca^{2+} channel openings per AZ. Similar results were

obtained from 8 nerve terminals and the mean number of openings evoked by a single AP was

0.18 ±0.07 per active zone (**Figure 3.5A**). This value was very close to our estimate of average

opening probability of individual Ca^{2+} channels, which provided further support for the

hypothesis that after exposure to 600 nM CgTX, the average number of available Ca^{2+} channels

A BTX labeling

B control

ΔF_s (%)

C 600 nM CgTX

ΔF_s (%)
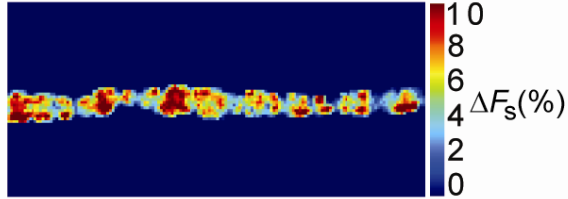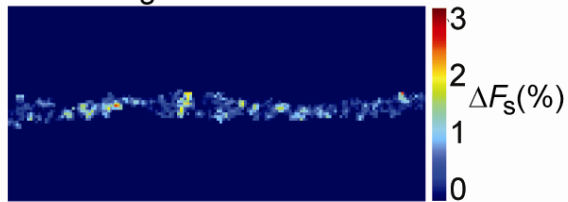
D opening of single channels

▲ trial1
□ trial2
● trial3
▲ trial4

E

— resting
— 600 nM CgTX
— 400 nM CgTX
— control

frequency (%)

Δf_s (%)

F

mEPPs

1 mV
100 ms

1 mV
10 ms

EPP
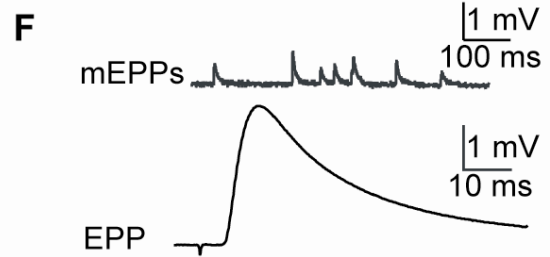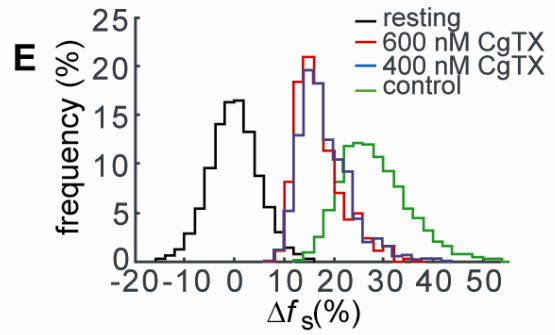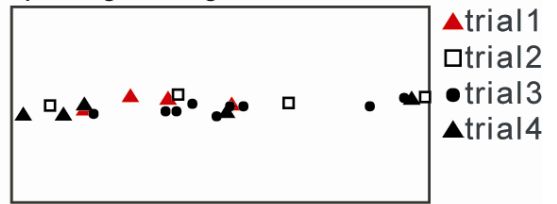
Figure 3.4 Imaging calcium entry through single Ca^{2+} channel openings at the frog motor nerve terminal.

(A)   Postsynaptic labeling of acetylcholine receptors is used for estimating the number of AZs in the corresponding presynaptic nerve terminal.

(B)   Average calcium signal for a representative control nerve terminal (100 stimuli at 0.5 Hz).

(C)   Average calcium signal remaining after block of presynaptic Ca^{2+} channels using a 60 minute exposure to 600 nM CgTX (100 stimuli at 0.5 Hz).

(D)   Representative display of the spatial location of imaged calcium entry sites after four single AP stimulus trials at low frequency. In this representation entry sites for each trial are depicted using a different symbol.

(E)   Histogram distribution of fluorescence intensity for pixels that detected calcium signals evoked by single AP stimulation at low frequency as compared with the distribution of pixel intensities in the resting nerve terminal. Exposure to 400 or 600 nM CgTX resulted in a distribution that took a lognormal form and was distinct from the distribution of resting intensities, and the distribution of intensities following stimulation under control conditions (no toxin block).

(F)   Representative recordings of mEPPs from a muscle fiber after exposure to 600 nM CgTX treatment (top), and averaged EPP response evoked by single nerve stimulation (bottom). Using these recordings, quantal content (QC) was calculated (QC = average EPP amplitude / average mEPP amplitude).

within single AZs is approximately reduced to 1. I also calculated the number of detected calcium entry sites for nerve terminals treated with 400 nM CgTX. In these experiments, I calculated that the number of Ca^{2+} channel openings per AZ per AP was 0.40 $\pm$0.11. This value is roughly double the value observed after treatment with 600 nM CgTX, which was consistent with a doubling in the measured total calcium entry that remained after block (15.3% vs 7% of control for 400 and 600 nM respectively). This linear relationship between block of Ca^{2+} entry and block of transmitter release when comparing these two relatively high concentrations of CgTX further supports the hypothesis that transmitter release under these conditions is triggered by the flux of Ca^{2+} through a single open Ca^{2+} channel.

Next I calculated the average release probability from single active zones following stimulation by a single AP. As I reported above, after a one hour exposure to high concentrations of CgTX, the quantal content (calculated using the direct method: EPP amplitude / mEPP amplitude) averaged 7.6 $\pm$4.9 per nerve terminal after exposure to 600 nM CgTX, and 15.1 $\pm$8.8 after exposure to 400 nM CgTX (n = 42 nerve terminals). I used confocal imaging of Alexa 594-conjugated α-bungarotoxin labeled postsynaptic folds, which are precisely aligned with presynaptic active zones, to measure the total number of active zones at each nerve terminal (Dittrich et al., 2009). The well-labeled postsynaptic folds were counted from brightest projection images taken from 27 motor nerve terminals. It was found that each frog motor nerve terminal had an average of 682 $\pm$338 active zones (mean $\pm$SD). By normalizing the quantal content to the average number of active zones within an entire frog motor nerve terminal, I can calculate the average release probability from individual active zones. Using this method, it was found that the release probability per AZ per AP was 0.5 for the control terminals, which was consistent with previous estimates (Katz and Meledi, 1979). After treatment with 600 nM or 400

nM CgTX, the average release probability per AZ per AP dropped to 0.011 or 0.022 respectively (see **Figure 3.5B**).

Finally, the probability that a single presynaptic Ca^{2+} channel opening would trigger synaptic vesicle release can be estimated by dividing the average number of release events per active zone (0.011 for 600 nM CgTX; see **Figure 3.5B**) by the average number of single calcium channel openings in each active zone (0.18 for 600 nM CgTX). Using this approach, I determined that the calcium flux through each isolated presynaptic Ca^{2+} channel opening triggers a vesicle fusion event about 6.1% of the time for the terminals treated with 600 nM CgTX.

3.4.5 Simulating transmitter release triggered by Ca^{2+} flux through a single Ca^{2+} channel opening

I also used our Monte Carlo simulation approach to examine the release of synaptic vesicles triggered when the number of Ca^{2+} channels in the active zone was reduced. Under the extreme conditions when very few Ca^{2+} channels were available, each simulated AP stimulation rarely opened Ca^{2+} channels, and most often only a single Ca^{2+} channel opened in the active zone. In these simulations, the probability that only a single Ca^{2+} channel opened clearly followed the binomial distribution. For example, if the total number of Ca^{2+} channels in each AZ was reduced to 3, the probability that only one channel opened per stimulation was predicted as $\frac{3!}{1! \times 2!} P^1 (1 - P)^2 = 0.37$ when P = 0.19. Indeed, I observed that 3823 out of 10,000 (38%, close to theoretical prediction) modeling runs (generated by distinct random number seeds) reported a single channel opening and 221 out of these released a synaptic vesicle. Therefore, the release probability per opening was equal to 5.8% (221/3823; see **Figure 3.6**), very close to our measured experimental
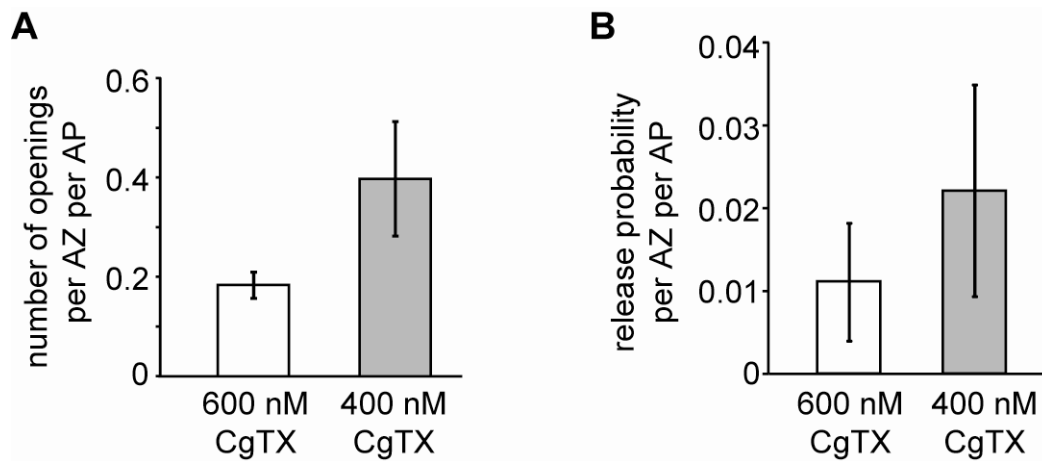
Figure 3.5 Ca^{2+} channel openings and transmitter release occur at low levels after exposure to a high concentration of CgTX

(A)   Normalized number of Ca^{2+} channel opening per AZ per AP after treatment with 400 nM or 600 nM CgTX.

(B)   Normalized release probability per AZ per AP after treatment with 400 nM or 600 nM CgTX determined by dividing the average quantal content under each treatment condition by the average number of active zones in adult frog cutaneous pectoris NMJs (700).

value (6.1%). For statistical analysis, I repeated the same procedure for the modeled AZs as I varied the total number of Ca^{2+} channels in the active zone (ranging from 1 to 10). In all cases, the results showed that the average release probability was 5.3 $\pm$ 0.3% (mean $\pm$ SD, n = 10) when only one Ca^{2+} channel opened per AZ per AP (see Table 5).

number of Ca^{2+} channel openings	1	2	3	4	5
total release probability (%)	5.3 $\pm$ 0.3	11.5 $\pm$ 0.8	18.9 $\pm$ 0.6	26.1 $\pm$ 3.7	33.6 $\pm$ 3.4
release probability per channel opening (%)	5.3 $\pm$ 0.3	5.8 $\pm$ 0.4	6.3 $\pm$ 0.2	6.5 $\pm$ 0.9	6.7 $\pm$ 0.7

Table 5: Simulated release probability from a single AZ in which the total number of Ca^{2+} channels is reduced.

I then asked whether additional channel openings in the active zone would affect release probability per opening. If each channel opening functioned nearly independently to trigger transmitter release, the release probability would be unaffected by the total number of Ca^{2+} channels that opened in the active zone. At the other extreme, if additional channel openings cooperate with one another to trigger synaptic vesicle release, release probability would increase with additional channel openings, perhaps even in a supralinear fashion. By addressing this question I further can test whether transmitter release is triggered predominately by the calcium flux through a single channel opening or by the summed flux through many Ca^{2+} channel openings in the active zone. As shown in **Figure 3.6** (and Table 5), the release probability per Ca^{2+} channel opening was little affected by the number of Ca^{2+} channels that opened in our modeled AZ. These data underscore the predominance of release triggered by calcium flux through a single open channel, even when several Ca^{2+} channels open in the active zone.
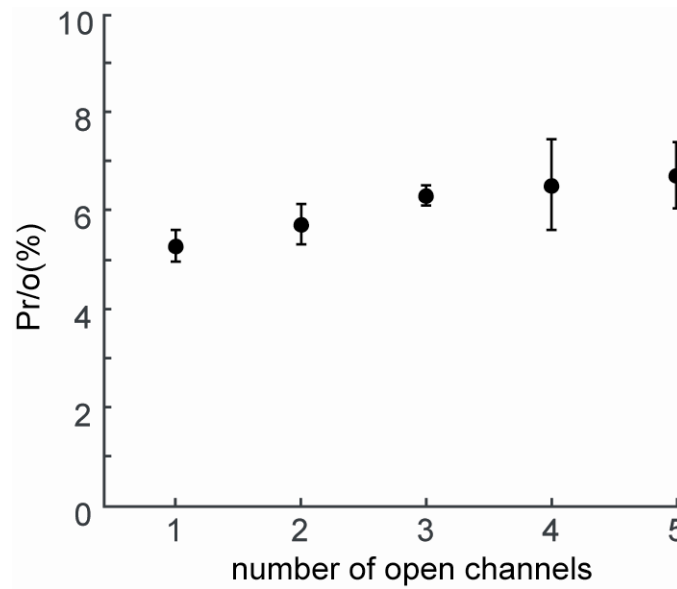
Figure 3.6 MCell modeling of the probability of transmitter release triggered by the opening of single Ca^{2+} channel.

Realistic simulations predict that release probability coupled with single Ca^{2+} channel openings is relatively small (5-6%), and remains relatively constant even as the number of open channels within an AZ increases.

3.4.6   Kinetics of transmitter release triggered by single Ca^{2+} channels

The kinetics of release is a major determinant of the timing of synaptic transmission and relies heavily on the coupling distance between presynaptic Ca^{2+} channels and the calcium sensor for exocytosis (Meinrenken et al., 2002; Lin and Faber, 2002). According to the results in the previous sections, transmitter release is controlled at the frog NMJ synapse primarily by calcium ions derived from the single, nearest Ca^{2+} channel in the active zone. Under this scenario, I would predict that the timing of transmitter release would be little affected by titrating a CgTX block as the normally tight Ca^{2+} channel release site topography would not be changed significantly. To test this idea, I compared the synaptic latency at control and 600 nM CgTX-treated motor nerve terminals. The release latency was measured as the interval between the stimulus artifact of the pulse triggering nerve stimulation and the onset of the EPP. This measure includes both the nerve conduction time and the synaptic delay between nerve depolarization and transmitter release. As shown in **Figure 3.7A**, exposure to 600 nM CgTX for one hour did not alter the synaptic latency as compared to control, indicating a similar distribution of latencies for transmitter release when release is triggered by a single Ca^{2+} channel opening as compared to the full complement of channels normally present in the active zone. These results were also predicted by our modeling work (Figure 3.7B). As the number of Ca^{2+} channels was reduced, the synaptic latency remained constant. These results are consistent with our conclusion that transmitter release at the frog NMJ synapse is primarily determined by the calcium flux through individual Ca^{2+} channel openings and that these channels are tightly associated with the synaptic vesicle that fuses. The unchanged synaptic latency observed after CgTX treatment was in sharp contrast to the effects of lowering extracellular calcium, which significantly increased the synaptic latencies (**Figure 3.7C**). These effects are also predicted by our model and consistent

97
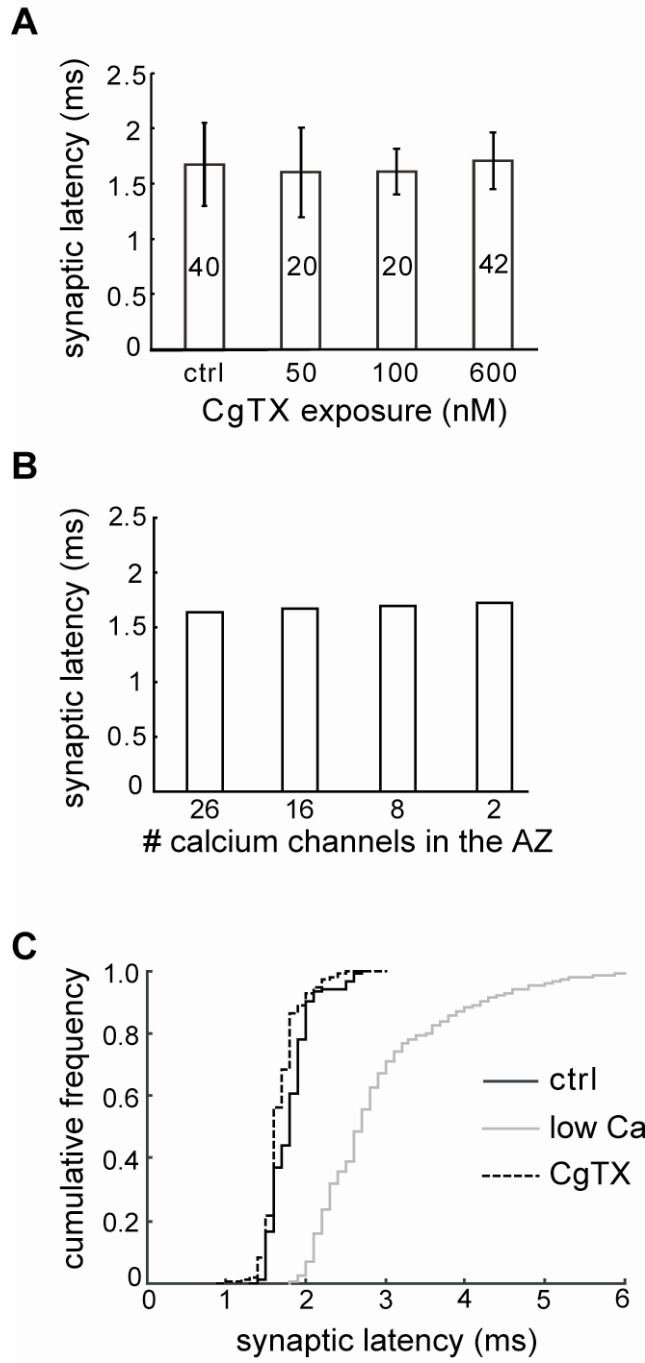
Figure 3.7 Synaptic latency remains constant after exposure to different doses of CgTX.

(A)   There was no difference in synaptic latency detected after single AP-evoked EPPs recorded before and after application of various doses of CgTX. The numbers in the bar are the total number of muscle fibers recorded for each experimental condition.

(B)   MCell computer simulations of synaptic latency remains constant as the number of available Ca^{2+} channels in the active zone is randomly reduced. Note the simulated synaptic latency does not include the conduction delay and time for postsynaptic response, these can be predicted to be less than 100 μs.

(C)   Representative example of the distribution of synaptic latencies in control, 600 nM CgTX, and low extracellular calcium conditions. No change was detected when comparing control and 600 nM CgTX, but synaptic latency increased when extracellular calcium was lowered.

with the idea that synaptic latency is very sensitive to the local concentration of calcium around docked synaptic vesicles (Bollmann et al., 2000; Schneggenburger and Neher, 2000).

3.5   DISCUSSION

In this chapter, I have provided evidence that the calcium flux through a single open voltage-gated Ca^{2+} channel at the frog motor nerve terminal can be imaged directly, and that such calcium flux is sufficient to trigger synaptic vesicle fusion with fast kinetics.

3.5.1   Imaging single Ca^{2+} channel openings within a single active zone

Optical single-channel recording of Ca^{2+} influx has been achieved previously by imaging Ca^{2+}-evoked fluorescence transients using a variety of optical techniques (Zou et al., 1999; Wang et al., 2001; Demuro and Parker, 2006). Functional studies of single Ca^{2+} channels controlling neurotransmitter release have primarily relied on patch clamp recordings from non-synaptic regions of the neuron. However, one previous study used cell-attached patch clamp recordings from the release face of the chick ciliary ganglion calyx nerve terminal (Stanley, 1993) and reported that a unitary Ca^{2+} channel opening (activated by ramps or steps to -30~-40 mV with an elevated extracellular calcium concentration of 6 mM) could cause quantal secretion. I have extended these studies to determine whether a single Ca^{2+} channel opening evoked by an action potential under physiological conditions would normally trigger synaptic vesicle fusion at the frog NMJ. Taking advantage of the linear spatial organization of presynaptic Ca^{2+} channels within hundreds of regularly spaced active zones at the adult frog NMJ, and high resolution

fluorescence imaging techniques, I have shown that the calcium influx through single Ca^{2+} channels under physiological conditions can be measured directly and that these openings can trigger the fusion of synaptic vesicles in the frog NMJ active zone.

3.5.2 Coupling of Ca^{2+} channels to transmitter release at presynaptic active zones

An ongoing debate centers on whether individual synaptic vesicle release is triggered by calcium flux through a single open Ca^{2+} channel that is tightly associated with the vesicle, or by multiple open Ca^{2+} channels in the active zone. Since the spatial relationship between docked synaptic vesicles and presynaptic Ca^{2+} channels is not known at most synapses, most studies rely on the measurement of the power relationship between transmitter release and calcium entry by altering the number of available Ca^{2+} channels using selective toxins or altered action potential waveforms (Yoshikami et al., 1989; Augustine, 1990; Mintz et al., 1995; Wu et al., 1999). Conceptually, the effectiveness of gradual Ca^{2+} channel blockade or activation on transmitter release is determined by the spatial relationship between Ca^{2+} channels and the calcium sensor, and therefore reflects the cooperativity (m) of Ca^{2+} channels in controlling vesicle secretion. This value of m has been shown to vary for different synapses and different subtypes of Ca^{2+} channels at a single synapse. For example at cerebellar parallel fiber synapses, Mintz et al. (1995) have determined that transmitter release triggered by N-type Ca^{2+} channels has an m value of 2.5, whereas when transmitter release is triggered by P/Q type Ca^{2+} channels m equals 4.0. Similarly, at the Calyx of Held synapse, the P/Q type Ca^{2+} channels control transmitter release more effectively ($m = 3.7$) than N-type Ca^{2+} channels ($m = 1.3$; Wu et al., 1999), and these m values can change with development of the synapse (Fedchyshyn and Wang, 2005), presumably as spatial relationships between Ca^{2+} channels and docked vesicles tighten.

However, at cultured hippocampal neurons, transmitter release triggered by either N-type or P/Q-type Ca^{2+} channels has a similar m value (~2.5) (Reid et al., 1998). At the chick ciliary ganglion calyx, where N-type channels trigger release, m equals 1.3 (Gentile and Stanley, 2005). Such a large variability in the cooperative degree to which Ca^{2+} channels couple to neurotransmitter release indicates a wide variety of spacing distances between elements within individual release sites at different synapses. Lower values of m (1~2) suggest that one or two open Ca^{2+} channels are sufficient for triggering the fusion of a synaptic vesicle which may be tightly associated with those open channels. In contrast, higher values of m (4~5) may indicate that many Ca^{2+} channels need to open simultaneously to contribute the calcium ions required to trigger the release of a single synaptic vesicle. Under these conditions, the Ca^{2+} channel cooperativity measurement is governed by the molecular cooperativity of the calcium sensor (Dodge and Rahamimoff, 1967) as titrating channel block is essentially similar to changing extracellular calcium concentration (Meinrenken et al., 2002).

At the adult frog neuromuscular junction, there have been two previous studies that have reached conclusions similar to the ones I have presented here. Yoshikami et al (1989) titrated the block of transmitter release using ω-conotoxin MVIIa (CmTX), another antagonist that reversibly blocks N-type Ca^{2+} channels with less potency than CgTX. In the Yoshikami et al (1989) study, calcium influx was not measured, but the fraction of Ca^{2+} channel block was estimated by assuming a similar K_d for Ca^{2+} channel block to that determined based on the block of transmitter release. Curve fitting with theoretical modeling of various channel cooperativity values (1-4) showed that the data fit best assuming that a single Ca^{2+} channel mediates the release of a single synaptic vesicle. In another study, Shahrezaei et al (2006) concluded that calcium ions from one or two Ca^{2+} channels cooperate to trigger neurotransmitter release at the

adult frog NMJ by simultaneously measuring the reduced calcium influx and postsynaptic potential after the application of a high concentration of CgTX, although they did not attempt to detect the imaged calcium flux through individual open Ca^{2+} channels, or study synaptic vesicle fusion triggered by a single open channel.

Using our MCell simulation approach, based on parameters constrained by our physiological data, I have fully investigated stoichiometric relationships between presynaptic Ca^{2+} channels and synaptic vesicles at adult frog NMJ synapses. In agreement with previous reports, I have shown that the steady-state calcium release relationship observed after exposure to various concentrations of CgTX exhibits a low power order (~2) that approaches 1 after exposure to very high concentration of CgTX. Consistently, the modeling data predicts that each fused synaptic vesicle bound calcium ions from an average of 2 open Ca^{2+} channels at control terminals (even though 4~5 Ca^{2+} channels open following each AP stimulation). However, tracing the origin of each calcium ion that bound synaptic vesicles triggered to fuse revealed that, in almost all cases, the single open Ca^{2+} channel tightly-associated with the vesicle contributed more than 80% of calcium ions bound. This means that even though the calcium flux through 2 Ca^{2+} channels commonly triggers release, the flux through only one of these channels predominated. Further, about one third of synaptic vesicle fusion events are triggered by calcium ions derived only from a single open channel and this percentage greatly increases as the number of available Ca^{2+} channels is reduced. Most importantly, by imaging the calcium influx through single open channels, I have provided direct evidence that isolated individual Ca^{2+} channel openings can evoke neurotransmitter release under physiological conditions. Based on this work, I predict that this type of coupling between presynaptic Ca^{2+} channels and vesicle fusion will predominate at synapses in which there is a relatively low probability of Ca^{2+} channel

opening during an action potential and a tight spatial relationship between Ca^{2+} channels and docked vesicles.

4.0   GENERAL DISCUSSION

4.1   SUMMARY OF FINDINGS

The major work presented in this dissertation is the quantitative analysis of presynaptic Ca^{2+} channels and their functional contribution to AP-evoked transmitter release, combining experimental data with Monte Carlo simulations, at a sub-active zone level. Based on these results, I propose the following working model of Ca^{2+}-triggered secretion within active zones at the adult frog NMJ. Only a small fraction (~15%) of the 200~250 intramembraneous particles observed at individual active zones by electron microscopy are functional Ca^{2+} channels, and these channels open with a very low probability during an AP (~0.2). The number of docked synaptic vesicles at a single active zone is about the same as the number of Ca^{2+} channels, suggesting that each vesicle may be tightly associated with a single Ca^{2+} channel. Such vesicle-Ca^{2+} channel topography is consistent with the realistic simulation results which indicate that a single Ca^{2+} channel adjacent to a synaptic vesicle primarily controls the exocytosis of that vesicle. My research further shows that the Ca^{2+} flux through a single Ca^{2+} channel opening is sufficient to trigger vesicle release, but at a relatively low probability (~5%). Together with the prediction that only 7-8 Ca^{2+} channels open within an active zone, this provides a mechanism underlying the low release probability from a single active zone following an AP stimulation at the frog NMJ synapse.

4.2   FUNCTIONAL ORGANIZATION OF PRESYNAPTIC ACTIVE ZONES

As described above, active zones are specialized regions of presynaptic nerve terminals where synaptic vesicle fusion is triggered by the AP-evoked Ca^{2+} flux through voltage-gated Ca^{2+} channels. The highly organized structure and molecular assembly of the active zone are designed to bring Ca^{2+} channels and docked synaptic vesicles into close proximity to one another as these are crucial components for presynaptic function (Rosenmund et al., 2003; Zhai and Bellen, 2004; Harlow et al., 2001).

4.2.1   Spatial organization of voltage-gated Ca^{2+} channels

At the nerve terminal, numerous studies have demonstrated that voltage-gated Ca^{2+} channels are restricted to active zone regions where transmitter is released, although it remains unclear whether or not Ca^{2+} channels are also present elsewhere throughout presynaptic terminals. The fast neurotransmitter release evoked by an AP, and the ineffectiveness of slow calcium buffers such as EGTA on neurotransmitter release at some synapses, support the idea that presynaptic Ca^{2+} channels must be located very close to the release sites, presumably in active zones. The best evidence for exclusive localization of Ca^{2+} channels within presynaptic active zones is provided by the staining of N-type Ca^{2+} channels using fluorescently labeled CgTX at the frog motor nerve terminals. In these studies, it is evident that fluorescently stained N-type Ca^{2+} channels are aligned perfectly with the postsynaptically labeled acetylcholine receptors (Robertaille et al., 1991; Cohen et al., 1991, see **Figure 1.5**). At *Drosophila* motor nerve terminals, transgenic expression of EGFP-tagged *cac* gene, which encodes the α1 subunit of a primary Ca^{2+} channel responsible for transmitter release, allows *in vivo* analysis of Ca^{2+} channel

localization at presynaptic nerve terminals (Kawasaki et al., 2004). Localization of Ca^{2+}

channels in this preparation has been visualized within active zones, but not distributed

throughout the presynaptic nerve terminals (Kawasaki et al., 2004). Furthermore, disruption of

Bruchpilot, a Drosophila protein showing some homology to the mammalian active zone protein

CAST, results in a severe reduction in the density of presynaptic Ca^{2+} channels at active zone

and an accompanying defective coupling of Ca^{2+} influx with synaptic vesicle fusion (Kittel et al.,

2006).

In contrast to the strong evidence for the localization of Ca^{2+} channels at presynaptic

active zones, little is known about the molecular mechanism underlying the active zone targeting

of Ca^{2+} channels. Multiple types of voltage-gated Ca^{2+} channels are expressed in the vertebrate

nervous system (see **Figure 1.3**). Proper targeting of distinct voltage-gated Ca^{2+} channels into

different sub-cellular compartments of the neuron is critical for their specific functioning during

neuronal activity. It is generally accepted that two types of voltage-gate Ca^{2+} channels (N and

P/Q) are most important in controlling fast neurotransmitter release from nerve terminals and are

enriched in their subcellular distribution to presynaptic active zones (Dunlap et al., 1995;

Catterall, 2000; Catterall and Few, 2008). At present, two cytoplasmic domains of presynaptic

Ca^{2+} channels have been identified and implicated in selective targeting to the nerve terminal. In

cultured hippocampal neurons, it has been proposed that a splice variant of N-type Ca^{2+} channels

containing PSD and SH3 domain-binding motifs in the C-terminus of the α1B subunit

specifically localizes to synapses through an interaction with the active zone specific proteins

Mint 1 and CASK (Maximov and Bezprozvanny, 2002). At an invertebrate synapse (*Lymnaea*),

Mint 1 and CASK are also required for presynaptic targeting of voltage-gated Ca^{2+} channels

(Spafford et al., 2003; Spafford and Zamponi, 2003). Interestingly, it has also been shown that

there is a specific splice variant of N-type Ca^{2+} channels that is mainly restricted to synapses of nociceptive neurons in the dorsal root ganglion (Bell et al., 2004). However, deletion of a homologous region of the α1A subunit has no effect on presynaptic targeting of P/Q type Ca^{2+} channels, suggesting different mechanisms for selective localization of N- and P/Q type Ca^{2+} channels at the nerve terminal (Hu et al., 2005). Secondly, a synprint motif in the cytoplasmic loop connecting domains II and III of α1A/B subunit has been shown to be necessary and sufficient for presynaptic targeting of N- and P/Q-type Ca^{2+} channels in superior cervical ganglion neurons (Mochida et al., 2003a and b), while in cultured hippocampal neurons, the synprint motif is necessary but not sufficient for presynaptic targeting of Ca^{2+} channels (Szabo et al., 2006). Interference of such interaction with injected synprint peptide reduces Ca^{2+} efficacy in triggering transmitter release, which may be caused by a reduction in Ca^{2+} channel density in nerve terminals due to improper targeting. However, it may also involve the disrupted organization of docked synaptic vesicles relative to other active zone proteins and the Ca^{2+} entry site (Keith et al., 2007). In summary, the precise molecular mechanisms underlying presynaptic targeting of N- and P/Q type are not well defined.

It seems that not all presynaptic Ca^{2+} channels are limited to the active zone. Several studies have shown that R-type Ca^{2+} channels are also present at the presynaptic terminal and may contribute to transmitter release. In the calyx of Held synapse, R-type Ca^{2+} channels contribute ~25% of the total Ca^{2+} influx during a presynaptic AP but only evoke a postsynaptic current of ~1% of control (Wu et al., 1998). This low efficacy in triggering transmitter release is consistent with the immunohistochemical finding of distant location of R-type Ca^{2+} channels relative to the release site (Wu et al., 1998, 1999). At the giant mossy fiber synapses in the CA3 area of hippocampus, R-type Ca^{2+} channels are also excluded from active zones and not involved

108

in fast synaptic transmission or paired-pulse facilitation (Dietrich et al., 2003). Interestingly, however, these R-type Ca^{2+} channels play an important role in the induction of mossy fiber LTP and posttetanic potentiation elicited by brief titanic stimulation (Dietrich et al., 2003). Since the R-type Ca^{2+} channel α1 subunit does not have the synprint motif, the molecular determinants for presynaptic targeting, yet active zone exclusion, of R-type Ca^{2+} channels remain unknown. Differential localization of various types of Ca^{2+} channels at the presynaptic nerve terminals may also by regulated due to some type of competition among Ca^{2+} channel subtypes for a limited number of 'channel slots' at release sites (Cao et al., 2004), the molecular identity of which remains to be characterized.

The Ca^{2+} transient at a release site can be significantly influenced by the geometric pattern of Ca^{2+} channel distribution in the active zone (assuming more than one channel opens with each action potential stimulation), and by the stoichiometric relationship between these Ca^{2+} channels and the Ca^{2+} sensor for transmitter release at release sites. But the spatial organization of most presynaptic Ca^{2+} channels has not been determined. Unfortunately, without this knowledge, the Ca^{2+} signal at the release site and the resultant release probability of the vesicle cannot be quantified, even when Ca^{2+} current amplitude, the biochemical properties of the cytoplasm, and the sensitivity of the Ca^{2+} sensor for release are known (Neher, 1998; Christopher et al., 2003).

Here I have taken advantage of the unique morphological features of the frog motor nerve terminal to explore the functional organization of Ca^{2+} channels at presynaptic active zones by first estimating the total number of Ca^{2+} channels within an entire active zone. The studies described above (Chapter 2) have shown that there are only 30~36 Ca^{2+} channels within individual active zones, which constitute a small proportion (~15%) of total intramembraneous

particles (200-250) observed in freeze-fracture replicas of the active zone. One implication of this finding is that the total number of presynaptic Ca^{2+} channels coincides roughly with the number of docked synaptic vesicles. This quantitative relationship suggests the interesting possibility that each docked synaptic vesicle is tightly associated with only a single voltage-gated Ca^{2+} channel (see next section). Although the idea that Ca^{2+} channels are homogenously distributed over the entire active zone is consistent with the known highly ordered structure of the release machinery within these active zones (Harlow et al., 2001), there still exists the possibility that Ca^{2+} channels are heterogeneously distribution along the active zone. This issue might be solved directly by applying sub-diffraction resolution microscopy techniques, such as STED (stimulated emission depletion; Kittle et al., 2006; Willig et al., 2006), which may provide the necessary optical resolution to differentiate individual Ca^{2+} channels separated from one another by ~40 nm. Using atomic force microscopy scanning of CgTX-tagged Ca^{2+} channels at the calyciform synapse of the chick ciliary ganglion, identified Ca^{2+} channels near the release face exhibit short linear or parallel linear array organization (Haydon et al., 1994). Recently, it has been shown that a similar organization of presynaptic Ca^{2+} channels within single AZs might exist at mouse NMJ (Nagwaney et al., 2009). Indeed, two parallel "double rows" of intramembraneous particles, which are ~80 nm long, have been observed on the replicas of freeze-fractured presynaptic membrane of mouse NMJ (Fukuoka et al., 1987). A reduction and disorganization of intramembraneous particles at active zone has been found in Lambert-Eaton myasthenic syndrome (LEMS), an autoimmune disease in which LEMS IgG attack the putative voltage-gated Ca^{2+} channels and therefore disrupt neuromuscular transmission (Fukuoka et al., 1987; Nagel et al., 1988; Vincent et al., 1989). It would be attractive to apply the experimental approaches described in this thesis to the mouse NMJ in the future and explore the number of

voltage-gated Ca^{2+} channels, which in this case are P/Q-type, and their opening probability during an AP. Such a study should provide important information that would increase our understanding of the spatial arrangement of Ca^{2+} channels at a neuromuscular active zone of different species, and the functional impact of such organizational differences in active zone structure on synaptic efficacy (Slater, 2008).

4.2.2 Topographic organization of Ca^{2+} channels and docked synaptic vesicles

Since Bernard Katz and his collaborators formulated the calcium hypothesis (Katz, 1969), it has been well established that Ca^{2+} ions are essential in triggering fast neurotransmitter release from presynaptic active zones of the nerve terminal. It has been further recognized that the characteristics of neurotransmitter release at a given synapse are precisely governed by the amplitude and spatiotemporal profile of AP-evoked Ca^{2+} transients within active zones (Barrett and Stevens, 1972; Llinas et al., 1981; Meinrenken et al., 2003; Bollmann et al., 2005). A large number of experimental and computational studies have suggested that such Ca^{2+} signals may last only a fraction of millisecond, with a rapid rise and fall as Ca^{2+} channels open and close rapidly following an AP (Yazejian et al., 1997; Sabatini and Regehr, 2002; Bischofberger et al., 2002). Furthermore, it has been proposed that these Ca^{2+} signals are spatially localized within the vicinity of open Ca^{2+} channels (Simon and Llinas, 1985; Yamada and Zucker, 1992), primarily due to the existence of a high concentration of Ca^{2+} buffer inside the terminal (Neher, 1998). Unfortunately, critically important information related to these hypotheses is lacking at most synapses, including the total number of Ca^{2+} channels, their spatial distribution at presynaptic active zones, and hence the stoichiometric and geometric relationship between Ca^{2+}

111

channels and synaptic vesicles. As a result, the quantitative characteristics of Ca^{2+} signals that trigger fast neurotransmitter release are still debated.

To aid in my discussion of Ca^{2+} channel-vesicle topography, I will clearly define two terms that are often used when discussing AP-evoked intracellular Ca^{2+} transients: "nanodomain" and "microdomain". These terms are used to distinguish two types of Ca^{2+} signals in functional studies at different synapses (Augustine 2001; Neher and Sakaba, 2008). Typically, a "nanodomain" is defined either as the localized Ca^{2+} signal at the mouth of a single open Ca^{2+} channel or as the localized Ca^{2+} signal in the immediate vicinity of a tight cluster of Ca^{2+} channels that open simultaneously, within the spatial dimension of ~10-100 nm (Neher and Sakaba, 2008). Because the size of a nanodomain is well below the diffraction limit of optical microscopy, this local Ca^{2+} signal is inaccessible for direct Ca^{2+} imaging study. Mathematical modeling of single Ca^{2+} channels predicts that at the mouth of open Ca^{2+} channels the nanodomain Ca^{2+} concentration can reach as high as ~100-200 μM (Neher, 1998). If a synaptic vesicle is located within this nanodomain, the influx of Ca^{2+} through a single open Ca^{2+} channels would be sufficient to trigger vesicle fusion and transmitter release. Using powerful computers and advanced quantitative modeling of buffered Ca^{2+} diffusion, many theoretical studies have explored the impact of single Ca^{2+} channel openings on the release probability of synaptic vesicles locating at various distances (Zucker and Fogelson, 1986; Yamada and Zucker, 1992; Chow et al. 1994; Cooper et al. 1996; Klingauf and Neher, 1997; Bennett et al. 2000; Gil et al. 2000). It has also been demonstrated experimentally that this nanodomain scenario might exist at several synaptic preparations. For example, at the squid giant synapse, injection of BAPTA, a Ca^{2+} chelator with fast kinetics, but not EGTA, a slow chelator, can efficiently block Ca^{2+}-triggered neurotransmitter release, indicating that synaptic vesicles are tightly coupled to the

112

Ca^{2+}-entry sites (Alder et al., 1991). Increasing the number of open Ca^{2+} channels by broadening the AP causes a linear increase in release probability, which lends strong support to the hypothesis that each open Ca^{2+} channel functions independently in controlling synaptic vesicle fusion (Augustine, 1990). Furthermore, the relative efficacy of BAPTA derivatives with different Ca^{2+} affinity in blocking transmitter release suggests that the AP-evoked peak Ca^{2+} transient may be on the order of 100 μM or greater (Alder et al., 1991; Augustine et al., 1991). A similar scenario has been observed at several other synapses, including the frog NMJ, and the ribbon synapse of the bipolar cell in the goldfish retina (Yoshikami et al., 1989; Heidelberger et al., 1994; von Gersdorff and Matthews, 1994; Burrone et al., 2002). The well documented direct interactions between SNARE proteins and N (or P/Q) type Ca^{2+} channels also support the idea that synaptic vesicles are close enough to active zone Ca^{2+} channels that nanodomain coupling could occur (Spafford and Zamponi et al., 2003; Few and Catterall, 2008). In fact, Stanley (1993) has reported that the flux of Ca^{2+} through a single open channel can stimulate a vesicle to fuse with plasma membrane at the chick ciliary ganglion calyx nerve terminal, providing direct support that the nanodomain produced by the flux of Ca^{2+} through a single Ca^{2+} channel opening is sufficient to trigger neurotransmitter release.

On the other hand, microdomain Ca^{2+} signals are produced by the summed Ca^{2+} entry through multiple open Ca^{2+} channels that are not tightly associated with one another or the vesicle release sites in an active zone, with a spatial dimension ranging from 100 nm to 1 μm (Sakaba and Neher, 2008). This situation is observed at the immature rat calyx of Held synapse, in which strong experimental evidence supports the hypothesis that neurotransmitter release is triggered by a microdomain of Ca^{2+} that is contributed by multiple open Ca^{2+} channels that appear to be loosely coupled to transmitter release sites (Borst and Sakmann, 1996, 1999; Wu et

al., 1999; Ballmann et al., 2000; Schneggenburger and Neher, 2000). First, it has been found that intraterminal injection of EGTA is almost as effective as BAPTA in attenuating transmitter release at this synapse, which indicates a relatively long distance between synaptic vesicles and the open Ca^{2+} channels (Borst and Sakmann, 1996). Second, a Ca^{2+} concentration of 20~30 μM produced by the Ca^{2+} uncaging technique is able to trigger fast transmitter release in a manner that is roughly equivalent to that evoked by an AP (Ballmann et al., 2000; Schneggenburger and Neher, 2000). Third, the release of a given synaptic vesicle is likely under the control of multiple types of voltage-gated Ca^{2+} channels (Wu et al., 1999). Finally, broadening the AP, which increases the number of open Ca^{2+} channels, leads to a superlinear change in release probability (Fedchyshyn and Wang, 2005). All these results are consistent with the idea that a Ca^{2+} microdomain, produced by many loosely coupled open Ca^{2+} channels, is responsible for initiating transmitter release at the immature calyx of Held synapse.

It should be noted, however, that the distinction between nanodomain and microdomain Ca^{2+} signals is not clear-cut, but complicated by many factors including the concentrations and kinetics of endogenous Ca^{2+} buffers, and the clustering pattern of Ca^{2+} channels at a particular synapse. Synaptic vesicles may dock at locations within an active zone region that have various coupling distances to Ca^{2+} entry sites. This type of non-uniform topographic relationship produces a large variability in the Ca^{2+} transient sensed by different vesicles, which may consequently lead to a vast heterogeneity in their release probability during an AP. Indeed, a numerical model that reproduced most experimental data of the calyx of Held synapse has predicted that vesicles locating at various distances would be released with probabilities that are inversely related to coupling distances, and range from 100% to less than 1% (Meinrenken et al., 2002). Interestingly, as the calyx of Held synapses mature during development, the effectiveness

114

of injecting EGTA in attenuating transmitter release decreases remarkably, suggesting a potential transformation of release site topography from microdomain to nanodomain (Fedchyshyn and Wang, 2005).

Therefore, it appears that Ca^{2+} signals that trigger transmitter release from different synapses can vary dramatically, with effective concentrations of Ca^{2+} ranging from as low as ~10 μM to as high as ~200 μM. Such variability is in part due to differences in the spatial arrangement of Ca^{2+} channels relative to the Ca^{2+} sensor proteins. Along these lines, by depleting fast-releasing vesicles during short term synaptic depression, it has been shown that the remaining vesicles have relatively high Ca^{2+} sensitivity and can be released rapidly by uniformly elevated Ca^{2+} using an uncaging technique, but not by the Ca^{2+} signal produced by an AP stimulus. This argues for a long distance between remaining competent synaptic vesicles and Ca^{2+} entry sites (Wadel et al., 2007). However, an alternative model which assumes an intrinsic heterogeneity of vesicles with different sensitivity of Ca^{2+} sensors may also explains the characteristics of release under these conditions (Trommershauser et al. 2003). Therefore, a determination of the spatial arrangement of Ca^{2+} channels in an active zone, and the topographical relationship between these Ca^{2+} channels and docked synaptic vesicles will be essential for differentiating these possibilities.

It remains unclear what mechanisms dictate the spatial coupling between Ca^{2+} channels and Ca^{2+} sensors in a particular synapse, and what functional significance a given topography might have to the control of neurotransmitter release and synaptic plasticity. One key insight may come from a parallel comparison of synapses between different types of interneurons and granule cells in the dentate gyrus of hippocampus. Cholecystokinin (CCK)-expressing interneurons form GABAergic synapses onto proximal dendrites of granule cells, whereas

parvalbumin (PV) interneurons innervate primarily the perisomatic region of granule cells (Hefft and Jonas, 2005). There are prominent differences in the functional characteristics of GABA release from CCK interneuron-granule cell synapses and from PV interneuron-granule cell synapses. First, neurotransmitter release from PV interneurons is more synchronous and faster as compared to CCK interneurons. Second, the GABA release from CCK interneurons is mediated exclusively by the Ca^{2+} influx through N-type Ca^{2+} channels, whereas GABA release from PV interneurons is controlled predominately by P/Q type Ca^{2+} channels (Hefft and Jonas, 2005). Third, bath application of 100 mM EGTA-AM abolished GABA release from CCK interneurons, but had no significant effect on fast transmitter release at PV interneuron-granule cell synapses. These data suggest a longer diffusion distance between Ca^{2+} entry sites and synaptic vesicles in CCK interneuron nerve terminals. Indeed, a nanodomain coupling between Ca^{2+} channels and Ca^{2+} sensors has been hypothesized at the PV interneuron-granule cell synapse (Bucurenciu et al., 2008). Distinct topographic organization of release sites at these two synapses is consistent with their respective features of transmitter release in response to single APs or high-frequency bursts of APs. In this regard, the nanodomain signaling at PV interneuron-granule cell synapses is thought to secure fast and efficient transmitter release from PV interneurons to their targets, which may provide a phasic inhibitory signal to synchronize the activity of principle cells in neuronal circuits (Hefft and Jonas, 2005; Bucurenciu et al., 2008). On the other hand, the microdomain signaling that appears to predominate at CCK interneuron-granule cell synapses may produce tonic inhibition on the principle cells (Hefft and Jonas, 2005).

4.3   FUNCTIONAL IMPLICATIONS OF ACTIVE ZONE ARCHITECTURE IN QUANTAL RELEASE

Remarkably, a single impulse at the motor nerve terminal normally triggers the release of hundreds of quanta, which is much more than that is required to bring the postsynaptic muscle fiber above threshold. The excess quanta released act as a "safety factor" ensuring the reliability of synaptic transmission between motor neurons and muscle cells, even during high frequency bursts of activity (Wood and Slater, 2001). What remains unknown is the biological mechanism controlling the number of quanta being released by a single AP in a given NMJ in different animal species. The frog NMJ has a unique and highly organized structure for effective synaptic transmission. The presynaptic nerve terminal consists of hundreds of linear active zones at a regularly spaced interval of ~1 µm. A single active zone, ~1 µm long, contains a linear array of ~200-250 intramembraneous particles and 25-40 docked synaptic vesicles lining up along both outside edges of the intramembraneous particle array (Pawson et al., 1998; Harlow et al., 2001; Rizo and Betz, 2005). It appears that only a small fraction of the intramembraneous particles (~15%) are Ca^{2+} channels, which is roughly equivalent to the number of docked synaptic vesicles, suggesting that each vesicle may be tightly associated with a single Ca^{2+} channel at the frog NMJ (Chapter 2). In contrast, the NMJs in mammals and lizards have a rather different structure and active zone organization. For example, the mouse NMJ consists of many swellings or boutons, each with an area of ~5-10 μm^2 that contain about 15-20 active zones (Slater, 2008). At these mammalian NMJs, each active zone is about ~100 nm long and contains ~20 intramembraneous particles and 2 vesicles docked in the middle of two double rows of intramembraneous particles (Nagwaney et al., 2009; see **Error! Reference source not found.**).

117

It might be expected that these different NMJ active zone structures may determine different release characteristics of neuromuscular transmission. In the frog NMJ, a single AP triggers the release of ~350 quanta from a total of ~700 active zones (Cho and Meriney, unpublished observations). Therefore, on average, each active zone releases one vesicle in response to every other AP. At a typical mouse NMJ, there are ~400-600 active zones, and quantal content is ~40-60. Under these conditions, one vesicle may be released from each active zone following one out of 10 AP stimuli. Considering that each active zone docks only 2 synaptic vesicles at the mouse NMJ, the release probability of individual vesicles is ~5%, nearly three-fold higher than that in frog NMJ active zone (1.6%). Assuming the same percentage of Ca^{2+} channels among 15-20 intramembraneous particles at the mouse NMJ, the higher release probability of synaptic vesicles is consistent with a tighter stoichiometric relationship, or coupling, between Ca^{2+} channels and synaptic vesicles that run down the middle of the active zone intramembraneous particle array. In this situation, docked vesicles would be in close proximity to more Ca^{2+} channels. It would be interesting to perform similar Ca^{2+} imaging experiments and variance analyses as described in this dissertation to estimate the number of Ca^{2+} channels and their opening probability during an AP at the mouse NMJ. This should provide important information for further comparisons and understanding of structure-function relationships in active zones.

Frog active zone

Mammalian active zone

N type Ca²⁺ channel

K$_{Ca}^+$ channels and other AZ proteins

P/Q type Ca²⁺ channel

Adapted from Urbano et al., 2003
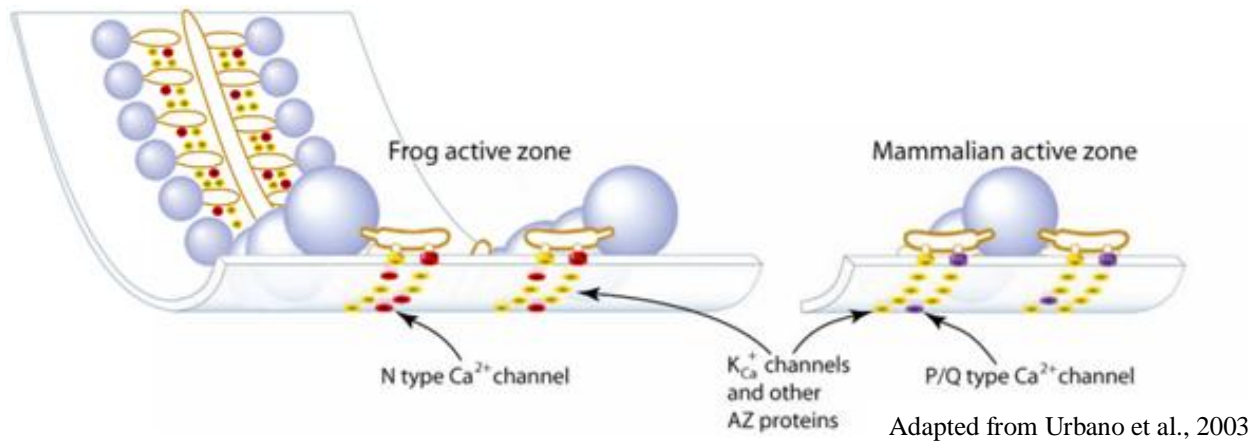
Figure 4.1 The architecture of active zone at frog and mouse neuromuscular junctions.

BIBLIOGRAPHY

Adler EM, Augustine GJ, Duffy SN, Charlton MP (1991) Alien intracellular calcium chelators attenuate neurotransmitter release at the squid giant synapse. J Neurosci 11:1496-1507

Albritton NL, Meyer T, Stryer L (1992) Range of messenger action of calcium ion and inositol 1,4,5-triphosphate. Science 258:1812–1815

Augustine GJ (2001) How does calcium trigger neurotransmitter release? Curr Opin Neurobiol 11: 320-326

Augustine GJ, Neher E (1992) Neuronal Ca^{2+} signalling takes the local route Curr Opin Neurobiol 2:302-307

Augustine GJ, Santamaria F, Tanaka K (2003) Local calcium signaling in neurons. Neuron 40: 331–346

Augustine GJ (1990) Regulation of transmitter release at the squid giant synapse by presynaptic delayed rectifier potassium current J Physiol (Lond) 431: 343-364

Augustine GJ, Charlton MP, Smith SJ (1987) Calcium action in synaptic transmitter release Annu Rev Neurosci 10, 633-693

Bertram R, Sherman A, Stanley EF (1996) Single-domain/bound calcium hypothesis of transmitter release and facilitation. J Neurophysiol 75: 1919-1931

Betz A, Thakur P, Junge HJ, Ashery U, Rhee JS, Scheuss V, Rosenmund C, Rettig J, Brose N (2001) Functional interaction of the active zone proteins Munc13–1 and RIM1 in synaptic vesicle priming. Neuron 30:183–196

Beutner D, Voets T, Neher E, Moser T (2001) Calcium dependence of exocytosis and endocytosis at the cochlear inner hair cell afferent synapse. Neuron 29: 681–690.

Bezprozvanny I, Scheller RH, Tsien RW (1995) Functional impact of syntaxin on gating of N-type and Q-type calcium channels. Nature 378: 623–626

Bischofberger J, Geiger JR, Jonas P (2002) Timing and efficacy of Ca^{2+} channel activation in hippocampal mossy fiber boutons J Neurosci 22: 10593-10602

Bollmann JH, Sakmann B (2005) Control of synaptic strength and timing by the release-site Ca^{2+} signal. Nat Neurosci 8:426-34

Bollmann JH, Sakmann B, Borst JG (2000) Calcium sensitivity of glutamate release in a calyx-type terminal. Science 289:953-7

Borst JG, Sakman B (1996) Calcium influx and transmitter release in a fast CNS synapse. Nature 383: 431–434

Borst JG, Sakmann B (1998) Calcium current during a single action potential in a large presynaptic terminal of the rat brainstem. J Physiol (Lond) 506: 143-157

Bostock H, Sears TA, Sherratt RM (1981) The effects of 4-aminopyridine and tetraethylammonium ions on normal and demyelinated mammalian nerve fibres. J Physiol 313: 301-315

Brenowitz S, Regehr W (2007) Reliability and heterogeneity of calcium signaling at single presynaptic boutons of cerebellar granule cells. J Neurosci. 27: 7888-7898

Brodin L, Low P, Shupliakov O (2000) Sequential steps in clathrin-mediated synaptic vesicle endocytosis. Curr. Opin. Neurobiol. 10:312–20.

Bucurenciu I, Kulik A, Schwaller B, Frotscher M, Jonas P (2008) Nanodomain coupling between Ca^{2+} channels and Ca^{2+} sensors promotes fast and efficient transmitter release at a cortical GABAergic synapse. Neuron 57:536-45

Catterall WA (1999) Interactions of presynaptic Ca^{2+} channels and snare proteins in neurotransmitter release. Ann NY Acad Sci 868: 144–159

Catterall WA, Few AP (2008) Calcium channel regulation and presynaptic plasticity. Neuron. 59:882-901

Ceccarelli B, Hurlbut WP, Mauro A (1973) Turnover of transmitter and synaptic vesicles at the frog neuromuscular junction. J Cell Biol 57:499–524

Chapman ER (2002) Synaptotagmin: a Ca^{2+} sensor that triggers exocytosis? Nat Rev Mol Cell Biol 3: 498-508

Chapman ER, Hanson PI, An S, Jahn R. (1995) Ca^{2+} regulates the interaction between synaptotagmin and syntaxin 1. J Biol Chem. 270:23667-71

Chicka MC, Hui E, Liu H, Chapman ER (2008) Synaptotagmin arrests the SNARE complex before triggering fast, efficient membrane fusion in response to Ca^{2+}. Nat Struct Mol Biol 15:827-35

Church PJ, Stanley EF (1996) Single L-type calcium channel conductance with physiological levels of calcium in chick ciliary ganglion neurons. J Physiol (Lond) 496: 59–68

Church PJ, Stanley EF (1996) Single L-type calcium channel conductance with physiological levels of calcium in chick ciliary ganglion neurons. J Physiol 496:59-68

Cohen MW, Jones OT, Angelides KJ (1991) Distribution of Ca^{2+} channels on frog motor nerve terminals revealed by fluorescent omega-conotoxin. J Neurosci 11: 1032-1039

Davis AF, Bai J, Fasshauer D, Wolowick MJ, Lewis JL, Chapman ER (1999) Kinetics of synaptotagmin responses to Ca^{2+} and assembly with the core SNARE complex into membranes. Neuron 24:363–376

DiGregorio DA, Peskoff A, Vergara JL (1999) Measurement of action potential-induced presynaptic calcium domains at a cultured neuromuscular junction. J Neurosci. 19:7846-59

Dittrich M, Pattillo JM, Luo F, King JD, Meriney SD, Stiles JR A novel excess calcium binding site model of neurotransmitter release. 2009 (submitted).

Dodge FA Jr, Rahamimoff R (1967) Co-operative action a calcium ions in transmitter release at the neuromuscular junction. J Physiol 193:419-32

Dunlap K, Luebke JI, Turner TJ (1995) Exocytotic Ca^{2+} channels in mammalian central neurons. Trends Neurosci. 18: 89–98

Ertel EA, Campbell KP, Harpold MM, Hofmann F, Mori Y, Perez-Reyes E, Schwartz A, Snutch TP, Tanabe T, Birnbaumer L, Tsien RW, Catterall WA (2000) Nomenclature of voltage-gated calcium channels. Neuron 25: 533–535

Evans RM, Zamponi GW (2006) Presynaptic Ca^{2+} channels-integration centers for neuronal signaling pathways. Trends Neurosci 29: 617–624

Faber, DS, Lin, JW, Korn, H (1991) Silent synaptic connections and their modifiability. Ann NY Acad Sci 627: 151-164

Fedchyshyn MJ, Wang LY (2005) Developmental transformation of the release modality at the calyx of Held synapse. J Neurosci 25:4131-40

Fernandez I, Ara çD, Ubach J, Gerber SH, Shin O, Gao Y, Anderson RG, S üdhof TC, Rizo J (2001) Three-dimensional structure of the synaptotagmin 1 C2B-domain: synaptotagmin 1 as a phospholipid binding machine. Neuron 32:1057-69

Fern ández-Chac ón R, K önigstorfer A, Gerber SH, Garc á J, Matos MF, Stevens CF, Brose N, Rizo J, Rosenmund C, S üdhof TC (2001) Synaptotagmin I functions as a calcium regulator of release probability. Nature 410:41-9

Fesce R, Grohovaz F, Valtorta F, Meldolesi J (1994) Neurotransmitter release: fusion or 'kiss-and-run'? Trends Cell Biol 4:1–4

Frank CA, Pielage J, Davis GW (2009) A presynaptic homeostatic signaling system composed of Eph receptor, ephexin, cdc42, and $Ca_v2.1$ calcium channels Neuron 61: 556-569

Frenguelli BG, Malinow R (1996) Fluctuations in intracellular calcium responses to action potentials in single en passage presynaptic boutons of layer v neurons in neocortical slices. Learning and Memory 3: 130-159

Fukuoka T, Engel AG, Lang B, Newsom-Davis J, Prior C, Wray DW (1987) Lambert-Eaton myasthenic syndrome: I Early morphological effects of IgG on the presynaptic membrane active zones. Ann Neurol 22:193-9

Gentile L, Stanley EF (2005) A unified model of presynaptic release site gating by calcium channel domains Eur J Neurosci 21: 278-282

Geppert M, Goda Y, Hammer RE, Li C, Rosahl TW, Stevens CF, Südhof TC (1994) Synaptotagmin I: A major Ca^{2+} sensor for transmitter release at a central synapse. Cell 79:717–27

Greengard P, Valtorta F, Czernik AJ, Benfenati F (1993) Synaptic vesicle phosphoproteins and regulation of synaptic function. Science 259:780–785

Hayashi T, McMahon H, Yamasaki S, Binz T, Hata Y, Sudhof TC, Niemann H (1994) Synaptic vesicle membrane fusion complex: action of clostridial neurotoxins on assembly. EMBO J 13:5051-5061

Heidelberger R, Heinemann C, Neher E, Matthews G (1994) Calcium dependence of the rate of exocytosis in a synaptic terminal. Nature 371:513-5

Hefft S, Jonas P (2005). Asynchronous GABA release generates long-lasting inhibition at a hippocampal interneuron principal neuron synapse. Nat Neurosci. 8:1319-28

Heuser JE, Reese TS, Landis DM (1974) Functional changes in frog neuromuscular junctions studied with freeze-fracture J Neurocytol 3:109-31

Heuser JE, Reese TS (1981) Structural changes after transmitter release at the frog neuromuscular junction J Cell Biol 88: 564-80

Heuser JE, Reese TS, Dennis MJ, Jan Y, Jan L, Evan L (1979) Synaptic vesicle exocytosis captured by quick freezing and correlated with quantal transmitter release. J Cell Biol 81: 275-300

Hilfiker S, Pieribone VA, Czernik AJ, Kao HT, Augustine GJ, Greengard P (1999) Synapsins as regulators of neurotransmitter release. Philos Trans R Soc Lond B Biol Sci 354:269–279

Hines ML, Carnevale NT (1997) The NEURON simulation environment. Neural Comput 9: 1179-209

Hodgkin AI, Huxley AF (1952) A quantitative description of membrane current and its application to conduction and excitation in nerve. J Physiol 117: 500-544

Hofmann F, Lacinová L, Klugbauer N (1999). Voltage-dependent calcium channels: from structure to function. Rev Physiol Biochem Pharmacol. 139:33-87

Hong SJ, Chang CC (1995) Inhibition of acetylcholine release from mouse motor nerve by a P-type calcium channel blocker, omega -agatoxin IVA. J Physiol (Lond) 482:283-290.

Hu Q, Saegusa H, Hayashi Y, Tanabe T (2005) The carboxy-terminal tail region of human Cav2.1 (P/Q-type) channel is not an essential determinant for its subcellular localization in cultured neurons. Genes Cells 10: 87–96

Jones SW, Marks TN (1989) Calcium currents in bullfrog sympathetic neurons I Activation kinetics and pharmacology. J Gen Physiol 94: 151-167

Katz B, Miledi R (1979) Estimates of quantal content during 'chemical potentiation' of transmitter release. Proc R Soc Lond B Biol Sci 205(1160):369-78

Katz B (1969) The release of Neural Transmitter substance (Liverpool; Liverpool University Press)

Kee Y, Scheller RH. (1996) Localization of synaptotagmin-binding domains on syntaxin. J Neurosci. 16:1975-81

Kerr LM, Yoshikami D (1984) A venom peptide with a novel presynaptic blocking action. Nature 308: 282-284

Kittel RJ, Wichmann C, Rasse TM, Fouquet W, Schmidt M, Schmid A, Wagh DA, Pawlu C, Kellner RR, Willig KI, Hell SW, Buchner E, Heckmann M, Sigrist SJ (2006) Bruchpilot promotes active zone assembly, Ca^{2+} channel clustering, and vesicle release. Science 312:1051–1054

Koh TW, Bellen HJ (2003) Synaptotagmin I, a Ca^{2+} sensor for neurotransmitter release. Trends Neurosci 26: 413-422

Lang B, Newsom-Davis J, Peers C, Prior C, Wray DW (1987) The effect of myasthenic syndrome antibody on presynaptic calcium channels in the mouse. J Physiol 390:257-70

Li C, Ullrich B, Zhang JZ, Anderson RG, Brose N, Südhof TC (1995) Ca^{2+}-dependent and -independent activities of neural and non-neural synaptotagmins Nature 375: 594-599

Lin JW, Faber DS (2002) Modulation of synaptic delay during synaptic plasticity. Trends Neurosci 25:449-55

Lin Z, Haus S, Edgerton J, Lipscombe D (1997) Identification of functionally distinct isoforms of the N-type Ca^{2+} channel in rat sympathetic ganglia and brain. Neuron 18: 153-166

Lin Z, Lin Y, Schorge S, Pan JQ, Beierlein M, Lipscombe D (1999) Alternative splicing of a short cassette exon in alpha1B generates functionally distinct N-type calcium channels in central and peripheral neurons J Neurosci 19: 5322-5331

Lipscombe D, Kongsamut S, Tsien RW (1989) Alpha-adrenergic inhibition of sympathetic neurotransmitter release mediated by modulation of N-type calcium-channel gating. Nature 340, 639-642

Littleton JT, Stern M, Schulze K, Perin M, Bellen HJ (1993) Mutational analysis of Drosophila synaptotagmin demonstrates its essential role in Ca^{2+}-activated neurotransmitter release Cell 74: 1125-1134

Llinás R, Sugimori M, Silver RB (1992) Microdomains of high calcium concentration in a presynaptic terminal. Science 256: 677-9

Llinás R, Steinberg IZ, Walton K (1981) Relationship between presynaptic calcium current and postsynaptic potential in squid giant synapse. Biophys J. 33: 323-51

Luo F, Dietrich M, Stiles JR, Meriney SD (2009) Quantitative analysis of single calcium channel openings and evoked transmitter release from presynaptic active zones. Submitted.

Luo F, Dietrich M, Stiles JR, Meriney SD (2009) Single pixel optical fluctuation analysis of Ca^{2+} channel function at presynaptic active zone. submitted.

Mackler JM, Drummond JA, Loewen CA, Robinson IM, Reist NE (2002) The C2B Ca^{2+}-binding motif of synaptotagmin is required for synaptic transmission in vivo Nature 418: 340-344

Maximov A, Sudhof TC (2005) Autonomous function of synaptotagmin 1 in triggering synchronous release independent of synchronous release. Neuron 48:547–54

Maximov A, Tang J, Yang X, Pang ZP, Südhof TC (2009) Complexin controls the force transfer from SNARE complexes to membranes in fusion. Science 323:516-21

Meinrenken CJ, Borst JG, Sakmann B (2002) Calcium secretion coupling at calyx of held governed by nonuniform channel-vesicle topography. J Neurosci 22:1648-67

Meriney SD, Grinnell AD (1991) Endogenous adenosine modulates stimulation-induced depression at the frog neuromuscular junction. J Physiol 443:441-55

Mintz IM, Sabatini BL, Regehr WG (1995) Calcium control of transmitter release at a cerebellar synapse. Neuron 15:675-88

Mochida S, Westenbroek RE, Yokoyama CT, Itoh K, Catterall WA (2003a). Subtype-selective reconstitution of synaptic transmission in sympathetic ganglion neurons by expression of exogenous calcium channels. Proc. Natl. Acad. Sci. USA 100, 2813–2818

Mochida S, Westenbroek RE, Yokoyama CT, Zhong H, Myers SJ, Scheuer T, Itoh K, Catterall WA (2003b) Requirement for the synaptic protein interaction site for reconstitution of synaptic transmission by P/Q-type calcium channels Proc Natl Acad Sci USA 100: 2819–2824

Murthy VN, Schikorski T, Stevens CF, Zhu Y (2001) Inactivity produces increases in neurotransmitter release and synapse size. Neuron 32:673-82

Nagel A, Engel AG, Lang B, Newsom-Davis J, Fukuoka T (1988) Lambert-Eaton myasthenic syndrome IgG depletes presynaptic membrane active zone particles by antigenic modulation. Ann Neurol 24:552-8

Neher E (1998a) Vesicle pools and Ca2+ microdomains: new tools for understanding their roles in neurotransmitter release. Neuron 20: 389–399

Neher E (1998b) Usefulness and limitations of linear approximations to the understanding of Ca2+ signals. Cell Calcium 24: 345–357.

Nishiki T, Augustine GJ (2004a) Dual roles of the C2B domain of synaptotagmin I in synchronizing Ca2+-dependent neurotransmitter release. J Neurosci 24:8542–50

Nishiki T, Augustine GJ (2004b) Synaptotagmin I synchronizes transmitter telease in mouse hippocampal neurons. J Neurosci 24:6127–32

Nonet ML, Grundahl K, Meyer BJ, Rand JB (1993) Synaptic function is impaired but not eliminated in C elegans mutants lacking synaptotagmin Cell 73: 1291-1305

Ohana O, Sakmann B (1998) Transmitter release modulation in nerve terminals of rat neocortical pyramidal cells by intracellular calcium buffers. J Physiol. 513: 135–148

Owald D, Sigrist SJ (2009) Assembling the presynaptic active zone. Curr Opin Neurobiol. 19: 1-8

Pang ZP, Melicoff E, Padgett D, Liu Y, Teich AF, Dickey BF, Lin W, Adachi R, Südhof TC. (2006a) Synaptotagmin-2 is essential for survival and contributes to Ca^{2+} triggering of neurotransmitter release in central and neuromuscular synapses. J Neurosci. 26:13493-504

Pang ZP, Sun J, Rizo J, Maximov A, Südhof TC (2006b) Genetic analysis of synaptotagmin 2 in spontaneous and Ca^{2+}-triggered neurotransmitter release. EMBO J. 25:2039-50.

Pattillo JM, Artim DE, Simples JE, Merieny SD (1999) Variations in onset of action potential broadening: effects on calcium current studied in chick ciliary ganglion neurons. J. Physiol. 514: 719-728.

Pawson PA, Grinnell AD, Wolowske B (1998) Quantitative freeze-fracture analysis of the frog neuromuscular junction synapse--I Naturally occurring variability in active zone structure. J Neurocytol. 27: 361-377.

Perin MS, Fried VA, Mignery GA, Jahn R, Sudhof TC (1990) Phospholipid binding by a synaptic vesicle protein homologous to the regulatory region of protein kinase C. Nature 345:260–63

Poage RE and Meriney SD (2002) Presynaptic calcium influx, neurotransmitter release and neuromuscular disease. Physiol and Behav 77: 507-512

Poirier MA, Xiao W, Macosko JC, Chan C, Shin YK, Bennett MK (1998) The synaptic SNARE complex is a parallel four-stranded helical bundle. Nat Struct Biol. 5:765-9

Pumplin DW, Reese TS, Llinás R (1981) Are the presynaptic membrane particles the calcium channels? Proc Natl Acad Sci USA 78: 7210-7213

Pun RY, Neale EA, Guthrie PB, Nelson PG (1986) Active and inactive central synapses in cell culture. J Neurophysiol 56: 1242-1256

Rajan S, Plant LD, Rabin ML, Butler MH, Goldstein SA (2005) Sumoylation silences the plasma membrane leak K+ channel K2P1 Cell 121: 37-47

Reid CA, Bekkers JM, Clements JD (1998) N- and P/Q-type Ca^{2+} channels mediate transmitter release with a similar cooperativity at rat hippocampal autapses. J Neurosci 18:2849-2855

Reid CA, Bekkers JM, Clements JD (2003) Presynaptic Ca^{2+} channels: a functional patchwork. Trends Neurosci 26: 683–687

Rettig J, Heinemann C, Ashery U, Sheng ZH, Yokoyama CT, Catterall WA, Neher E (1997) Alteration of Ca^{2+} dependence of neurotransmitter release by disruption of Ca^{2+} channel/syntaxin interaction J Neurosci 17: 6647–6656

Rizzoli SO, Betz WJ (2005) Synaptic vesicle pools. Nat Rev Neurosci 6: 57-69

Roberts WM, Jacobs RA, Hudspeth AJ (1990) Colocalization of ion channels involved in frequency selectivity and synaptic transmission at presynaptic active zones of hair cells. J Neurosci 10: 3664–3684

Robinson IM, Ranjan R, Schwarz TL (2002) Synaptotagmins I and IV promote transmitter release independently of Ca^{2+} binding in the C2A domain Nature 418: 336-340

Robitaille R, Adler EM, Charlton MP (1990) Strategic location of calcium channels at transmitter release sites of frog neuromuscular synapses Neuron 5: 773-779

Robitaille R, Garcia ML, Kaczorowski GJ, Charlton MP (1993) Functional colocalization of calcium and calcium-gated potassium channels in control of transmitter release Neuron 11: 645-55

Rosenmund C, Stevens CF (1996) Definition of the readily releasable pool of vesicles at hippocampal synapses. Neuron 16:1197–201

Royle SJ, Lagnado L (2003) Endocytosis at the synaptic terminal. J Physiol (Lond) 553:345–355

Rozov A, Burnashev N, Sakmann B, Neher E (2001) Transmitter release modulation by intracellular Ca^{2+} buffers in facilitating and depressing nerve terminals of pyramidal cells in layer 2/3 of the rat neocortex indicates a target cell-specific difference in presynaptic calcium dynamics. J. Physiol. 531: 807–826

Sabatini BL, Regehr WG (1997) Control of neurotransmitter release by presynaptic waveform at the granule cell to Purkinje cell synapse. J Neurosci 17: 3425-3435

Sabatini BL, Svoboda K (2000) Analysis of calcium channels in single spines using optical fluctuation analysis. Nature 408: 589-593

Sätzler K, Söhl LF, Bollmann JH, Borst JGG, Frotscher M, Sakmann B, Lubke JH (2002) Three-dimensional reconstruction of a calyx of Held and its postsynaptic principal neuron in the medial nucleus of the trapezoid body. J Neurosci 22:10567-10579

Schiavo G, Benfenati F, Poulain B, Rossetto O, Polverino de Laureto P, DasGupta BR, Montecucco C (1992) Tetanus and botulinum-B neurotoxins block neurotransmitter release by proteolytic cleavage of synaptobrevin. Nature 359:832-835

Schikorski T, Stevens CF (1997) Quantitative ultrastructural analysis of hippocampal excitatory synapses. J Neurosci 17:5858-5867

Schikorski T, Stevens CF (1999) Quantitative fine-structural analysis of olfactory cortical synapses. Proc Natl Acad Sci USA 96:4107-4112

Schikorski T, Stevens CF (2001) Morphological correlates of functionally defined synaptic vesicle populations. Nat Neurosci 4:391-395

Schneggenburger R, Neher E (2000) Intracellular calcium dependence of transmitter release rates at a fast central synapse. Nature 406:889-93

Shahrezaei V, Cao A, Delaney KR (2006) Ca^{2+} from one or two channels controls fusion of a single vesicle at the frog neuromuscular junction. J Neurosci 26:13240-9

Simon SM, Llinás RR (1985) Compartmentalization of the submembrane calcium activity during calcium influx and its significance in transmitter release. Biophys J 48:485-98

Slepnev VI, De Camilli P (2000) Accessory factors in clathrin-dependent synaptic vesicle endocytosis. Nat. Rev. Neurosci. 1:161–72

Söllner T, Whiteheart SW, Brunner M, Erdjument-Bromage H, Geromanos S, Tempst P, Rothman JE (1993) SNAP receptors implicated in vesicle targeting and fusion. Nature 362:318-24

Spafford JD and Zamponi GW (2003) Functional interactions between presynaptic calcium channels and the neurotransmitter release machinery. Curr. Opin. Neurobiol. 13: 308–314

Spafford JD, Munno DW, Van Nierop P, Feng ZP, Jarvis SE, Gallin WJ, Smit AB, Zamponi GW, Syed NI (2003). Calcium channel structural determinants of synaptic transmission between identified invertebrate neurons. J. Biol. Chem. 278: 4258–4267

Stanley EF (1993) Single calcium channels and acetylcholine release at a presynaptic nerve terminal Neuron 11:1007-11

Stanley EF (1997) The calcium channel and the organization of the presynaptic transmitter release face. Trends Neurosci 20: 404–409

Stea A, Dubel SJ, Snutch TP (1999) alpha 1B N-type calcium channel isoforms with distinct biophysical properties. Ann NY Acad Sci 868: 118-130

Stevens CF (2003) Neurotransmitter Release at Central Synapses. Neuron 40: 381–388

Stevens CF, Tsujimoto T (1995) Estimates for the pool size of releasable quanta at a single central synapse and for the time required to refill a pool. Proc Natl Acad Sci USA 92: 846–849

Stevens CF, Sullivan JM (1998) Regulation of the readily releasable vesicle pool by protein kinase C. Neuron 21:885-93

Stevens CF, Sullivan JM (2003) The synaptotagmin C2A domain is part of the calcium sensor controlling fast synaptic transmission. Neuron 39:299-308

Stewart BA, Mohtashami M, Trimble WS, Boulianne GL (2000) SNARE proteins contribute to calcium cooperativity of synaptic transmission. Proc Natl Acad Sci U S A. 97:13955-60.

Stiles JR, Bartol TM (2001) Monte Carlo methods for simulating realistic synaptic microphysiology using MCell In Computational Neuroscience: Realistic Modeling for Experimentalists, ed De Schutter, E (Boca Raton, FL; CRC Press), pp 87-127

Stiles JR, Van Helden D, Bartol TM, Jr Salpeter EE, Salpeter MM (1996) Miniature endplate current rise times <100 μs from improved dual recordings can be modeled with passive acetylcholine diffusion from a synaptic vesicle Proc Natl Acad Sci USA 93:5747-5752

Stocker JW, Nadasdi L, Aldrich RW, Tsien RW (1997) Preferential interaction of omega-conotoxins with inactivated N-type Ca^{2+} channels J Neurosci 17: 3002-3013

Südhof TC (2002) Synaptotagmins: why so many? J Biol Chem 277: 7629-7632

Sun YA, Poo MM (1987) Evoked release of acetylcholine from the growing embryonic neuron. Proc Natl Acad Sci U S A. 84:2540-4

Sutton RB, Fasshauer D, Jahn R, Brunger AT (1998) Crystal structure of a SNARE complex involved in synaptic exocytosis at 2.4 A resolution. Nature. 395: 347-53

Szabo Z, Obermair GJ, Cooper CB, Zamponi GW, Flucher BE (2006) Role of the synprint site in presynaptic targeting of the calcium channel CaV22 in hippocampal neurons. Eur J Neurosci 24: 709–718

Takamori S, Holt M, Stenius K, Lemke EA, Grønborg M, Riedel D, Urlaub H, Schenck S, Brügger B, Ringler P, Müller SA, Rammner B, Gräter F, Hub JS, De Groot BL, Mieskes G, Moriyama Y, Klingauf J, Grubmüller H, Heuser J, Wieland F, Jahn R. (2006). Molecular anatomy of a trafficking organelle. Cell. 127:831-46

Tang J, Maximov A, Shin OH, Dai H, Rizo J, Südhof TC (2006) A complexin / synaptotagmin 1 switch controls fast synaptic vesicle exocytosis. Cell 126:1175-87

Thomsen RH, Wilson DF (1983) Effects of 4-aminopyridine and 3,4 diaminopyridine on transmitter release at the neuromuscular junction J Pharmacol Exp Ther 227: 260-265

Toselli M, Biella G, Taglietti V, Cazzaniga E, Parenti M (2005) Caveolin-1 expression and membrane cholesterol content modulate N-type calcium channel activity in NG108-15 cells Biophys J 89: 2443-2457

Tucker WC, Weber T, Chapman ER (2004) Reconstitution of Ca^{2+}-regulated membrane fusion by synaptotagmin and SNAREs. Science 304:435-8

Ubach J, Zhang X, Shao X, Südhof TC, Rizo J (1998) Ca^{2+} binding to synaptotagmin: how many Ca^{2+} ions bind to the tip of a C2-domain? EMBO J 17: 3921-30.

Uchitel OD, Protti DA, Sanchez V, Cherksey BD, Sugimori M, Llinás R (1992) P-type voltage-dependent calcium channel mediates presynaptic calcium influx and transmitter release in mammalian synapses. Proc Natl Acad Sci USA 89:3330-3333

Vacher H, Mohapatra DP, Trimmer JS (2008). Localization and targeting of voltage-dependent ion channels in mammalian central neurons. Physiol Rev 88: 1407–1447

Vincent A, Lang B, Newsom-Davis J (1989) Autoimmunity to the voltage-gated calcium channel underlies the Lambert-Eaton myasthenic syndrome, a paraneoplastic disorder. Trends Neurosci 12:496-502

Von Gersdorff H, Vardi E, Matthews G, Sterling P (1996) Evidence that vesicles on the synaptic ribbon of retinal bipolar neurons can be rapidly released. Neuron 116:1221-1227

Voronin LL, Cherubini E (2004) 'Deaf, mute and whispering' silent synapses: their role in synaptic plasticity J Physiol (Lond) 557: 3-12

Wachman ES, Poage RE, Stiles JR, Farkas DL, Meriney SD (2004) Spatial Distribution of calcium entry evoked by single action potentials within the presynaptic active zone. J Neurosci 24: 2877-2885

Wadel K, Neher E, Sakaba T (2007) The coupling between synaptic vesicles and Ca^{2+} channels determines fast neurotransmitter release. Neuron. 53:563-75

Wang LY, Neher E, Taschenberger H. (2008) Synaptic vesicles in mature calyx of Held synapses sense higher nanodomain calcium concentrations during action potential-evoked glutamate release. J Neurosci. 28:14450-8

Wang X, Engisch KL, Li Y, Pinter MJ, Cope TC, Rich MM (2004) Decreased synaptic activity shifts the calcium dependence of release at the mammalian neuromuscular junction in vivo. J Neurosci 24: 10687-10692

Weber T, Zemelman BV, McNew JA, Westermann B, Gmachl M, Parlati F, Söllner TH, Rothman JE (1998) SNAREpins: minimal machinery for membrane fusion. Cell 92:759-72

Wheeler DB, Randall A, Tsien RW (1994) Roles of N-type and Q-type Ca^{2+} channels in supporting hippocampal synaptic transmission. Science 264:107-111

Willig KI, Rizzoli SO, Westphal V, Jahn R, Hell SW (2006) STED microscopy reveals that synaptotagmin remains clustered after synaptic vesicle exocytosis. Nature. 440:935-9

Wilson VG, Rosas-Acosta G (2005) Wrestling with SUMO in a new arena Sci STKE 290, 32

Wilson RI, Nicoll RA (2001). Endogenous cannabinoids mediate retrograde signalling at hippocampal synapses. Nature 410: 588–592

Wiser O, Bennett MK, Atlas D (1996) Functional interaction of syntaxin and SNAP-25 with voltage-sensitive L- and N-type Ca^{2+} channels. EMBO J 15: 4100–4110

Wood SJ, Slater CR (2001) Safety factor at the neuromuscular junction. Prog Neurobiol 64: 393-429

Wu LG, Borst JG, Sakmann B (1998) R-type Ca^{2+} currents evoke transmitter release at a rat central synapse. Proc Natl Acad Sci U S A 95:4720-5

Wu LG, Westenbroek RE, Borst JG, Catterall WA, Sakmann B (1999) Calcium channel types with distinct presynaptic localization couple differentially to ransmitter release in single calyx-type synapses. J Neurosci 19:726-36

Wucherpfennig T, Wilsch-Brauninger M, Gonzalez-Gaitan M (2003). Role of Drosophila Rab5 during endosomal trafficking at the synapse and evoked neurotransmitter release. J. Cell Biol. 161:609–24

Xu-Friedman MA, Harris KM, Regehr WG (2001) Three-dimensional comparison of ultrastructural characteristics at depressing and facilitating synapses onto cerebellar Purkinje cells. J Neurosci 21:6666-6672

Yamada WM, Zucker RS (1992) Time course of transmitter release calculated from simulations of a calcium diffusion model. Biophys J 61:671-82

Yazejian B, Sun XP, Grinnell AD (2000) Tracking presynaptic Ca^{2+} dynamics during neurotransmitter release with Ca^{2+}-activated K^+ channels. Nat Neurosci 3:566-71

Yoshihara M, Littleton T (2002) Synaptotagmin I Functions as a Calcium Sensor to Synchronize Neurotransmitter Release. Neuron 36: 897–908.

Yoshikami D, Bagabaldo Z, Olivera BM (1989) The inhibitory effects of omega-conotoxins on Ca channels and synapses. Ann NY Acad Sci 560, 230–248

Zenisek D, Davila V, Wan L, Almers W (2003) Imaging calcium entry sites and ribbon structures in two presynaptic cells. J Neurosci 23: 2538–2548

Zhai RG and Bellen HJ (2004) The architecture of the active zone in the presynaptic nerve terminal. Physiology (Bethesda) 19: 262-70

Zucker RS and Fogelson AL (1986) Relationship between transmitter release and presynaptic calcium influx when calcium enters through discrete channels. Proc Natl Acad Sci USA 83: 3032–3036